Vol. 59 • No. 6

June 2016

Microwave Journal.com

MVP

ADI's Integrated Transceiver

horizon house®

Founded in 1958

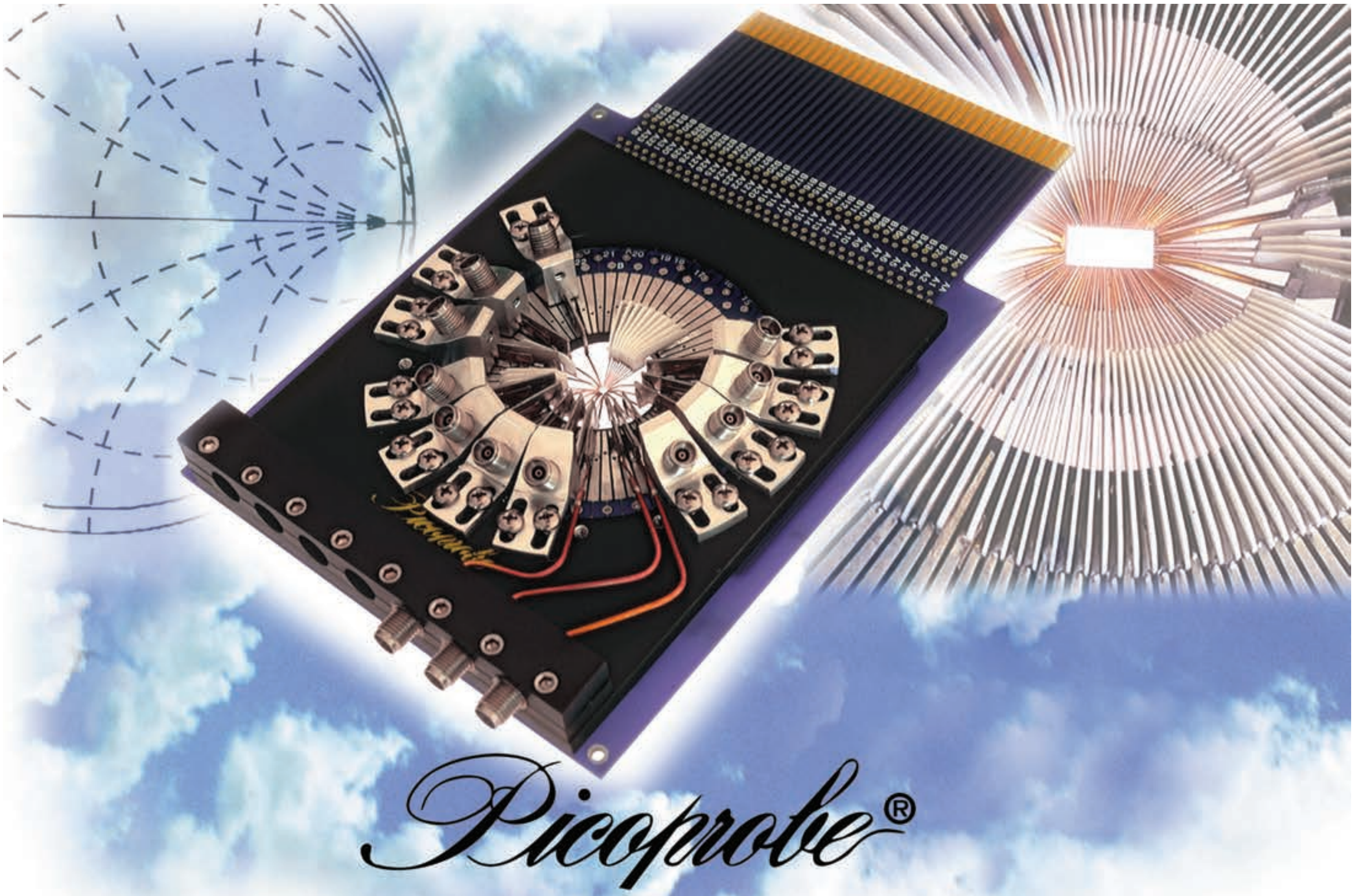

Picoprobe elevates probe cards to a higher level…

(…110 GHz to be exact.)

Since 1981, GGB Industries, Inc., has blazed the on-chip measurement trail with innovative designs, quality craftsmanship, and highly reliable products. Our line of custom microwave probe cards continues our tradition of manufacturing exceptional testing instruments.

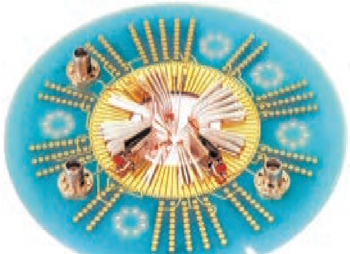

Through unique modular design techniques, hundreds of low frequency probe needles and a variety of microwave probes with operating frequencies from DC to 40, 67, or even 110 GHz can be custom configured to your layout.

Our patented probe structures provide the precision and ruggedness you require for both production and characterization testing. And only Picoprobe® offers the lowest loss, best match, low inductance power supplies, and current sources on a single probe card.

Our proven probe card design technology allows full visibility with inking capability and ensures reliable contacts, even when probing non-planar structures.

Not only do you get all the attractive features mentioned, but you get personal, professional service, rapid response, and continuous product support--all at an affordable price so your project can be completed on time and within budget.

Typical Specs	10GHz	20GHz	40GHz
Insertion Loss	0.6 dB	0.8 dB	1.3 dB
Return Loss	22 dB	18 dB	15 dB

For technical assistance, custom product designs, or off-the-shelf delivery,call GGB Industries, Inc., at (239) 643-4400.

GGB INDUSTRIES, INC. • P.O. BOX 10958 • NAPLES, FL 34101

Telephone (239) 643-4400 • Fax (239) 643-4403 • E-mail email@ggb.com • www.picoprobe.com

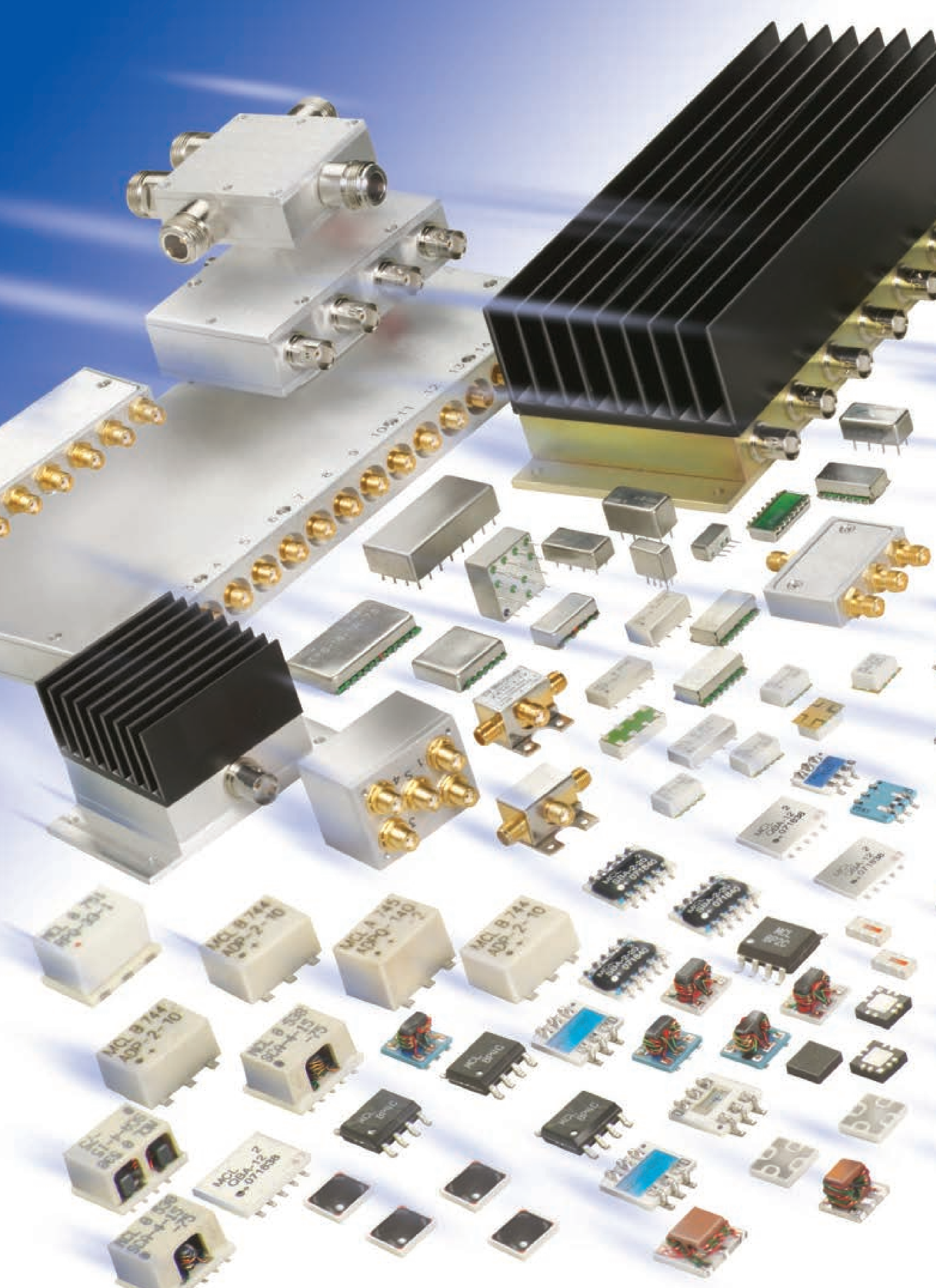
MCL B 744
ADP-2-10
MCL B 744
ADP-2-10
MCL B 744
ADP-2-10

Technology On the Move™

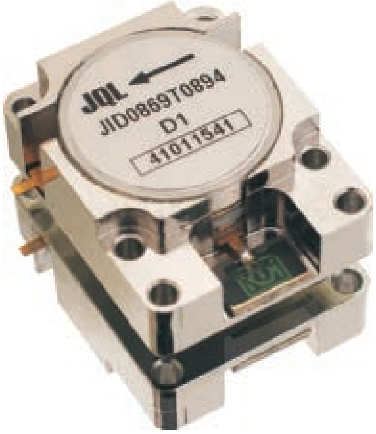

Drop-in Isolators

Cavity Filters

Surface Mount Circulators

Waveguide Isolators

Power Combiners

Coaxial Circulators

JQL

Tel:1(888)236-9828(US&Canada)
1(630)930-9917(Worldwide)
www.jqlelectronics.com sales@jqlelectronics.com

Closer to the *"Perfect Notch"*

Engineers know the **'perfect notch'** in YIG band-reject filters is an unattainable goal. However, Teledyne Microwave Solutions (TMS) has developed a new patent-pending technology to deliver a **YIG Tuned Notch Filter Line** that brings the technology *far closer to the ideal 'notch' than ever before.*

Introducing Teledyne's

New YIG Tuned Band-Reject Filters

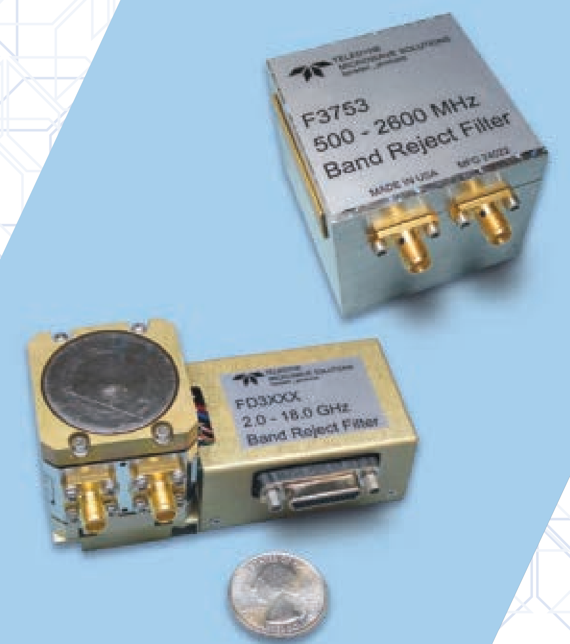

A Design Trifecta:

- **Wider Notch Bandwidth**
- **Greater Notch Depth**
- **Narrower 3dB BW**

These TMS BRFs deliver ***improved performance at lower frequencies with reduced spurious responses.*** *Add these benefits to the "TMS Design Trifecta," and it becomes clear that TMS should be your* ***ONE SOURCE*** *for demanding YIG band-reject filter requirements.*

TELEDYNE
MICROWAVE SOLUTIONS
Everywhere**you**look™

teledynemicrowave.com
1.800.832.6869 or 1.650.962.6944
microwave@teledyne.com

TMS: The Power of Consolidation

Cougar • MEC • LabTech • Microwave • Paradise Datacom • Defence Ltd.

Microwave Journal
June 2016
Vol. 59 • No. 6
Semiconductors/
MMICs/RFICs
mwjournal.com

CONTENTS

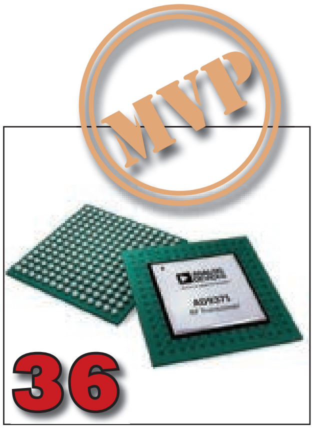

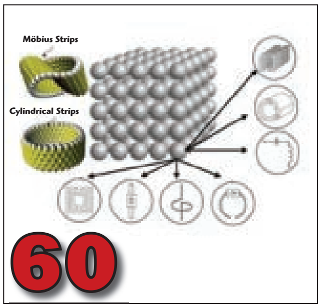

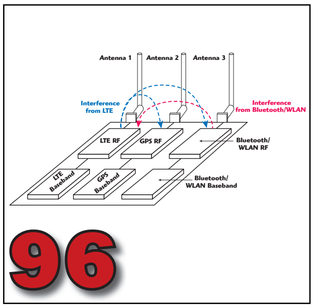

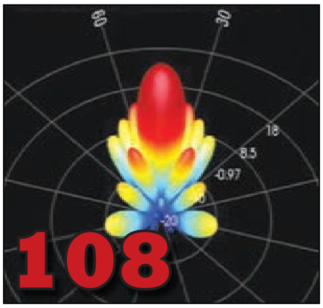

AUGMENTED REALITY: HOW IT WORKS

STEP 1
Download the free Layar app from the iTunes (iOS) or Google Play (Android) store.

STEP 2
Launch the app to view enhanced content on any page with the layar logo.

STEP 3
Frame the entire page in the screen and tap to experience enhancements (tap screen again for full screen view).

Look for the Layar logo on participating pages. **AR pages may expire after 30 days.**

59 YEARS OF PUBLISHING EXCELLENCE

If your 5G idea works here...

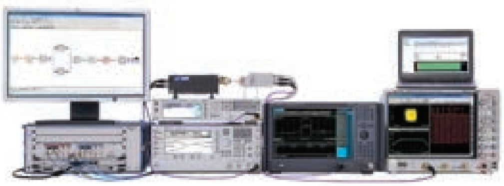

it will work here.

50,000 soccer fans streaming live-action mobile video. All at once.

Soon it will be reality. A world connected as never before. Always on. Amazingly fast. Massive traffic. Instant information. That's the promise of 5G. New spectrum. New waveforms. Millimeter-waves. Massive MIMO. More. Keysight offers the world's first 5G simulation, design and test environment able to emulate your real-world 5G wireless thesis. With deep expertise to help you tackle 5G risk and complexity. So you can go from 5G ideas to 5G reality faster.

HARDWARE + SOFTWARE + PEOPLE = 5G INSIGHTS

5G **Get the latest app notes, white papers and tutorials**
www.keysight.com/find/5G-Insight

USA: 800 829 4444 CAN: 877 894 4414

KEYSIGHT TECHNOLOGIES
Unlocking Measurement Insights

Agilent's Electronic Measurement Group is now **Keysight Technologies**.

CONTENTS

mwjournal.com

Product Feature

Tech Briefs

Departments

Microwave Journal (USPS 396-250) (ISSN 0192-6225) is published monthly by Horizon House Publications Inc., 685 Canton St., Norwood, MA 02062. Periodicals postage paid at Norwood, MA 02062 and additional mailing offices.

POSTMASTER: Send address corrections to *Microwave Journal*, PO Box 1143, Skokie, IL 60076 or e-mail mwj@halldata.com. Subscription information: (847) 763-4943. This journal is issued without charge upon written request to qualified persons working in the RF & microwave industry. Other subscriptions are: domestic, $120.00 per year, two-year subscriptions, $185.00; foreign, $200.00 per year, two-year subscriptions, $370.00; back issues (if available) and single copies, $10.00 domestic and $20.00 foreign. Claims for missing issues must be filed within 90 days of date of issue for complimentary replacement.

STAFF

EXECUTIVE EDITORIAL OFFICE
685 Canton Street, Norwood, MA 02062
Tel: (781) 769-9750
FAX: (781) 769-5037
e-mail: mwj@mwjournal.com

EUROPEAN EDITORIAL OFFICE
16 Sussex Street, London SW1V 4RW, England
Tel: Editorial: +44 207 596 8730 Sales: +44 207 596 8740
FAX: +44 207 596 8749

SUBSCRIPTION SERVICES
Send subscription inquiries and address changes to:
Tel: (847) 763-4943
e-mail: mwj@halldata.com

BPA WORLDWIDE

www.mwjournal.com

Printed in the USA

Microwave Journal Online

Scan page using layar app

Visit us @ mwjournal.com

eLEARNING free webinars

Expanding the Possibilities of Cellular Wireless Infrastructure with GaN
Sponsored by: Qorvo 6/7

Practical Antenna Design for Advanced Wireless Products
Sponsored by: National Instruments 6/14

Technical Education Training
Sponsored by: National Instruments 6/16

Faster Analysis of Complex RF Signals
Sponsored by: Boonton (Wireless Telecom Group) 6/23

Radar Signal Generation with up to 2 GHz Bandwidth for Single-Channel and Multichannel Receiver Testing
Sponsored by: Rohde & Schwarz 6/28

Web Survey

Which market will drive high volume GaN?

Look for our multiple choice survey online at mwjournal.com

April Survey

What acquisition or merger will have the biggest impact on the wireless industry?

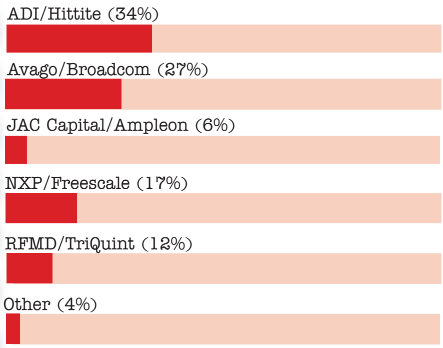

Executive Interviews

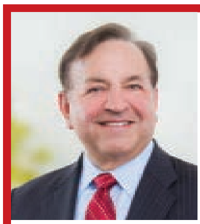

Bami Bastani, SVP of RF Business Unit at **GLOBALFOUNDRIES**, discusses trends in foundry services, RF SOI technology and their recent acquisition of IBM's foundries.

C. G. Shih, president of "pure play" foundry **Wavetek Microelectronics**, discusses their process technologies, the markets they serve and what differentiates Wavetek among global foundries.

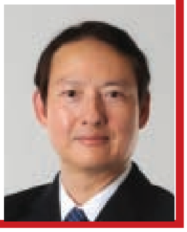

WHITE PAPERS

Altair

molex

Richardson Electronics POWER & MICROWAVE TECHNOLOGIES

Wolfspeed

Catch *Frequency Matters*, the industry update from *Microwave Journal*, www.microwavejournal.com/FrequencyMatters

Join Us Online

Follow us @Pathindle

Become a fan at facebook.com/microwavejournal

COM

6/26–7/1 AP-S/URSI 2016
Fajardo, Puerto Rico

This symposium is the premier international forum for the exchange of information on state-of-the-art research in antennas, electromagnetic wave propagation, radio science and electromagnetic engineering. Both events are co-sponsored by the IEEE Antennas and Propagation Society (AP-S) and U. S. Committee of the International Union of Radio Science (USNC-URSI). The symposium attracts over 1,500 attendees from around the world.
www.2016apsursi.org

25–29 EMC 2016
Ottawa, Canada

The 2016 IEEE International Symposium on Electromagnetic Compatibility, sponsored by the IEEE EMC Society, is a must-attend event for EMC engineers of all levels and specialties. The symposium provides knowledge and tools that help engineers address electromagnetic environmental effects and electromagnetic compatibility. Topics include: Signal & Power Integrity, EMC for Emerging Technologies and Space EMC.
www.emc2016.emcss.org

WEBINAR 24
Sponsored by: IDT

27–29 NEMO2016
Beijing, China

NEMO is a new annual focal event on electromagnetic and multiphysics-based computer-aided design (EM-CAD), rotating between Europe, North America and Asia. NEMO2016 aims to stimulate discussion and exploration of "disruptive" technologies of EM-CAD in addition to traditional topics. The conference features an exciting technical program, an industry exhibition and invited talks by internationally recognized experts in electromagnetic and multiphysics modeling and optimization.
www.nemo-ieee.org

24 RWW2017 Call for Papers Deadline

Authors are invited to submit papers for presentation at RWW2017. All papers accepted will be published in a digest and included in IEEE Xplore. Topics include: RF/microwave physical layer, devices, algorithms and implementation to applications; RF/microwave power amplifiers; wireless sensors and sensor networks, RFID, localization and six-port technology; silicon technologies for microwave and mmWave applications; and space- and suborbital-based high-data-rate communications networks.
www.radiowirelessweek.org

EDI CON 2016
COMING September 20-22

Hynes Convention Center
Boston, Mass.

Register now at
www.ediconusa.com

FOR DETAILS, VISIT MWJOURNAL.COM/EVENTS

Coming**Events**

CALL FOR PAPERS

RWW2017
July 24, 2016

IEDM 2016
August 10, 2016

88th ARFTG Conference
October 7, 2016

mwjournal.com

JULY

IEEE EMC
July 25–29, 2016 • Ottawa, Canada
www.emc2016.emcss.org

NEMO 2016
July 27–29, 2016 • Beijing, China
www.nemo-ieee.org

AUGUST

NIWeek 2016
August 1–4, 2016 • Austin, Texas
www.ni.com/niweek

RFIT 2016
August 24–26, 2016 • Taipei, Taiwan
www.rfit2016.org

SEPTEMBER

CTIA Super Mobility
September 7–9, 2016 • Las Vegas, Nev.
www.ctiasupermobility2016.com

Tower and Small Cell Summit
September 7–9, 2016 • Las Vegas, Nev.
www.towersummit.com

IEEE AUTOTESTCON 2016
September 12–15, 2016 • Anaheim, Calif.
www.autotestcon.com

ION GNSS+ 2016
September 12–16, 2016 • Portland, Ore.
www.ion.org/gnss

Metamaterials 2016
September 17–22, 2016 • Crete, Greece
http://congress2016.metamorphose-vi.org

EDI CON USA
September 20–22, 2016 • Boston, Mass.
www.ediconusa.com

IRMMW-THz 2016
September 25–30, 2016 • Copenhagen, Denmark
www.irmmw-thz2016.org

OCTOBER

EuMW 2016
October 3–7, 2016 • London, UK
www.eumweek.com

ICUWB 2016
October 16–19, 2016 • Nanjing, China
http://icuwb2016.njupt.edu.cn

Phased Array 2016
October 18–21, 2016 • Waltham, Mass.
www.array2016.org

IME/China 2016
October 19–21, 2016 • Shanghai, China
www.imwexpo.com/siteengine.php?do=en/index

IEEE CSICS 2016
October 23–26, 2016 • Austin, Texas
www.csics.org

AMTA 2016
October 30–November 4, 2016 • Austin, Texas
www.amta2016.org

NOVEMBER

MILCOM 2016
November 1–3, 2016 • Baltimore, Md.
www.milcom.org

ITC/USA
November 7–10, 2016 • Glendale, Ariz.
www.telemetry.org

DECEMBER

IEEE International Electron Devices Meeting
December 3–7, 2016 • San Francisco, Calif.
www.ieee-iedm.org

APMC 2016
December 5–9, 2016 • New Delhi, India
www.apmc2016.org

88th ARFTG Microwave Measurement Conference
December 6–9, 2016 • Austin, Texas
www.arftg.org

JANUARY

RWW2017
January 15–18, 2017 • Phoenix, Ariz.
www.radiowirelessweek.org

DesignCon 2017
January 31–February 2, 2017 • Santa Clara, Calif.
www.designcon.com

COVER FEATURE
INVITED PAPER

Get Your GaN Here: RF GaN Foundry Survey

Patrick Hindle, Gary Lerude and Richard Mumford
Microwave Journal

The GaN market seems poised to take off this year as it becomes mainstream and starts penetrating some of the higher volume commercial markets. It has taken a strong foothold in most high power military applications and captured some of the cable TV and cellular infrastructure markets, but LDMOS still has the largest market share in the infrastructure and industrial markets. That might change soon, as GaN has as good or better performance than LDMOS and is now addressing the cost issue that seems to be the only advantage favoring LDMOS in most applications. Recent announcements by Qorvo, to move to 6 inch GaN on SiC, and MACOM, to prove 8 inch GaN on Si processed on low cost CMOS lines, will greatly reduce the cost of GaN, probably making it competitive with LDMOS. GaN also competes with GaAs in many of the higher frequency power markets and has displaced it in most of the future military applications where power is the most important performance specification.

If you do not have access to RF GaN device manufacturing within your company, you need to find a reliable GaN foundry service. While there are many RF GaN wafer fabrication facilities around the world, many of them are captive and not available to design companies that need their products manufactured. There does not seem to be much information generally available about RF GaN foundry services, so *Microwave Journal* surveyed as many of the GaN foundry services as we could identify and have summarized our findings.

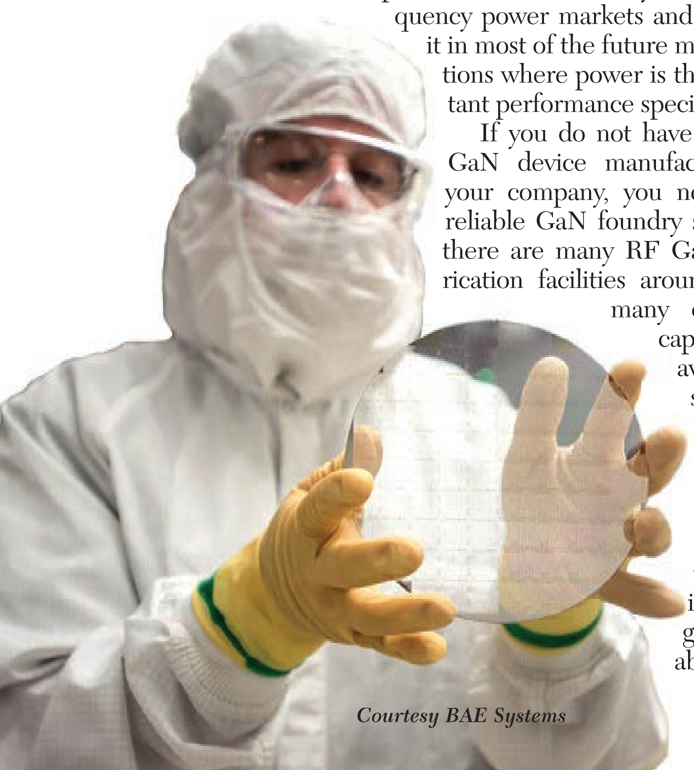

Courtesy BAE Systems

GENERAL LANDSCAPE

There are several GaN foundries in North America (including one in Canada), a couple in Europe, and Taiwan's WIN Semiconductors is the largest non-captive compound semiconductor foundry. Although the Japanese have a large market share in RF GaN, we did not find any Japanese companies offering foundry services, including Sumitomo, one of the largest GaN producers. China has been buying and launching semiconductor companies at a fast rate to build a presence in both the analog and digital markets. Chengdu HiWafer Semiconductor Co. and Xiamen San'an Integrated Circuit Co. offer compound semiconductor foundry services, and both state they have 6 inch GaN processes released or under development. We were not able to obtain detailed information about their capabilities in time for this article.

In the U.S., a majority of customers use Wolfspeed (a Cree Company), while many European companies, especially in the aerospace and defense market, use United Monolithic Semiconductors (UMS) or OMMIC. Several companies have strategic relationships with specific foundries, with proprietary processes that are not available to other companies. An example is GCS, based in Torrance, Calif., who declined to provide process information for this survey, since their engagements are typically ITAR controlled or proprietary; they do partner with some companies to provide RF GaN foundry services. There are several captive RF GaN foundries, such as Raytheon, MACOM and Qorvo. As separate companies, RFMD and TriQuint offered GaN foundry services;

since merging to become Qorvo, they only work with "strategic" customers, from the feedback we received.

SUBSTRATES

Most RF GaN devices are produced on SiC substrates, which offer a good lattice match and provide the high thermal conductivity that GaN demands—since its power density is very high compared to other semiconductor materials. Getting the heat out of the device is a huge challenge, so substrate and package materials are both critical. One company bucking that trend is MACOM, as they have the IP rights to International Rectifier's original patents for GaN on Si (which MACOM acquired with Nitronex). Si substrates are much lower in cost than SiC but have lower thermal conductivity than SiC. The lower thermal conductivity arguably puts Si at a disadvantage compared to SiC. However, MACOM has published data showing with appropriate design, GaN on Si performs as reliably as GaN on SiC in many applications.[1] GaN on Si could have the advantage of being processed on larger wafers on standard, low cost CMOS production lines. MACOM, however, does not offer foundry services; while they partner with GCS to produce GaN on Si devices, it is a proprietary process not available to other companies. We did find that OMMIC offers a GaN on Si process as a foundry service. OMMIC is the only company other than MACOM that we found offering RF GaN on Si devices.

All of the foundries surveyed process on 3 or 4 inch GaN wafers, but many plan to migrate to 6 inch as demand increases. Several have already announced plans to convert to 6 inch within the next year or two. BAE Systems estimates that converting from 4 to 6 inch GaN wafers (see ***Figure 1***) will reduce the cost from ~$3/mm^2 to ~$1.50/mm^2, as the usable area about doubles.

FOUNDRY PROCESS OVERVIEW

In general, most foundries offer two or three standard processes: a 0.5 µm, high voltage (40 to 50 V) process aimed at high power devices for frequencies below approximately 8 GHz and a 0.25 µm, medium voltage (28 to 30 V) process for higher frequency applications (up to approximately 18 GHz). Some offer a third option, an even smaller gate length (typically, about 0.15 µm) for millimeter wave applications (up to 100 GHz). See ***Table 1*** for a full listing of the processes offered by the seven companies that responded to our RF GaN foundry services survey.

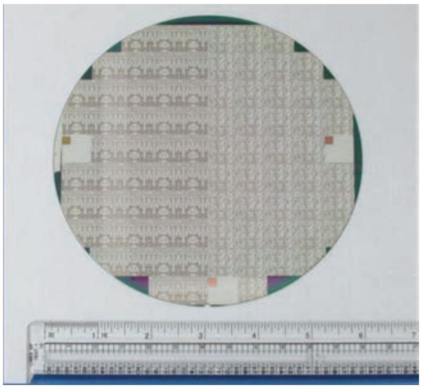

▲ *Fig. 1 6 inch GaN on SiC wafer (courtesy BAE Systems).*

Maximum power densities ranged from 6 to 8 W/mm, with Wolfspeed reporting a high of 8 W/mm for their 50 V, 0.4 µm G50V3 process. Other high power density processes of 6 W/mm or greater are available from BAE Systems, Fraunhofer, National Research Council of Canada, WIN Semiconductors and Wolfspeed. The highest operating frequency processes were Fraunhofer's GaN10, with 0.1 µm devices operating to 94 GHz, and OMMIC's D006GH (in development), with a 60 nm device operating to 100 GHz. Several foundries have efficiency exceeding 60 percent, including BAE, Fraunhofer, Wolfspeed, UMS and WIN. Most of the processes have field plates or offer them as an option. All of the foundries surveyed are using either 3 or 4 inch wafers, and a couple plan to move to 6 inch wafers relatively soon.

BAE Systems (Nashua, N.H.)

BAE Systems acquired the Lockheed Martin Sanders facilities in 2000. Their GaN processes are based on SiC substrates for best thermal properties, since they are geared to high performance military applications (with selected dual-use commercial markets when their process and/or design expertise are a good fit). This approach for military applications was first baselined by DARPA in 2005 under the Wide Bandgap Semiconductor-RF Program. Current wafer size is 4 inch. In 2014, they demonstrated high yield processing of MMIC power amplifiers (PA)

TABLE 1

GaN FOUNDRY PROCESSES

Company and Process	Gate Length (µm)	Bias (V)	BVdg (V)	Density (W/mm)	Max Frequency (GHz)	Efficiency	Field Plate	Wafer Size	Substrate
BAE Systems									
0.2 µm FP	0.2	40	>100	6	40 (Ft)	60% at 10 GHz	Yes	4	SiC
0.18 µm NFP	0.18	30	140 typ	3	57 (Ft)	45% at 30 GHz	No	4	SiC
Fraunhofer									
GaN50	0.5	50	150	6	6	65% at 3 GHz	Yes	4	SiC
GaN25	0.25	28	100	5	20	55% at 10 GHz	Yes	4	SiC
GaN10	0.1	15	30	2	94	40% at 30 GHz	No	4	SiC
National Research Council									
GaN500v3	0.5	40	180	5	13 (Ft)	N/A	Yes	3	SiC
GaN150v1	0.15	30	120	7	35 (Ft)	33% at 18 GHz	Optional	3	SiC
E-GaN (Under Development)	0.15	30	180	N/A	20 (Ft)	N/A	Optional	3	SiC
OMMIC									
D01GH	0.1	25 V (12 V typ)	40	3.5	50/110 (Ft)	48% at 40 GHz	No	3	Si, SiC
D006GH (Under Development)	0.06	20 V (8 V typ)	25	1	100/170 (Ft)	N/A	No	3	SiC
United Monolithic Semiconductors									
GH50	0.5	50	>200	>5	7	>65% at 2 GHz	Yes	4	SiC
GH25	0.25	30	>100	>4	20	50% at 10 GHz	Yes	4	SiC
WIN Semiconductors									
NP45	0.45	50	>160	>6.5	12 (Ft)	60 to 75% at 2.7 GHz	Yes	4	SiC
NP25	0.25	28	120	4.2	25 (Ft)	50% at 6 GHz	Yes	4	SiC
Wolfspeed (Cree)									
G50V3 MMIC	0.4	50	>150	8	6	65%	Yes	4	SiC
G28V3 MMIC	0.4	28	>120	4.5	8	65%	Yes	4	SiC
G284V4 MMIC	0.25	28	>120	4.5	18	65%	Yes	4	SiC
G40V4 MMIC	0.25	40	>120	6	18	65%	Yes	4	SiC

on 6 inch wafers, using their field plate (FP) GaN process[2] and are planning production release of a "no field plate" (NFP) process on 6 inch wafers in 2017.

BAE's 0.2 µm field plate process, originally developed in the 2005 to 2008 timeframe, is now an industry standard process, with performance that is widely available in the market. Their newer NFP process offers high performance at an affordable cost. This includes high power, gain and efficiency up to 50 GHz. Using 2 mil thick wafers, small vias can be placed under every source for low inductance grounding. This, combined with reduced output capacitance (C_{ds}) devices, enables wideband amplifiers with enhanced gain and power-added efficiency (PAE).[3] The 140 V typical BV_{gd} of the NFP process provides a high degree of robustness to high instantaneous voltages in PA designs, as well as high P_{in} survivability for low noise amplifiers (LNA). The 6 inch NFP GaN process will offer lower cost and leverage BAE Systems' experience running 6 inch PHEMT processes for more than 10 years.[4]

Fraunhofer IAF (Freiburg, Germany)

Fraunhofer offers high performance processes with high efficiency. The company manufactures products for research, base stations, electronic warfare, point-to-point radio links and radar. Based on 4 inch GaN on SiC wafers, Fraunhofer offers three processes providing DC to 100 GHz coverage: 1) 0.5 µm gate length, 50 V operating voltage and a frequency range up to 6 GHz; 2) 0.25 µm, 28 V, to 20 GHz and 3) 0.1 µm, 15 V, to 94 GHz. The 0.5 µm process provides an efficiency of 65 percent with a power density of 6 W/mm. The 0.5 and 0.25 µm processes are fabricated on 4 mil thick wafers with 50 µm vias, while the 0.1 µm process is on 3 mil thick wafers with 30 µm vias. Fraunhofer allows foundry access every 4 months using pizza masks, with nearly arbitrary chip sizes in small quantities. Overall, they have good breath of frequency coverage with three gates lengths and provide high efficiency.

National Research Council of Canada (Ottawa, Canada)

We were surprised that the Canadian government, through the National Research Council (NRC), offers a full line of GaN foundry processes and is the only Canadian source for GaN electronics. Intended to aid Canadian industry and technology — but

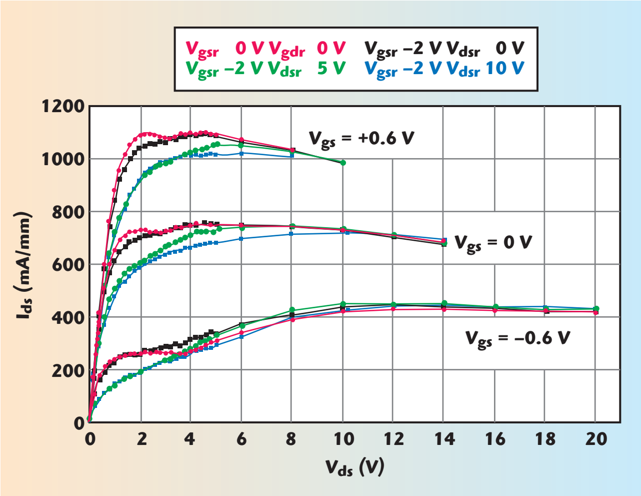

▲ *Fig. 2 Pulsed I-V measurement on 2 × 20 µm cell, showing less than 10 percent gate lag on OMMIC's D01GH GaN on Si process.*

not restricted to working only within Canada's borders — NRC serves both academic and commercial markets, leveraging its significant processing know-how. They offer one 0.5 µm and two 0.15 µm processes, operating up to 35 GHz, including probably the only enhancement mode process available on the market. The 0.15 µm depletion mode process has a power density of 7 W/mm, and the 0.5 µm process has a high breakdown of 180 V.

OMMIC (Limeil-Brévannes, France)

OMMIC offers foundry services and custom designs using its D01GH GaN on Si process that offers cost advantages over GaN on SiC. The process has a 0.1 µm gate length and runs on 3 inch wafers, planned to move to 6 inch in 2017. While this process was developed for power applications and provides 3.3 W/mm power density, it is also good for LNAs from 15 to 50 GHz, achieving a 1 dB noise figure at 30 GHz. Due to their ohmic contact regrowth process, D01GH devices exhibit very low noise performance, equivalent to state-of-the-art GaAs processes. In-situ passivation limits gate lag effects to less than 10 percent (see ***Figure 2***), enabling better performance in switched mode applications such as radar. Their lower bias, 30 V breakdown devices, can be biased around 12 V V_{DD} for PAs, with LNAs operating around 5 V. This is lower than other processes on the market, which mainly operate at 28 V.

OMMIC's D006GH is a GaN on SiC process with 60 nm gate length. Still in development, the process will be released for foundry access in the first quarter of 2017. It is intended to support power and low noise applications from 40 to 100 GHz.

OMMIC's development efforts are focused on PAs for Ka-Band satellite communications and X- and Ku-Band LNAs for military applications. In the next three years, they plan to focus on commercial markets, such as 5G base stations requiring Ka- and W-Band transmit/receive chips and instrumentation requiring DC to 67 GHz coverage and 32 dBm output power at 1 dB compression.

United Monolithic Semiconductors (Yvette, France)

Serving military, space and commercial (primarily telecom infrastructure and automotive) markets, UMS has developed and qualified two GaN on SiC processes. The 0.5 µm GH5010 process is suitable for power amplifiers operating up to C-Band and provides 5 W/mm with 50 V bias. The process is already listed in the European Space Agency (ESA) European Preferred Parts List (EPPL). The 0.25 µm GH25 MMIC process provides more than 4 W/mm with high efficiency up to Ku-Band (see ***Figure 3***). Typical operating voltage is 30 V. This process also has good noise performance, typically 1.8 dB noise figure at 15 GHz with 11 dB associated gain. More than 60 GH25 foundry projects have already been launched.

To address higher frequency applications, to K- and Ka-Bands, UMS is de-

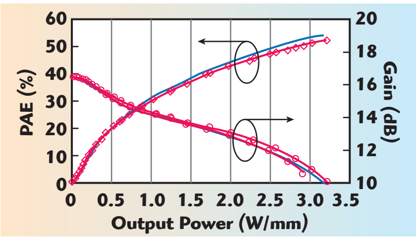

▲ *Fig. 3 4 GHz PAE and gain vs. power density for 8 × 100 µm cell on UMS' GH25 GaN on SiC process.*


38GHz
60GHz
24GHz
79GHz

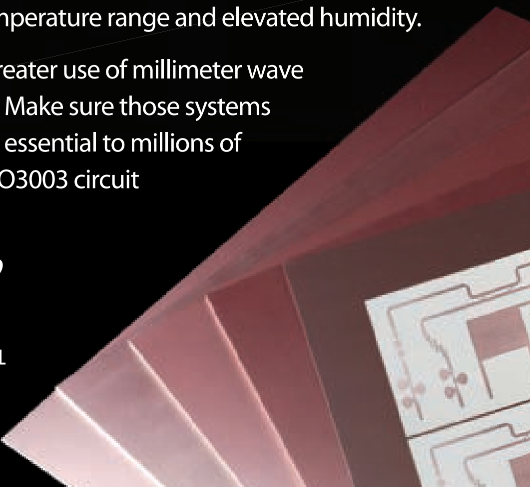

veloping a 0.15 µm process. UMS cites their EPPL listing as an indication that their process technology is high quality and reliable. They have a close link between their foundry technologies and UMS products, which ensures that the processes and models align with the needs of designers, are kept up to date and continuously improved. They offer express lots for short cycle time.

WIN Semiconductors (Tao Yuan City, Taiwan)

WIN Semiconductors, the largest compound semiconductor foundry, offers two GaN processes. As a pure-play foundry, WIN provides this technology via a non-competitive business model that insulates customers from potential conflict and supply chain risk. WIN's GaN processes leverage their extensive GaAs production capabilities, and they support both discrete transistors as well as MMICs. They also offer a 28 V, high power, passive device process on 6 inch GaAs wafers and provide high Q passive networks for cost effective hybrid GaN products.

WIN's primary commercial market for GaN technology is PAs used in wireless infrastructure. For military applications, their technology addresses PAs and LNAs used in radar systems. WIN presently offers two GaN HEMT technologies: NP25 and NP45. Both are fabricated on 4 inch SiC substrates. NP25 has a 0.25 µm gate with a source-coupled field plate and operates at 28 V. Typical power performance is 4 W/mm, with greater than 50 percent efficiency measured on a 1.25 mm cell at 6 GHz, biased at 28 V and 100 mA/mm. Linear gain is 17 dB. At 15 GHz, the process provides greater than 12 dB linear gain and 4.2 W/mm, with greater than 40 percent efficiency. The NP45 process has a 0.45 µm gate with a source-coupled field plate and operates at 50 V. Typical device performance is greater than 16 dB linear gain with greater than 6.5 W/mm and 60 percent efficiency, measured on a 4 mm cell tuned for peak output power at 2.7 GHz and biased at 50 V. The same device tuned for maximum efficiency (also at 2.7 GHz and 50 V bias) achieves over 75 percent efficiency, with approximately 5 W/mm and greater than 17 dB gain. This was the highest efficiency reported.

Wolfspeed (Durham, N.C.)

Wolfspeed, a Cree Company, is one of the most widely used foundries, offering four processes, all on 4 inch wafers. They cater to many military and commercial applications, such as wireless infrastructure, radar (both commercial and military), ISM, LMR, satellite communications, avionics, data links, space and CATV. They have 0.4 µm gate length processes with 50 and 28 V operating voltage, with the higher voltage process having a power density of 8 W/mm and a breakdown voltage exceeding 150 V. This was the highest reported power density we found for a GaN process. For higher frequency applications, Wolfspeed offers 0.25 µm processes that operate with 40 and 28 V bias that cover up to 18 GHz. All of their processes have efficiencies of 65 percent, which is very competitive among those reported.

Wolfspeed recently announced that their discrete transistors and multi-stage GaN MMICs have exceeded 100 billion total hours of field operation, the largest known body of field data accumulated by any domestic GaN supplier. Sumitomo is probably the only other RF GaN supplier that might have accumulated this history of field operation. Wolfspeed has achieved Category 1A trusted-foundry status through certification from the Defense MicroElectronics Activity (DMEA). Additionally, they have been assessed by the U.S. Department of Defense (DoD) as being at Manufacturing Readiness Level 8 or higher.

RELIABILITY

Many of the military applications at BAE Systems impose challenging reliability requirements for their GaN MMICs. High baseplate temperatures and wideband CW operation result in high channel temperatures. All of their production GaN processes have been tested and qualified to ensure devices meet these demanding requirements. They perform accelerated life testing under RF drive at multiple temperatures, from which the activation energy is estimated and lifetime (MTTF) at actual operating temperatures calculated. The typical MTTF derived in this manner for BAE Systems' 0.18 µm NFP GaN process is 10^7 hr at 200°C channel temperature, at its maximum recommended operating voltage of 30 V.

Fraunhofer performs DC, HTRB and RF testing at 2 and 10 GHz for their GaN50 and GaN25 processes. For the GaN10 process, they just test at 10 GHz.

NRC reports that reliability measurements for the GaN150 process are in progress. MTTF measurements on a previous process (GaN800) yielded an MTTF of 2.5×10^7 hours at a channel temperature of 200°C.

OMMIC's preliminary reliability tests show no significant degradation after 2000 hours of DC life testing with a case temperature of 80°C, V_{ds} = 12 V and I_{ds} = 200 mA/mm, which equates to a channel temperature of 200°C. Other reliability tests are underway.

UMS qualifies their processes by performing storage, HTRB, HTOL and DC life tests, as well as RF step stress and RF life testing. This enables them to determine maximum ratings and guarantee at least 20 years reliability at 200°C junction temperature. These qualification tests are performed on elementary cells, typical of those used in discrete devices and MMICs with larger gate widths.

For reliability verification, WIN provides customers with a full qualification report that includes four temperature MTTF results.

Wolfspeed's processes have delivered more than 100 billion total hours of field operation with a FIT rate of less than 5 per billion device hours for discrete GaN RF transistors and multistage GaN MMICs. The company recently announced that their GaN RF power transistors completed testing and demonstrated compliance with NASA reliability standards for satellite and space systems. They partnered with KCB Solutions on a comprehensive testing program to demonstrate that their GaN on SiC devices meet NASA EEE-INST-002 Level 1 reliability and performance standards, derived from the MIL-STD requirements for Class S and Class K qualifications.

BACKEND SERVICES

BAE Systems offers on-wafer test and wafer dicing, chip picking and inspection. First-level packaging is also offered to some customers. For example, they can deliver die soldered onto CTE-matched shims or assembled in simple packages.

All Fraunhofer SiC processes include full backside processing, including via holes with metallization upon request. They perform extensive testing (DC, small signal and load-pull wafer mapping) as well as full MMIC testing. They provide fast packaging of power bars for high-power characterization.

NRC offers on-wafer testing but no mounting or packaging.

OMMIC offers on-wafer test services, visual inspection (commercial and space grade), lot acceptance testing (LAT) and wafer acceptance testing (WAT) for space programs. Every design can be packaged in either plastic QFN (with up to 30 GHz operation) or air cavity packages. They also offer hermetic packaging services for space applications.

UMS offers a wide and flexible range of back-end services, including on-wafer noise and power testing. They also offer visual inspection, picking and packaging.

WIN provides high voltage DC product testing, dicing and inspection services for GaN customers.

Wolfspeed provides dicing, on-wafer DC/RF probe and fixtured DC/RF characterization.

EDA SOFTWARE SUPPORT

BAE Systems offers design services on a case-by-case basis. They also provide design support to customers who wish to design their own MMICs. They have an internally-developed modified Angelov nonlinear model that is very accurate for nonlinear circuit simulation. They provide all necessary device models and layout information to foundry customers. ADS-compatible PDKs are under development and will be available in late 2016.

Fraunhofer has Keysight PDKs for microstrip and grounded coplanar transmission lines for ADS (ADS DRC included), including full auto-layout functions.

For the GaN500 process, NRC offers both Root and Angelov models in ADS. For GaN150, they only offer a Root model. No models are available for the 0.15 µm E-GaN process.

OMMIC PDKs are available on their website for the latest 32- and 64-bit versions of ADS and for the 32-bit version of NI/AWR Microwave Office. The 64-bit NI/AWR design kit is under development. For all design kits, they provide nonlinear models and noise models, all over temperature. They also provide a DRC and LVS checking service in house, if needed. They have a team of modeling engineers dedicated to customer support and offer a multi-project wafer (pizza mask) service with four runs a year per process, for small prototyping quantities.

UMS' GH25 PDKs are compatible with ADS and Microwave Office. They include nonlinear, electro-thermal scalable models for power generation, linear models for LNA design, cold FET models for switches and diodes and passive elements for MMIC designs. Their PDKs include additional features such as DRC and 3D view generation for EM simulation.

WIN design kits are available for ADS and NI/AWR platforms and contain internally developed and optimized nonlinear models, models for small-signal and noise and load-pull data. WIN offers 24-hour design rule checking using a web-based tool, WebDRC. Layout verification (LVS) is done through Cadence as well as the ADS and AWR platforms.

Wolfspeed offers PDKs with ADS and NI/AWR's Microwave Office.

MARKET OPPORTUNITIES

Similar to the path taken by GaAs devices, expect GaN to mature and become the technology of choice for a diverse range of applications, especially the high power markets. As the technology proliferates and its cost declines, GaN will provide the best value for many PA functions where it offers an optimum trade-off. As communication and military systems become more complex, device specifications for transmit power, efficiency, linearity, frequency/bandwidth and operating temperature will become more challenging and GaN will offer many advantages over GaAs and Si. For example, in military applications, it improves size, weight and power (SWaP), and will continue to make inroads in those systems.

Most GaN suppliers see the base station and satellite markets as areas for major growth in the near term,

with one foundry mentioning automotive. The millimeter wave portion of 5G could also be a large opportunity, as GaN performs well in broadband, high frequency applications. The RF Energy market is a good fit for GaN technology as well. Aerospace and defense markets that foundries see having the most growth include wideband, high power amplifiers for electronic warfare, phased arrays for radar and a wide range of millimeter wave applications.

GaN'S FUTURE

The main competition for GaN is LDMOS at RF frequencies and GaAs for higher frequencies. LDMOS still dominates the high volume commercial markets for high power applications. While GaN will not completely replace any one technology, it is bound to further penetrate these higher volume markets as it becomes more price competitive. LDMOS continues to improve its performance each year, so it will remain competitive in these markets, yet it is bound to yield significant market share in the future.

BAE Systems thinks that in the long term, GaN for microwave applications will flourish in the applications where it is best suited: predominantly high power at frequencies from 1 to 100 GHz. Nonetheless, it won't completely replace GaAs and Si, as these both have their own unique performance characteristics and associated economies that will ensure continued viability for certain markets. Further expansion of GaN will occur as high yield processes mature and wafer sizes increase, reducing costs. GaN clearly is a disruptive semiconductor technology, with no other semiconductor technology emerging to threaten it for at least the next decade.

Expect continued evolution of GaN variants such as GaN on Si for reduced cost and GaN on diamond for enhanced thermal properties for high performance applications. GaN will also be used more widely for functions other than PAs, such as LNAs, switches and multi-function MMICs. A combination LNA/limiter is well suited for GaN, with its combination of low noise performance and high breakdown voltage, the latter good for limiters.

The most interesting evolution will be the fight between GaN on SiC and GaN on Si. Will one technology win out in the industry? GaN on Si has the promise of being lower cost — offering larger wafer sizes and lower substrate and processing costs, if processed on standard CMOS production lines. If its performance is close to that of GaN on SiC, arguably, the cost advantage will be too great for SiC to overcome. On the other hand, SiC will have thermally-driven performance advantages that are required by some applications, ensuring a place for both technologies. ■

References

1. Doug Carlson, "Commercialization of GaN," *Microwave Journal*, June 2014, Vol. 57, No. 6, pp. 34–40.
2. Isaak et al., "The First 0.2 µm 6-Inch GaN-on-SiC MMIC Process," CS ManTech, 2014, pp. 229–231.
3. Komiak et al., "Decade Bandwidth 2 to 20 GHz GaN HEMT Power Amplifier MMICs in DFP and No FP Technology," IMS 2011.
4. Gunther et al., The First 0.1 µm 6-Inch GaAs PHEMT MMIC Process," CS ManTech, 2006, pp. 23–26.

UP TO **100 Watt**

AMPLIFIERS

NOW! 100 kHz to 26.5 GHz

from $995 ea. qty. (1-9)

High-powered performance across wide frequency ranges. Mini-Circuits' class A/AB linear amplifiers have set a standard for wideband high-power performance throughout the RF and microwave industry. Rugged and reliable, they feature over-voltage and over-temperature protections and can withstand opens and shorts at the output! Available with or without heat sinks, they're perfect for demanding test lab environments and for integrating directly into customer assemblies. With standard models covering frequencies from 100 kHz up to 26.5 GHz, chances are we have a solution for your needs in stock. Place your order on minicircuits.com today for delivery as soon as tomorrow! Need a custom model? Give us a call and talk to our engineers about your special requirements!

Model	Frequency (MHz)	Gain (dB)	Pout @ Comp. 1 dB (W)	Pout @ Comp. 3 dB (W)	$ Price* (Qty. 1-9)
NEW! ZVM-273HP+	13000-26500	14.5	0.5	0.5	2195
ZVE-3W-83+	2000-8000	35	2	3	1295
ZVE-3W-183+	5900-18000	35	2	3	1295
ZHL-4W-422+	500-4200	25	3	4	1160
ZHL-5W-422+	500-4200	25	3	5	1670
ZHL-5W-2G+	800-2000	45	5	5	995
ZHL-10W-2G+	800-2000	43	10	12	1295
• ZHL-16W-43+	1800-4000	45	12	16	1595
• ZHL-20W-13+	20-1000	50	13	20	1395
• ZHL-20W-13SW+	20-1000	50	13	20	1445
LZY-22+	0.1-200	43	16	30	1495
ZHL-30W-262+	2300-2550	50	20	32	1995
ZHL-30W-252+	700-2500	50	25	40	2995
LZY-2+	500-1000	47	32	38	2195
LZY-1+	20-512	42	50	50	1995
• ZHL-50W-52+	50-500	50	63	63	1395
• ZHL-100W-52+	50-500	50	63	79	1995
• ZHL-100W-GAN+	20-500	42	79	100	2395
ZHL-100W-13+	800-1000	50	79	100	2195
ZHL-100W-352+	3000-3500	50	100	100	3595
ZHL-100W-43+	3500-4000	50	100	100	3595

Listed performance data typical, see minicircuits.com for more details.

• Protected under U.S. Patent 7,348,854

**Price Includes Heatsink*

Mini-Circuits®

www.minicircuits.com P.O. Box 350166, Brooklyn, NY 11235-0003 (718) 934-4500 sales@minicircuits.com

MVP

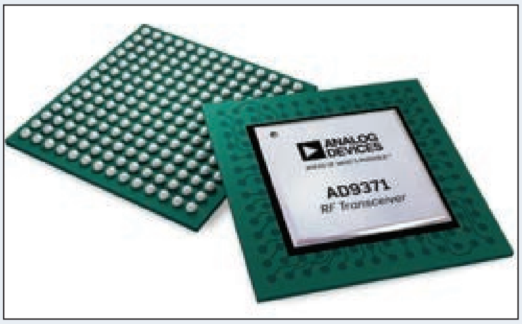

New Radio Ecosystem for a Changing Wireless World

Analog Devices Inc.
Norwood, Mass.

The nature of wireless communications is changing. The number of antennas is exploding in the never-ending search for improved spectral efficiency and range. Band proliferation in cellular wireless is increasing network capacity — but also interference. There is a boom in ISM-band applications and air interface standards. Even applications such as wireless video for drones need improved RF performance to tolerate increasing interference and avoid dreaded "fly aways." Wireless connectivity is taken for granted — it's expected to be everywhere, on all the time and on a very fast pace of evolution.

The traditional IF radio architecture is struggling to keep up. The number of discrete components and band-specific filters slows development time, and it's increasingly hard to find a workable frequency plan. These challenges require not only radio solutions with breakthrough versatility and performance but also an ecosystem of development tools to get products to market with the speed that today's world demands.

Based on innovative transceiver architectures and advanced digital algorithms, Analog Devices (ADI) is leveraging its silicon design and system expertise to shift focus to what matters most: reducing system cost while reducing the time to get a product to market. ADI's RadioVerse™ technology and design ecosystem provide customers with integrated transceiver technologies, a robust design environment and market-specific technical expertise to quickly move their radio designs from concept to creation.

The foundation of the RadioVerse technology and design ecosystem is zero IF (ZIF) transceiver technology with breakthrough performance. In a ZIF receiver, the desired RF signal — or band — is down-converted directly to baseband. Likewise, in the transmitter, the digital baseband signal is converted directly to RF. The advantages are profound:

- Band-specific IF filters on the PCB are eliminated. Instead, on-chip high dynamic range analog-to-digital converters (ADC) and digital filters, which benefit from Moore's Law, are optimally configured in software for each application.
- Clocking the ADCs, digital-to-analog converters (DAC) and digital at the lowest possible rate results in the lowest possible power dissipation.
- There are no out-of-band impairments such as images, N x M mixing products or aliases which increase RF filter rejection requirements.
- In addition to bandwidth agility, ZIF maximizes

RF agility, since most of the signal processing is at baseband.

For these reasons, ZIF is the dominant radio architecture in consumer applications, such as cellular handsets and Wi-Fi. ADI's transceivers bring this technology to applications requiring much wider bandwidth and dynamic range. Through heavy use of "digitally-assisted analog," in-band impairments such as images are suppressed by more than 70 dB.

The latest addition to ADI's wideband transceiver family is the AD9371. This wideband transceiver covers 300 MHz to 6 GHz with 100 MHz signal bandwidth. The AD9371 is a highly integrated, RF agile transceiver offering dual channel transmitters and receivers, a two input observation receiver for digital predistortion (DPD) and power control, integrated synthesizers and digital signal processing functions (see ***Figure 1***). The IC delivers a versatile combination of high performance and low power consumption and can operate in both half and full duplex non-contiguous multicarrier applications. Along with its predecessor, the AD9361 56 MHz RF transceiver, this family of products covers a wide range of applications, ranging from small cells, wireless pro audio and video, LTE macro base stations, portable signal analyzers and hand held and vehicle radios.

With the integration of the LO and high speed converter clocks, only a low frequency reference clock is needed, simplifying system clock generation and distribution. Monolithic integration enables the transceiver IC to be powered by few power rails: a typical configuration requires only three supplies (1.2 , 1.8 and 2.5 V). Eliminating additional power supplies decreases system cost and size and simplifies the PCB power plane decoupling design. The extremely low power consumption of the ADI transceivers eases thermal management, i.e., the

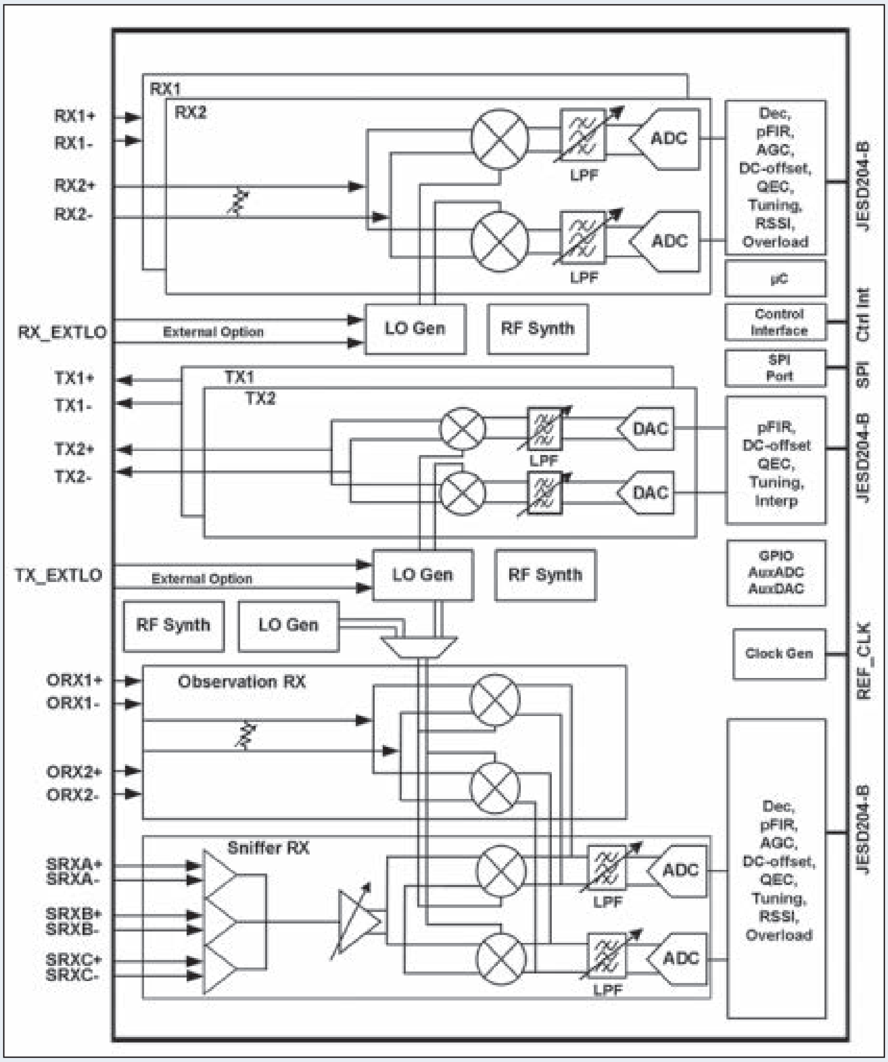

▲ *Fig. 1 Functional block diagram of the AD9371 transceiver.*

MostValuable**Product**

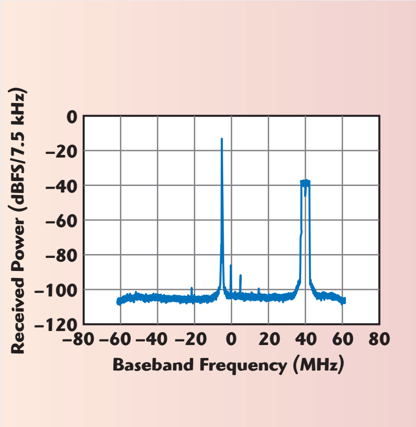

▲ *Fig. 2 Linearity of the receiver portion of the AD9371, showing the performance of quadrature error correction.*

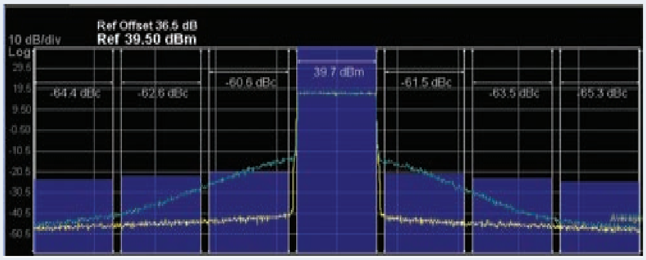

▲ *Fig. 3 Linearity of the AD9371 transmitter portion with a 2.6 GHz, 20 MHz LTE signal.*

need for heat sinking and other thermal management techniques — further reducing product size and development cost.

Figure 2 shows the performance of the AD9371 receiver with a -15 dB full scale (FS) CW input 5 MHz below the LO and a -10 dB FS (rms), 5 MHz wide LTE carrier that is 40 MHz above the LO, which is at 2.6 GHz. The advanced wideband quadrature error correction (QEC) algorithms simultaneously reject errors across the entire, wider bandwidth, resulting in nearly 80 dB rejection across temperature. ***Figure 3*** shows the linearity performance of the transmitter, which has better than 60 dBc adjacent channel rejection with a 2.6 GHz, 20 MHz LTE waveform with 40 dBm total carrier power. The AD9371 transmitter is followed by power amplifier that delivers the +40 dBm output; the chain is linearized using the transceiver's integrated observation receivers and a DPD algorithm.

ADI's RadioVerse technology and design ecosystem will enable faster time to market (see ***Figure 4***). A product like the AD9371 is necessarily complex, but ADI's application programming interface (API) simplifies software integration by replacing complicated sequences of register writes with single high level commands. RadioVerse includes evaluation kits, development graphical user interfaces (GUI), simulation models, reference designs, best-of-breed partnerships, technical content for specific applications and access to ADI's EngineerZone online technical community. The ecosystem is in place and growing, enabling engineers to harness the capabilities of ADI's transceiver technology.

VENDOR**VIEW**

Analog Devices Inc.
Norwood, Mass.
www.analog.com

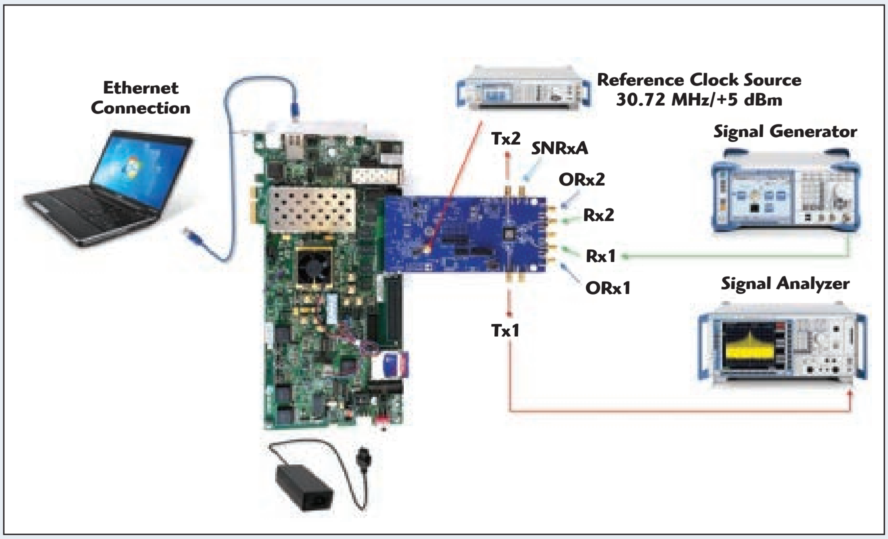

▲ *Fig. 4 The AD9371 can be used with ADI's evaluation software or custom code, including MATLAB and LabVIEW.*

RF Amplifiers and Sub-Assemblies for Every Application

Delivery from Stock to 2 Weeks ARO from the catalog or built to your specifications!

- Competitive Pricing & Fast Delivery
- Military Reliability & Qualification
- Various Options: Temperature Compensation, Input Limiter Protection, Detectors/TTL & More
- Unconditionally Stable (100% tested)

ISO 9001:2000 and AS9100B CERTIFIED

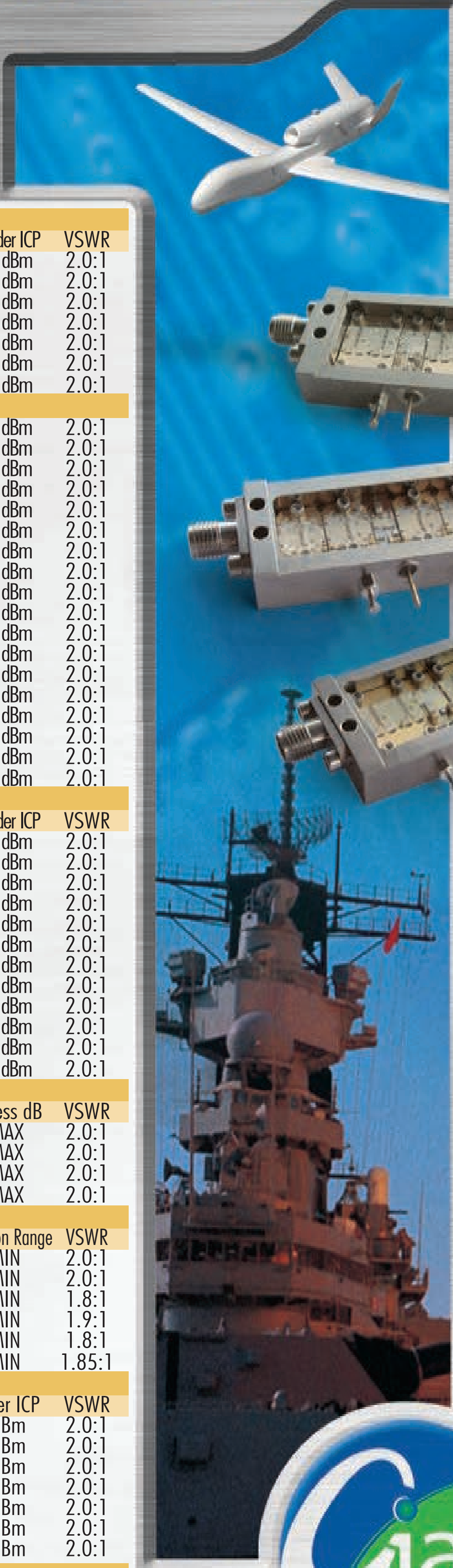

OCTAVE BAND LOW NOISE AMPLIFIERS

Model No.	Freq (GHz)	Gain (dB) MIN	Noise Figure (dB)	Power-out @ P1-dB	3rd Order ICP	VSWR
CA01-2110	0.5-1.0	28	1.0 MAX, 0.7 TYP	+10 MIN	+20 dBm	2.0:1
CA12-2110	1.0-2.0	30	1.0 MAX, 0.7 TYP	+10 MIN	+20 dBm	2.0:1
CA24-2111	2.0-4.0	29	1.1 MAX, 0.95 TYP	+10 MIN	+20 dBm	2.0:1
CA48-2111	4.0-8.0	29	1.3 MAX, 1.0 TYP	+10 MIN	+20 dBm	2.0:1
CA812-3111	8.0-12.0	27	1.6 MAX, 1.4 TYP	+10 MIN	+20 dBm	2.0:1
CA1218-4111	12.0-18.0	25	1.9 MAX, 1.7 TYP	+10 MIN	+20 dBm	2.0:1
CA1826-2110	18.0-26.5	32	3.0 MAX, 2.5 TYP	+10 MIN	+20 dBm	2.0:1

NARROW BAND LOW NOISE AND MEDIUM POWER AMPLIFIERS

Model No.	Freq (GHz)	Gain (dB) MIN	Noise Figure (dB)	Power-out @ P1-dB	3rd Order ICP	VSWR
CA01-2111	0.4 - 0.5	28	0.6 MAX, 0.4 TYP	+10 MIN	+20 dBm	2.0:1
CA01-2113	0.8 - 1.0	28	0.6 MAX, 0.4 TYP	+10 MIN	+20 dBm	2.0:1
CA12-3117	1.2 - 1.6	25	0.6 MAX, 0.4 TYP	+10 MIN	+20 dBm	2.0:1
CA23-3111	2.2 - 2.4	30	0.6 MAX, 0.45 TYP	+10 MIN	+20 dBm	2.0:1
CA23-3116	2.7 - 2.9	29	0.7 MAX, 0.5 TYP	+10 MIN	+20 dBm	2.0:1
CA34-2110	3.7 - 4.2	28	1.0 MAX, 0.5 TYP	+10 MIN	+20 dBm	2.0:1
CA56-3110	5.4 - 5.9	40	1.0 MAX, 0.5 TYP	+10 MIN	+20 dBm	2.0:1
CA78-4110	7.25 - 7.75	32	1.2 MAX, 1.0 TYP	+10 MIN	+20 dBm	2.0:1
CA910-3110	9.0 - 10.6	25	1.4 MAX, 1.2 TYP	+10 MIN	+20 dBm	2.0:1
CA1315-3110	13.75 - 15.4	25	1.6 MAX, 1.4 TYP	+10 MIN	+20 dBm	2.0:1
CA12-3114	1.35 - 1.85	30	4.0 MAX, 3.0 TYP	+33 MIN	+41 dBm	2.0:1
CA34-6116	3.1 - 3.5	40	4.5 MAX, 3.5 TYP	+35 MIN	+43 dBm	2.0:1
CA56-5114	5.9 - 6.4	30	5.0 MAX, 4.0 TYP	+30 MIN	+40 dBm	2.0:1
CA812-6115	8.0 - 12.0	30	4.5 MAX, 3.5 TYP	+30 MIN	+40 dBm	2.0:1
CA812-6116	8.0 - 12.0	30	5.0 MAX, 4.0 TYP	+33 MIN	+41 dBm	2.0:1
CA1213-7110	12.2 - 13.25	28	6.0 MAX, 5.5 TYP	+33 MIN	+42 dBm	2.0:1
CA1415-7110	14.0 - 15.0	30	5.0 MAX, 4.0 TYP	+30 MIN	+40 dBm	2.0:1
CA1722-4110	17.0 - 22.0	25	3.5 MAX, 2.8 TYP	+21 MIN	+31 dBm	2.0:1

ULTRA-BROADBAND & MULTI-OCTAVE BAND AMPLIFIERS

Model No.	Freq (GHz)	Gain (dB) MIN	Noise Figure (dB)	Power-out @ P1-dB	3rd Order ICP	VSWR
CA0102-3111	0.1-2.0	28	1.6 Max, 1.2 TYP	+10 MIN	+20 dBm	2.0:1
CA0106-3111	0.1-6.0	28	1.9 Max, 1.5 TYP	+10 MIN	+20 dBm	2.0:1
CA0108-3110	0.1-8.0	26	2.2 Max, 1.8 TYP	+10 MIN	+20 dBm	2.0:1
CA0108-4112	0.1-8.0	32	3.0 MAX, 1.8 TYP	+22 MIN	+32 dBm	2.0:1
CA02-3112	0.5-2.0	36	4.5 MAX, 2.5 TYP	+30 MIN	+40 dBm	2.0:1
CA26-3110	2.0-6.0	26	2.0 MAX, 1.5 TYP	+10 MIN	+20 dBm	2.0:1
CA26-4114	2.0-6.0	22	5.0 MAX, 3.5 TYP	+30 MIN	+40 dBm	2.0:1
CA618-4112	6.0-18.0	25	5.0 MAX, 3.5 TYP	+23 MIN	+33 dBm	2.0:1
CA618-6114	6.0-18.0	35	5.0 MAX, 3.5 TYP	+30 MIN	+40 dBm	2.0:1
CA218-4116	2.0-18.0	30	3.5 MAX, 2.8 TYP	+10 MIN	+20 dBm	2.0:1
CA218-4110	2.0-18.0	30	5.0 MAX, 3.5 TYP	+20 MIN	+30 dBm	2.0:1
CA218-4112	2.0-18.0	29	5.0 MAX, 3.5 TYP	+24 MIN	+34 dBm	2.0:1

LIMITING AMPLIFIERS

Model No.	Freq (GHz)	Input Dynamic Range	Output Power Range Psat	Power Flatness dB	VSWR
CLA24-4001	2.0 - 4.0	-28 to +10 dBm	+7 to +11 dBm	+/- 1.5 MAX	2.0:1
CLA26-8001	2.0 - 6.0	-50 to +20 dBm	+14 to +18 dBm	+/- 1.5 MAX	2.0:1
CLA712-5001	7.0 - 12.4	-21 to +10 dBm	+14 to +19 dBm	+/- 1.5 MAX	2.0:1
CLA618-1201	6.0 - 18.0	-50 to +20 dBm	+14 to +19 dBm	+/- 1.5 MAX	2.0:1

AMPLIFIERS WITH INTEGRATED GAIN ATTENUATION

Model No.	Freq (GHz)	Gain (dB) MIN	Noise Figure (dB)	Power-out @ P1-dB	Gain Attenuation Range	VSWR
CA001-2511A	0.025-0.150	21	5.0 MAX, 3.5 TYP	+12 MIN	30 dB MIN	2.0:1
CA05-3110A	0.5-5.5	23	2.5 MAX, 1.5 TYP	+18 MIN	20 dB MIN	2.0:1
CA56-3110A	5.85-6.425	28	2.5 MAX, 1.5 TYP	+16 MIN	22 dB MIN	1.8:1
CA612-4110A	6.0-12.0	24	2.5 MAX, 1.5 TYP	+12 MIN	15 dB MIN	1.9:1
CA1315-4110A	13.75-15.4	25	2.2 MAX, 1.6 TYP	+16 MIN	20 dB MIN	1.8:1
CA1518-4110A	15.0-18.0	30	3.0 MAX, 2.0 TYP	+18 MIN	20 dB MIN	1.85:1

LOW FREQUENCY AMPLIFIERS

Model No.	Freq (GHz)	Gain (dB) MIN	Noise Figure dB	Power-out @ P1-dB	3rd Order ICP	VSWR
CA001-2110	0.01-0.10	18	4.0 MAX, 2.2 TYP	+10 MIN	+20 dBm	2.0:1
CA001-2211	0.04-0.15	24	3.5 MAX, 2.2 TYP	+13 MIN	+23 dBm	2.0:1
CA001-2215	0.04-0.15	23	4.0 MAX, 2.2 TYP	+23 MIN	+33 dBm	2.0:1
CA001-3113	0.01-1.0	28	4.0 MAX, 2.8 TYP	+17 MIN	+27 dBm	2.0:1
CA002-3114	0.01-2.0	27	4.0 MAX, 2.8 TYP	+20 MIN	+30 dBm	2.0:1
CA003-3116	0.01-3.0	18	4.0 MAX, 2.8 TYP	+25 MIN	+35 dBm	2.0:1
CA004-3112	0.01-4.0	32	4.0 MAX, 2.8 TYP	+15 MIN	+25 dBm	2.0:1

CIAO Wireless can easily modify any of its standard models to meet your "exact" requirements at the Catalog Pricing.

Visit our web site at **www.ciaowireless.com** for our complete product offering.

Ciao wireless

Ciao Wireless, Inc. 4000 Via Pescador, Camarillo, CA 93012

Tel (805) 389-3224 Fax (805) 389-3629 sales@ciaowireless.com

Successful Flight Test for Ground-Breaking Integrated Battle Command System (IBCS)

VIEW VIDEO

U.S. Army soldiers have executed a successful dual engagement flight test of the Northrop Grumman Corp.-developed Integrated Air and Missile Defense (IAMD) Battle Command System (IBCS) to identify, track, engage and defeat ballistic and cruise missile targets.

Building upon previous successful flight tests, the April 8 event validated the ability of IBCS to manage multiple threats. The test included joint sensors providing data to the IBCS engagement operations center to augment Army sensor data for a single integrated air picture, and the IBCS selecting from different missile types to defeat multiple threats arriving at the same time.

"This IBCS test demonstrated the benefit of giving warfighters expanded combinations of radars and weapon systems to achieve any-sensor, best-shooter capability," said Dan Verwiel, vice president and general manager, missile defense and protective systems division, Northrop Grumman Mission Systems. "Together with the Army, we look forward to realizing the advances offered by the IBCS open architecture, including taking advantage of sensors that look in all directions to facilitate 360-degree protection for air and missile defense missions."

> IBCS enables integration of current and future sensors and weapon systems and interoperability with joint C2 and the ballistic missile defense system.

The IBCS utilized sensors and interceptors from different air defense systems connected at the component level to operate on the IBCS integrated fire control network. Using tracking data from Sentinel and Patriot radars, the IBCS provided the command-and-control (C2) for a Patriot Advanced Capability Three (PAC-3) interceptor to destroy a ballistic missile target and a PAC-2 interceptor to destroy a cruise missile target.

Additionally, the IBCS flight test architecture included the Marine Corps Tactical Air Operations Module for joint C2 situational awareness. Air defenders from Fort Bliss, Texas, conducted all IBCS operations as part of the Limited User Test system evaluation ahead of a Milestone C decision later this year.

IBCS replaces seven legacy C2 systems to deliver a single integrated air picture and offer the flexibility to deploy smaller force packages. By networking sensors and interceptors, IBCS provides wider area surveillance and broader protection areas. With its truly open systems architecture, IBCS enables integration of current and future sensors and weapon systems and interoperability with joint C2 and the ballistic missile defense system.

GXV-T Revs up Research into Nimbler, Faster, Smarter Armored Ground Vehicles

Today's ground-based armored fighting vehicles are better protected than ever, but face a constantly evolving threat: weapons increasingly effective at piercing armor. While adding more armor has provided incremental increases in protection, it has also hobbled vehicle speed and mobility and ballooned development and deployment costs. To help reverse this trend, DARPA's Ground X-Vehicle Technology (GXV-T) program recently awarded contracts to eight organizations.

"We're exploring a variety of potentially groundbreaking technologies, all of which are designed to improve vehicle mobility, vehicle survivability and crew safety and performance without piling on armor," said Maj. Christopher Orlowski, DARPA program manager. "DARPA's performers for GXV-T are helping defy the 'more armor equals better protection' axiom that has constrained armored ground vehicle design for the past 100 years, and are paving the way toward innovative, disruptive vehicles for the 21st century and beyond."

DARPA has awarded contracts for GXV-T to Carnegie Mellon University (Pittsburgh, Pa.), Honeywell International Inc. (Phoenix, Ariz.), Leidos (San Diego, Calif.), Pratt & Miller (New Hudson, Mich.), QinetiQ Inc. (QinetiQ UK, Farnborough, UK), Raytheon BBN (Cambridge, Mass.), Southwest Research Institute (San Antonio, Texas) and SRI International (Menlo Park, Calif.).

GXV-T is pursuing research in the following four technical areas:

- Radically Enhanced Mobility—Ability to traverse diverse off-road terrain, including slopes and various elevations.
- Survivability through Agility—Autonomously avoid incoming threats without harming occupants through technologies that enable, for example, agile motion and active repositioning of armor.
- Crew Augmentation—Improved physical and electronically assisted situational awareness for crew and passengers; semi-autonomous driver assistance and automation of key crew functions similar to capabilities found in modern commercial airplane cockpits.
- Signature Management—Reduction of detectable signatures, including visible, infrared (IR), acoustic and electromagnetic (EM).

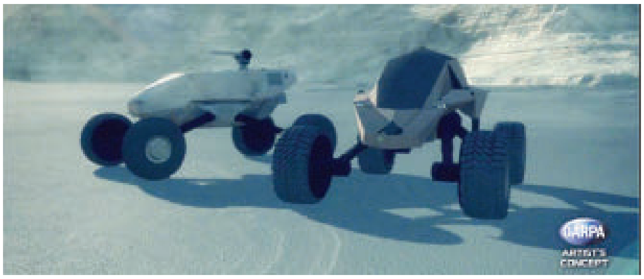

DARPA Image

For More Information Visit mwjournal.com for more defense news

Miniaturized Circulator Opens Way to Doubling Wireless Capacity

A DARPA-funded team has drastically miniaturized highly specialized electronic components called circulators and for the first time integrated them into standard silicon-based circuitry. The feat could lead to a doubling of RF capacity for wireless communications—meaning even faster web-searching and downloads—as well as the development of smaller, less expensive and more readily upgraded antenna arrays for radar, signals intelligence and other applications.

The defining feature of circulators is that RF signals, in the form of electronic waves in the circuitry, travel only in a forward direction with reverse propagation forbidden by the physics of the circuit. That's what you need for minimizing on-chip interference and for keeping signals separated. Most materials can't play this role because RF traffic can flow both ways through them; these materials exhibit what engineers refer to as reciprocal behavior. Nonreciprocal components like the new circulator, on the other hand, act like one-way highways for RF signals. Traditionally, circulators have relied on external, ferrite-based magnets to force RF signals into a one-way course through downstream circuitry. Those magnets and ferrite materials have rendered the circulators bulky, expensive, and incompatible with the workhorse microcircuit technology, known by insiders as complementary metal oxide semiconductor, or CMOS.

The Columbia researchers' design achieves the one-way RF flow with a series of capacitors coordinated with a minuscule and precise clock, electronically emulating the direction-dictating magnetic "twist" that in conventional ferrite circulators is imposed on RF signals by an external magnetic field. That novel design makes possible an unprecedented microelectronic assemblage: A receiver connected to one "on-ramp" (or port) of the new circulator structure; a transmitter connected to another port of that same circulator; and an antenna shared by those two tiny devices, itself coupled to the circulator via a third port situated between the other two. Since the RF propagation is one way (non-reciprocal) in the circulator, the transmitted and received signals smoothly traverse their respective paths without getting mixed up with one another.

That clean segregation of received and transmitted signals opens a powerful new capability. In most two-way RF systems, transmission and reception at a given frequency must be staggered in time with a switching process, slowing communication speeds. The way around this bottleneck has been to transmit and receive at two different frequencies, which requires twice as much spectrum—a limited resource. The new pinky-nail-sized circulator opens the door to communications and radar systems operating in full duplex mode—transmitting and receiving at the same frequency at the same time with a single shared antenna.

The 2016 Defence, Security and Space Forum

At European Microwave Week

EuMA

Microwave Journal
Frequency Matters.

Wednesday, 5 October – ExCel, London – Rooms 8 to 11

A focused Forum addressing the application of RF and microwave technology to Complex Urban Environments.

The emphasis will be on complex urban environments, encompassing the challenges and opportunities for indoor/enclosed and urban communications and sensing technologies. The Forum has the scope to cover topics including: Smart City initiatives; 3D tracking technologies in complex and indoor environments; sensing complex targets in dense target environments; congested spectrum and network issues.

Programme:

09:00 – 10:40 EuRAD Opening Session

11:20 – 13:00 Complex Urban Sensing and Communication

Speakers from industry and academia will present RF solutions and systems that address the challenges imposed by operation in complex urban environments. Confirmed speakers include:

- New Transceiver Technology Applied to Standoff Submillimetre-Wave Imaging Radar – *Ken Cooper, JPL*
- Indoor and Urban Environment Location of Moving People and Vehicles Using Signals of Opportunity – *Pierfrancesco Lombardo, University of Rome*
- Communication Satellite Impact on TV and Data Broadcasting Through Urban Environments – *Erdem Demircioğlu, Turksat International*

© Shmuel Auster

13:10 – 14:10 Strategy Analytics Lunch & Learn Session

This session will add a further dimension by offering a market analysis perspective, illustrating the status, development and potential of the market.

14:20 – 16:00 *Microwave Journal* Industry Panel Session

The session offers an industrial perspective on the key issues facing the defence, security and space sector. In accordance with the theme for 2016, the Panel will address: *Complex Urban environments, encompassing the challenges and opportunities for indoor/enclosed and urban communications and sensing technologies*.

16:40 – 18:20 EuMW Defence & Security Executive Forum

High-level speakers from leading defence and security companies present their views and experiences on RF microwave technology trends and its use in urban environments. Confirmed presentations include:

- Challenges for Maritime Border Surveillance Radar –*Tony Brown, EASAT*
- Challenges in the 'Future Borders' Concept - Combining Technology, People and Processes – *Roger Cumming, Fenley-Martel (ex UK Home Office)*
- Challenges in Urban Sensing and Communications [Preliminary Title] –*Ian Beresford, QinetiQ*

18:20 – 19:00 Cocktail Reception

Registration and Programme Updates

Registration fees are £10 for those who have registered for a conference and £40 for those not registered for a conference.

As information is formalized, the Conference Special Events section of the EuMW website will be updated on a regular basis.

Register online at www.eumweek.com

EuMW 2016
Microwaves Everywhere

Sponsors:

KEYSIGHT TECHNOLOGIES · Peregrine Semiconductor · QinetiQ · qorvo all around you · ROHDE&SCHWARZ

China Unicom and Ericsson to Cooperate on 5G, Cloud and IoT

Ericsson and China Unicom have signed a Memorandum of Understanding (MoU) to collaborate on next-generation networks. The two companies aim to accelerate the development of next-generation network standardization and the maturity of network infrastructure, to establish cross-industry ecosystems and to foster innovation for new business. The agreement will help drive innovation and early application of 5G mobile network technology.

Under the terms of the MoU, Ericsson and China Unicom will cooperate on network architecture, 5G, cloud and the Internet of Things (IoT), including: Next-generation network architecture for fixed mobile convergence; cooperation on 5G standardization, research into key technologies and joint testing; studies of network visualization and 5G network slicing; joint promotion of software-defined networking (SDN) projects in standardization groups and SDN solution verification; mobile cellular IoT network end-to-end solutions and services, as well as support China Unicom's 'Focus Strategy', commercial network evolution solution and low-cost coverage solution deployment and practice.

> "...embrace the opportunities of network transformation."

Guanglu Shao, vice president, China Unicom, said, "Ericsson is a long-term strategic partner of China Unicom. As the transformation toward next-generation networks approaches, we hope to strengthen the partnership with Ericsson, the world-leading company, in technology and business development — especially in 5G, IoT and cloud — in order to win the future."

Chris Houghton, head of Region North East Asia, Ericsson, commented, "With Ericsson's industry leading technology, portfolio and global experience, China Unicom will be more competitive in networks and get ready to embrace the opportunities of network transformation."

Stratobus Project Takes Off

Thales Alenia Space has officially kicked off its Stratobus research and development project. Stratobus is an autonomous stratospheric airship that has been approved by the French government's 'investment in the future' programme, with funding of €17 million. Since the project has also won support from four different French regions, additional funding of about €3 million is expected.

Stratobus will be positioned at an altitude of about 20 km over its theatre of operations, in the lower layer of the stratosphere, which offers sufficient density to provide lift for the balloon. It will carry payloads to perform missions such as the surveillance of borders or high-value sites, on land or at sea (video surveillance of offshore platforms, etc.), security (the fight against terrorism, drug trafficking, etc.), environmental monitoring (forest fires, soil erosion, pollution, etc.) and telecommunications (Internet, 5G).

"The new market for high-altitude pseudo satellites, or HAPS, is estimated at one billion dollars from now to 2020, but is awaiting a product. With Stratobus offering a field of view of 500 km, we're convinced that it will win a large share of this market," said Jean-Loic Galle, president and chief executive officer of Thales Alenia Space.

Thales Alenia Space project manager Jean-Philippe Chessel added, "Stratobus is midway between a drone and a satellite, making a low-cost product offering permanent regional coverage and ideally complementing satellite solutions. Using only solar energy and green technologies, Stratobus has a very small carbon footprint – much smaller than that of a small private plane."

Thales Alenia Space and partners plan to launch a demonstrator in 2018, followed by the first qualification and certification flights in 2020.

Photo Courtesy: Thales

Georgia Joins Horizon 2020

Researchers and innovators from Georgia will now be able to participate in Horizon 2020, the European Union's framework programme for research and innovation, under the same conditions as their counterparts from EU Member States and other associated countries. The agreement was signed on behalf of the European Commission by Carlos Moedas, European Commissioner for Research, Science and Innovation, and Tamar Sanikidze, Georgian Minister for Education and Science.

This agreement allows for Georgia's enhanced cooperation with the EU in research and innovation, which are vital for successful and modern economies. It shows the commitment of the Union to develop the scientific and innovation capacity of its associated partners. It also represents another step towards reaching the EU goal of opening research and innovation to the world.

Georgian research institutes, universities and individual researchers will now have access to all opportunities offered by Horizon 2020 that funds diverse scientific areas, from blue sky research to demonstration projects. Georgian SMEs and businesses will also be able to benefit from

For More Information
Visit mwjournal.com for more international news

increased support to develop new ideas and bring products and services to the market.

Commissioner Carlos Moedas said, “I am very pleased to welcome Georgia into Horizon 2020, the world’s largest public funding programme for research and innovation. EU research, science and innovation is open to the world for collaboration and we value working together with our partners to invest in knowledge and innovation for the future. Georgia’s association will bring a diversity of expertise and ideas, enriching our international research cooperation.”

Johannes Hahn, commissioner for European Neighbourhood Policy and Enlargement Negotiations added: “The full association of Georgia into Horizon 2020 will allow its enterprises and research institutions to become even more competitive and resilient.”

e2v Hosts Defence and Security Quantum Technology Community Meeting

On behalf of the Defence Science and Technology Laboratory (Dstl), e2v hosted the fifth Defence and Security Quantum Technology Community meeting. The event brought together a community of experts from industry, government and academia to accelerate the commercialisation of Quantum Technology and to maintain the UK as a world leader in the field.

Experts delivered a series of informative presentations on their latest advancements, and on display were exhibits and demonstrations from the National Quantum Technology hubs including representatives and equipment from the Universities of Birmingham, Strathclyde, Nottingham, Southampton, Oxford and Warwick.

Trevor Cross, chief technology officer at e2v, said, “Our collaboration with the Quantum Community brings together world class research, Dstl’s ambitious technology demonstrator programme and proven industrial expertise to deliver a collective vision. This will enable us together with our partners to translate state-of-the-art laboratory technology into deployable practical devices. These crucial partnerships support the development of smaller, lighter and cheaper components to make quantum devices a commercially viable reality that will ultimately improve, save and protect people’s lives.”

Neil Stansfield, technical strategy lead, Knowledge, Innovation, and Futures Enterprise, Dstl said, “A cornerstone of the UK National Quantum Technologies Programme is to form strategic collaborations between UK industry, academia and government partners. We are delighted that this meeting, the first hosted by an industrial partner, has helped strengthen that collaboration and further developed our understanding of how early engagement of UK industry will contribute to successful exploitation of the science in the academic base. This contributes to both our needs in defence and security, but also to supporting wealth creation in the UK.”

5G Worldwide Service Revenue to Reach $247B in 2025

VIEW VIDEO

ABI Research projects that mobile broadband operators will reap 5G revenues of $247 billion in 2025 with North America, Asia-Pacific and Western Europe being the top markets. Specifically, network operators, vendors and standards bodies will finalize technical details concerning millimeter wave by 2020, with rollout ramping up afterward.

"5G will be a fast growing cellular technology, most probably faster than preceding generations including 4G," says Joe Hoffman, managing director and vice president at ABI Research. "The technology migration over the next few years will mean the continued decline of 2G. 3G and 4G will grow in many markets but 5G will generate new use cases and market revenues."

As infrastructure vendors and mobile operators prepare for the future of 5G, the market faces several key challenges. Obstacles include spectrum fragmentation, standards development, coverage range, availability of devices and CAPEX/OPEX, and most importantly, the development of use cases that ensure profitable outcomes from the unique competitive advantages of 5G.

> "It will be better, cheaper, greener and incredibly high-speed wireless data access for the mass market that will cause business innovation to explode."

Unlike the case with LTE, 5G stakeholders are trying hard to achieve spectrum harmonization. As with LTE, however, 5G will also include unlicensed and shared spectrum schemes. Government organizations worldwide will need to work together to regulate the 5G spectrum and set the new standard.

Additionally, Enhanced Mobile Broadband coverage will be best achieved in urban areas that require faster speeds and greater capacity. While smart antenna technology can extend coverage reach, it will mean a small cells deployment. ABI Research forecasts 8.5 million small cells to be deployed by 2020, setting in place the infrastructure for a rapid 5G millimeter wave rollout. And in-band backhaul is a new tool to solve connectivity issues.

At the early stage of deployment, the leading 5G use case is enhanced mobile broadband, closely followed by critical and massive machine type communications. Leading mobile operators in North America and Asia-Pacific recently announced projects and plans to roll out their own 5G initiatives. For example, Verizon Wireless, NTT DoCoMo, KT and SK Telecom formed the 5G Open Trial Specification Alliance. In addition, Verizon Wireless's acquisition of XO Communications' fiber network business brings strategic access to licensed millimeter wave spectrum with which to deploy 5G.

"The 5G Network of Tomorrow will, over time, evolve to embrace cellular, Wi-Fi and wired connectivity, in addition to millimeter wave," concludes Hoffman. "It will be better, cheaper, greener and incredibly high-speed wireless data access for the mass market that will cause business innovation to explode."

Non-Cellular Wireless Markets to Reach More Than 10 Billion Annual IC Shipments by 2021

ABI Research forecasts the global wireless connectivity market, excluding cellular connectivity, to reach more than 10 billion annual IC shipments by 2021. While smartphones will continue to represent the largest market, the introduction of Bluetooth mesh networking, emerging Wi-Fi protocols, enhancements to 802.15.4, such as ZigBee 3.0 and Thread, and the growing trend to develop multi-protocol connectivity system on chips (SoCs), will create new opportunities in various verticals of the IoT market.

Bluetooth will be in 60 percent of total devices by 2021. The mobile phone market will account for less than 45 percent total Bluetooth shipments by this time as Bluetooth Smart continues to grow and branch into new verticals. Bluetooth Smart will be in 16 percent of devices by this time, with strong growth in smart home and beacon applications, in addition to a significant presence in the connected home and wearable space.

> It is the growing prevalence of combo ICs that will help drive the market forward, particularly in IoT verticals.

Wi-Fi will see its most significant growth in IoT verticals, such as wearables, automotive, the smart home, and other nascent IoT verticals. However, by 2021, mobile phones will still account for 55 percent of the Wi-Fi-enabled device market. Wi-Fi is also branching out into new frequency bands, including 802.11ad (WiGig) for high-speed wireless data transfer and sub-1GHz Wi-Fi HaLow (802.11ah). This will open up new opportunities for 802.11ad in the networking, mobile device, computing, and peripheral space, and in low power IoT devices and wireless sensor network applications for 802.11ah. By 2021, Wi-Fi will be found in 47 percent of all devices.

802.15.4-based technologies, such as ZigBee and Thread, are set to find success in the smart home, achieving a CAGR of 60 percent between 2016 and 2021. The technology will also see growth in energy management and smart city applications, such as building automation, smart metering, smart lighting and industrial applications, accounting for more than 28 percent of devices by this time.

NFC is also targeting new opportunities for mobile payments in smartphones and wearables, as well as secure

For More Information
Visit mwjournal.com for more commercial market news

pairing and provisioning of IoT devices. It is the growing prevalence of combo ICs, though, that will help drive the market forward, particularly in IoT verticals.

"These solutions can help eliminate the need for multiple connectivity ICs, reduce complexity and cost, and give manufacturers greater flexibility in targeting multiple applications and use cases using a single SoC," says Andrew Zignani, industry analyst at ABI Research. "Devices incorporating multiprotocol chipsets will be more future-proof and faster to market. Ultimately, this will enable greater scalability and afford OEMs more flexibility and confidence when designing a connected device."

Booming Opportunities in IoT Cybersecurity

VIEW VIDEO

While it remains a fragmented market that has yet to consolidate, the ecosystem is expanding with vendors finding their way into three groups: hardware (chipset/SoC/microcontroller), firmware/software (embedded OS/RTOS/hypervisor), and applications (platform/cloud/service/analytics) across a wide range of verticals, including automotive, smart home, healthcare and energy.

"There is growing interest and requirement for improved levels of security to be designed into products, devices, and networks to protect data, combat fraud, and prevent criminal hacking," says Michela Menting, research director at ABI Research. "While there is no one 'go-to' company, with so many IoT and security vendors making a stake, the prospects for successfully penetrating the market are high for new players and entrenched leaders alike. Promising opportunities, and undeniably challenges, will center on securing assets, protecting data and ensuring privacy."

> "Promising opportunities, and undeniably challenges, will center on securing assets, protecting data and ensuring privacy."

Market players pioneering the expansion of the IoT cybersecurity vendor ecosystem include Qualcomm, Gemalto, G&D, ARM, Imagination Technologies, Deutsche Telekom, Symantec, Wind River, QNX, Green Hills, Freescale, General Dynamics, Commsignia, Covisint, Cryptosoft, Waterfall Security, Oracle, Intel, Harman (TowerSec), Bastille, Rambus, Escrypt, Inside Secure and ForgeRock among many others.

Numereous groups are working on different aspects of security standards, from hardware designs to network connectivity.

Around the **Circuit**

Barbara Walsh, Multimedia Staff Editor

The Industry Mourns the Passing of a Colleague and Friend

Tim Dolan, longtime vice president of engineering at K&L Microwave in Salisbury, Md., passed away on April 15, 2016, after several weeks of illness. Tim is survived by his wife Diane, daughter Elizabeth, sons Tommy and Jeffrey, daughter-in-law Jillian, close relatives including three siblings and numerous cousins, and many grieving co-workers and business associates.

Tim was born on June 19, 1957, and grew up in Philadelphia. A master electrician grandfather helped stoke a lifelong love of circuits, and a powerful work ethic produced a teenaged Jersey Shore charter fishing boat captain. Tim began his college education at California State University at Los Angeles and completed his electrical engineering degree in 1982 at Penn State, where he met Diane. He launched his career at the Optimax division of Alpha Industries and joined K&L Microwave in 1992, achieving company officer in two years.

Tim profoundly influenced innovation and design at K&L. Special expertise included amplifiers and integrated assemblies, power and heat dissipation, and corona and multipaction effects. He played major roles on classified defense programs, the formalization of K&L's quality system and the development of the Filter Wizard® selection software. Tim worked with university and industry researchers on marketable and patentable product innovations, academic and trade papers, and software advances. He supported science and engineering education and spearheaded efforts to expand company technical knowledge.

▲ *Tim Dolan*

An imposing figure with a wonderful sense of humor, Tim's enthusiasm, generosity, enjoyment of people and passion for technical topics won affection throughout the industry. Co-workers recall a "go-to" guy for explanations and assistance. Customers and reps have expressed gratitude for his honesty and drive. He was a welcomed travel companion and trade show presence. For Tim, professional problem-solving seemed a vehicle for friendship and helping others, as well as an end in itself. His contributions to lives, programs and organizations are lasting, and he is already sorely missed.

MERGERS & ACQUISITIONS

Qorvo Inc. announced that it has signed a definitive agreement to acquire privately-held **GreenPeak Technologies**, a leader in ultra-low power, short range RF communication technology. The acquisition of Netherlands-based GreenPeak will allow Qorvo to expand its customer offering to include highly integrated RF solutions and systems-on-a-chip for the connected home and the rapidly growing Internet of Things.

Teledyne LeCroy Inc. announced that it has entered into an agreement to acquire **Quantum Data Inc.**, the market leader in HDMI and SDI signal generators and protocol analyzers as well as test tools for other digital video technologies. Teledyne LeCroy is the market leader in protocol test tools for well known serial data standards like USB, PCI Express, SAS and SATA. The company's strategy is to continue to expand its protocol offerings into additional wired and wireless data communication standards with the goal to be the market leader in each protocol standard.

Mitel and **Polycom** announced that they have entered into a definitive merger agreement in which Mitel will acquire all of the outstanding shares of Polycom common stock in a cash and stock transaction valued at approximately $1.96 billion. The transaction represented a 22 percent premium to Polycom shareholders based on Mitel's and Polycom's "unaffected" share prices as of April 5, 2016 and is expected to close in the third quarter of 2016, subject to shareholder and regulatory approvals and other customary closing conditions.

MaxLinear Inc., a provider of RF and mixed-signal integrated circuits for cable and satellite broadband communications, the connected home, and data center, metro and long-haul fiber networks, announced the acquisition of certain assets and the assumption of certain liabilities related to **Microsemi Corp.'s Broadband Wireless Division**, which was previously part of PMC-Sierra Inc. These acquired assets and assumed liabilities specifically address wireless infrastructure markets, including wideband RF transceivers and synthesizers for 3G, 4G and future 5G cellular base station and remote radio head unit platforms.

COLLABORATIONS

Anritsu Co. and **TRX Systems** announce that they have entered into a partnership whereby Anritsu's handheld analyzers are integrated with a 3D indoor location and mapping solution from TRX Systems to create the industry's first automatically geo-referenced RF signal mapping solutions. The MA8100A series TRX NEON® Signal Mapper simplifies and dramatically reduces the time required for

For More Information
For up-to-date news briefs, visit mwjournal.com

DUAL or SINGLE LOOP

SYNTHESIZER & PLO MODULES

Up to 30 GHz*

Features:

- Proprietary digital Integer and Fractional PLL technology
- Lowest digital noise floor available -237 dBc/Hz figure of merit
- Output frequencies from 100 MHz locked crystal to 30 GHz
- Available with reference clean up dual loop, or single loop for very low noise reference
- Parallel fixed band stepping or SPI interface synthesized up to octave bandwidths
- Reference input range 1 MHz to 1.5 GHz
- Dual RF output or reference sample output available
- +12 dBm standard output power +16 dBm available
- Standard module size 2.25 X 2.25 X 0.5 Inches (LxWxH)
- Standard operating temperature -10 to 60 °C, -40 to +85 °C available

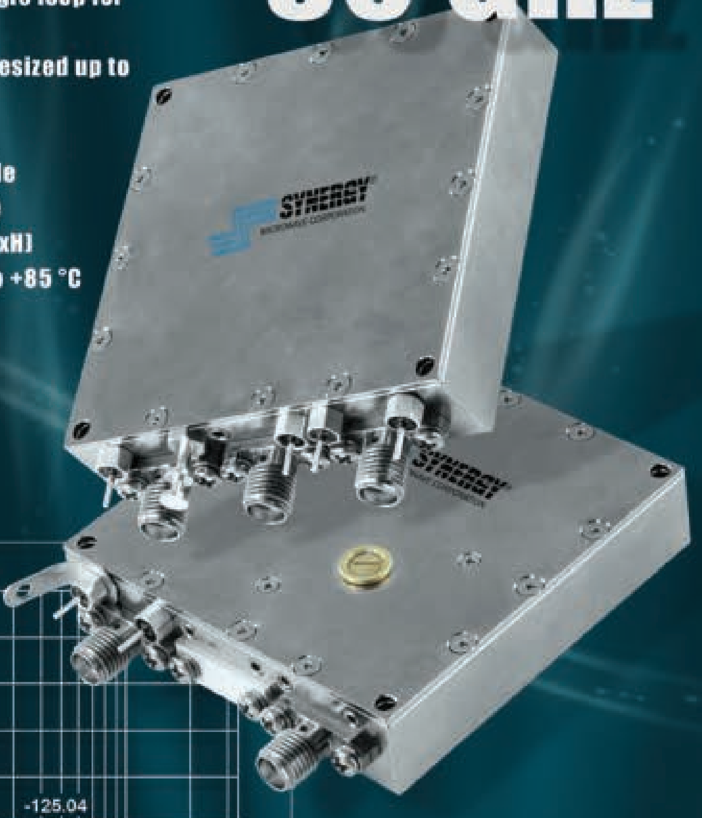

Applications:

- SATCOM, RADAR, MICROWAVE RADIO

** 16 - 30 GHz with added x2 module < 1" in height.*

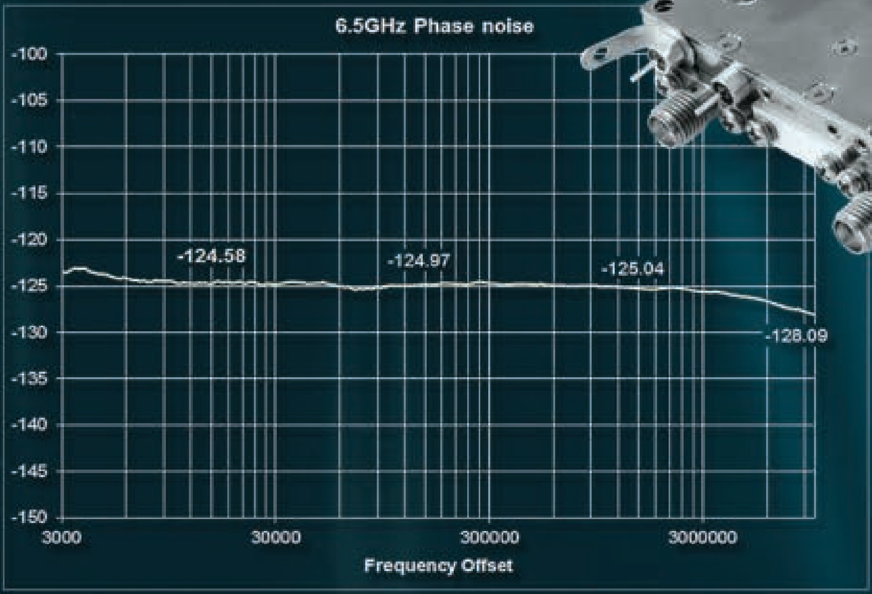

RoHS

Talk To Us About Your Custom Requirements.

SYNERGY®
MICROWAVE CORPORATION

Phone: (973) 881-8800 | Fax: (973) 881-8361
E-mail: sales@synergymwave.com
Web: WWW.SYNERGYMWAVE.COM
Mail: 201 McLean Boulevard, Paterson, NJ 07504

indoor signal testing, making it an ideal solution for professionals who conduct in-building testing of public safety and commercial networks, including public safety organizations, network operators and DAS installers.

Sivers IMA announced that **Inxpect**, the developer of the first radar-based intelligent motion sensing platform for the industrial safety, smart home and security markets, has selected Sivers IMA as the partner for some of their upcoming products. Under the agreement, Sivers IMA will enhance and customize its FMCW radar technology allowing Inxpect to leapfrog current performance and cost benchmarks.

UTAC Holdings Ltd., a semiconductor assembly and test services provider in Asia, announced a joint collaboration with **AT&S**, a global manufacturer of high-end printed circuit boards with headquarters in Leoben, Austria, to provide complete turnkey supply chain solutions for three-dimensional system-in-package (3D SiP) requirements. The collaboration combines UTAC's established packaging and test services and AT&S' embedded chip in substrate technology. This will offer customers a full turnkey supply chain assembly and test flow for applications that require the heterogeneous integration benefits that the 3D SiP with embedded chip architecture provides.

Eutelsat Communications announced its selection of **Gilat Satellite Networks Ltd.** to power a new range of broadband services in Western Russia. Eutelsat has selected Gilat's SkyEdge II-c hub with X-Architecture and SkyEdge II-c small user terminals to deliver broadband services using the new Express AMU1/EUTELSAT 36C satellite. The hub will be installed at the Dubna satellite centre operated by RSCC, near Moscow. The satellite's high throughput payload comprises 18 Ka-Band beams delivering continuous coverage of Western Russia, from the Arctic coastline to the Caspian Sea.

NEW STARTS

Antenova Ltd., a manufacturer of antennas and RF antenna modules for M2M, has expanded its design and development facility in Taipei's technology quarter Nei Hu District, Taiwan. This is in direct response to the increasing demand from customers for antennas for M2M and IoT applications. Antenova's engineering resources cover the USA, Europe and Asia, with a specialist RF team in Taipei leading the company's antenna design and development operations. As well as designing the company's antennas, the same RF engineers also provide support to Antenova's customers, assisting by providing antenna integration and matching services throughout the entire design process.

ACHIEVEMENTS

Anritsu Co. announced that its ME7873LA RF/RRM conformance test system (CTS) leads the industry in total number of validated PTCRB 3CA LTE test cases supported by any platform. This leadership position was achieved based on approvals gained at the recent PTCRB #83 meeting held March 14-17 in Tampa, Fla. The ME7873LA RF/RRM CTS is a scalable GCF, PTCRB, and carrier-validated test system that enables certification of LTE and W-CDMA devices to industry and carrier standards. The ME7873LA provides test coverage for 3GPP 36.521-1 (Tx, Rx and performance), 36.521-3 (Radio Resource Management – RRM), 34.121-1 (Tx, Rx, performance and RRM), and carrier-specific Supplementary RF/RRM test packages.

Altair invites engineering students from across the globe to participate in the 14th annual FEKO Student Competition. The competition is open to all students who work on a supervised project in electromagnetic engineering and make use of FEKO, Altair's HyperWorks solution for electromagnetic simulation. The Altair competition is an ideal opportunity for students to showcase their work with FEKO. In addition to international recognition, some attractive prizes are up for grabs this year — a state-of-the-art laptop computer or a ticket to attend any one of the Altair ATC or ATCx events, which are hosted around the world each year.

Lime Microsystems announced the launch of a crowdfunding campaign to bring their LimeSDR software defined radio platform into full-scale production. The campaign, hosted on the Crowd Supply platform, aims to raise $500,000 to fund the final stages of development and mass production of the LimeSDR. The LimeSDR platform is a low cost application-enabled software defined radio (SDR) platform that can be programmed to support virtually any type of wireless standard.

CONTRACTS

Harris Corp. has received an $88 million order to supply electronic jammers for U.S. Navy F/A-18 Hornet and Super Hornet aircraft. The jammers protect the Navy jets from sophisticated electronic threats, including modern integrated air defense systems. The order was received during the third quarter of Harris' fiscal 2016. Under the modification to the contract awarded in July 2015, Harris will manufacture and deliver 48 on-board electronic warfare jamming systems for the Integrated Defensive Electronic Countermeasures (IDECM) program. Deliveries are expected to be completed by December 2018.

PEOPLE

▲ *Alexander Everke*

ams AG, a provider of high performance sensor and analog solutions, announced **Alexander Everke** as CEO, effective immediately. Bringing more than 24 years of semiconductor industry experience to the company, Everke joined ams' management board as CEO designate in October 2015. Everke has held senior executive positions with Siemens, Infineon and NXP during his career. Prior to joining ams, he was a member of the NXP management team serving as executive vice president and general manager for NXP's multimarket semiconductors, high performance mixed signal and infrastructure & industrial business units.

Communications & Power Industries

Beverly Microwave Division

For more information contact us at:
150 Sohier Road • Beverly, MA 01915
+1 (978) 922-6000 • bmdmarketing@cpii.com
www.cpii.com/bmd

Solid State Power Amplifiers

State of the art design; designed for all military environments

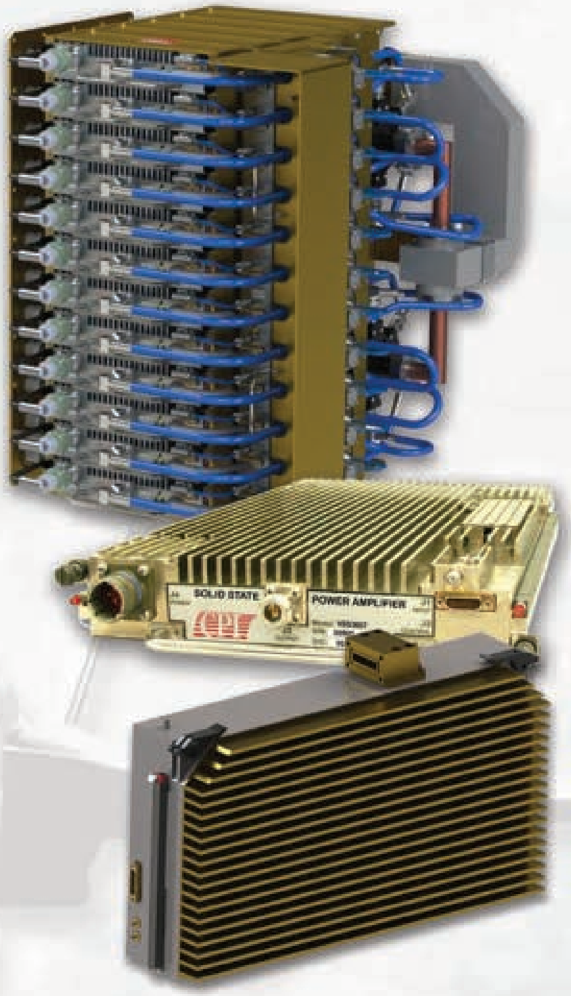

Features:

- High efficiency pulsed modules (10% duty)
- BIT and controls via EIA-422
- Compact light weight
- 9.0 - 9.2 GHz X-Band: 1 kW modules
- 2.7 - 2.9 GHz S-Band: 1.3 kW modules
- 1.2 - 1.4 GHz L-Band: 700 W modules
- Power combine modules up to 25 kW

Benefits:

- High reliability
- Field replaceable modules

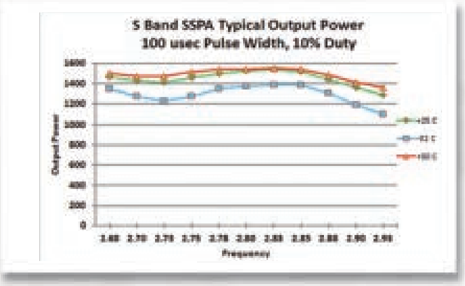

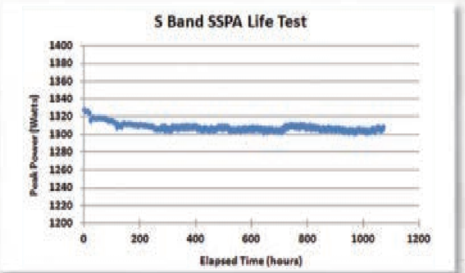

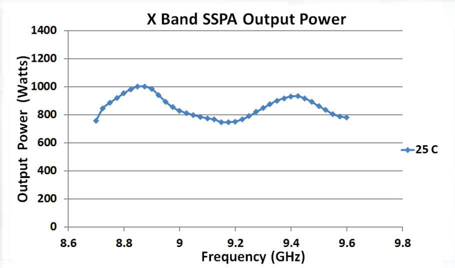

• Solid State Power Amplifiers • Integrated Microwave Assemblies • Receiver Protectors
• Control Components • Transmitters • Amplifiers • Modulators • Magnetrons • Crossed Field Amplifiers
• Ring Loop Traveling Wave Tubes • Power Couplers

Around the **Circuit**

▲ *Andreas Karch*

Indium Corp. has hired **Andreas Karch** as regional technical manager, Germany, Austria and Switzerland. Karch provides support, including sharing process knowledge and making technical recommendations for the use of Indium Corp.'s materials, including solder paste, solder preforms, fluxes and thermal management materials. Karch has more than 20 years of automotive industry experience, including the advanced development of customized electronics. He is an ECQA-certified integrated design engineer and has a Six Sigma Yellow Belt. He was recently the recipient of the top 10 innovative patents for an automotive LED assembly. Karch maintains a thorough understanding of process technologies and project management skills.

REP APPOINTMENTS

Amplical Corp. announced the appointment of the following regional sales representatives: **MC Microwave**, San Jose, Calif. (northern California). **RF Alliance Technical Marketing**, Ocean, N.J. (greater New York Metropolitan area including Long Island, New Jersey and eastern Pennsylvania). **TE Repco**, West Palm Beach, Fla. (Florida).

GigOptix Inc. announced that it has signed **Avnet**, a global technology distributor, as its distributor for all GigOptix product lines sales in China. Establishing the partnership with Avnet marks an important milestone for GigOptix, enhancing the already solid business of GigOptix in the Chinese Enterprise and Cloud connectivity markets, and supporting the anticipated rapid growth of the business over the next few years.

RFMW Ltd. and **SANAV** announce a distribution relationship allowing RFMW to promote and sell SANAV products worldwide. SANAV offers both standard and custom antenna solutions for multiple markets. Under the agreement, RFMW will support SANAV's antenna activity, including sales of their GPS, GNSS, 4G, UHF, WiFi and MIMO antennas. With years of manufacturing experience combined with innovative design capabilities, SANAV offers antennas capable of supporting the latest technologies such as GPS/GNSS+3G, GPS/Glonass+3G+UHF, GPS+4G+WiFi, GPS+LTE- MIMO + WiFi - MIMO and so on.

PLACES

AmpliTech Inc. recently completed the move to a new facility at 620 Johnson Avenue in Bohemia, N.Y. They are now located in the heart of the Industrial Center in Bohemia — minutes from the Islip MacArthur Airport, a main business hub for Long Island. This new location doubles the space of their previous location, allowing the company to increase productivity and exposure to larger OEM customers.

photo courtesy of the
U.S. Military & NASA

ULTRA-REL® *10 MHz to 7GHz*

CERAMIC MMIC AMPLIFIERS

Low NF from 0.5 dB *High IP3 up to +42 dBm* *Low DC current 65 mA* from $4[95] ea. (qty 20)

When failure is not an option. Our CMA family of ceramic MMIC amplifiers is expanding to meet your needs for more critical applications. Designed into a nitrogen-filled, hermetic LTCC package just 0.045" high, these rugged models have been qualified to meet MIL standards for a whole battery of harsh environmental conditions:

Qualified for: *(see website for complete list and details)*

Gross and Fine Leak	*HTOL (1700 hours @ +105°C)*
Mechanical Shock	*Steam Aging*
Vibration	*Solder Heat Resistance*
Acceleration	*Autoclave*
PIND	*And More!*

Robust performance across wide bandwidths makes them ideal for instrumentation, or anywhere long-term reliability adds bottom-line value. Go to minicircuits.com for all the details today, and have them in your hands as soon as tomorrow!

Electrical Specifications *(-55 to +105°C)*

3 x 3 x 1.14 mm

	Model	Freq. (GHz)	Gain (dB)	P_{OUT} (dBm)	IP3 (dBm)	NF (dB)	DC (V)	Price $ ea. (qty 20)
New	CMA-81+	DC-6	10	19.5	38	7.5	5	6.45
New	CMA-82+	DC-7	15	20	42	6.8	5	6.45
New	CMA-84+	DC-7	24	21	38	5.5	5	6.45
	CMA-62+	0.01-6	15	19	33	5	5	4.95
	CMA-63+	0.01-6	20	18	32	4	5	4.95
	CMA-545+	0.05-6	15	20	37	1	3	4.95
	CMA-5043+	0.05-4	18	20	33	0.8	5	4.95
	CMA-545G1+	0.4-2.2	32	23	36	0.9	5	5.45
	CMA-162LN+	0.7-1.6	23	19	30	0.5	4	4.95
	CMA-252LN+	1.5-2.5	17	18	30	1	4	4.95

RoHS compliant

Mini-Circuits®

www.minicircuits.com P.O. Box 350166, Brooklyn, NY 11235-0003 (718) 934-4500 sales@minicircuits.com

503 Rev H

EDITOR'S NOTE

This is the second of a three-part series on Möbius metamaterials. This month, the authors delve into the theory and interesting applications: signal sources, wearable and implantable electronics, and gravitational field research.

Möbius Metamaterial Inspired Signal Sources and Sensors

Ulrich L. Rohde
Brandenburgische Technische Universitat, Cottbus, Germany
Ajay K. Poddar
Synergy Microwave, Patterson, N.J.

Metamaterial Möbius strips (MMS) have captured the interest of research scientists because of their distinctive properties, such as topological symmetry, which is conserved when the system undergoes an alteration such as deformation, twisting and stretching; and a negative index of refraction (i.e., $n=-\sqrt{\varepsilon\mu}$; $\varepsilon < 0$, $\mu < 0$). ***Figure 1*** shows typical negative index ($\varepsilon < 0$, $\mu < 0$) Möbius strips formed by graphene nano-ribbons that are used to create topologically-induced high Q-factor components with desirable electromagnetic properties. Unlike conventional materials, which interact with electromagnetic waves based on their chemical compositions, the properties of negative index materials (NIM), otherwise known as metamaterials, come from their geometric topological structures.

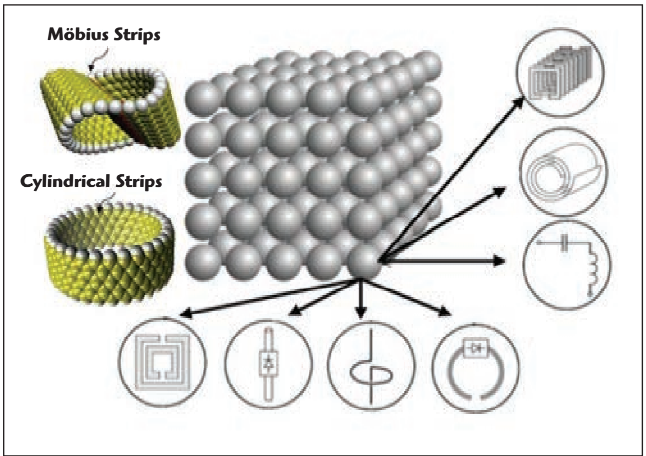

▲ *Fig. 1 Möbius strips formed by graphene nanoribbons exhibit negative index properties suitable for high Q-factor microwave components.*

NIMs, as shown in Figure 1, are artificial engineered topological structures intended to modify the bulk permeability and permittivity of the medium. This is realized by constraining the size of periodically unit cell NIMs structures size to typically less than the wavelength of incident EM waves. It is interesting to note that by changing the position, orientation and excitation of the NIMs structures, important parameters such as permittivity, permeability, refractive index, transmission, reflection, impedance and coupling can be tuned and optimized for desired applications. There are many ways to vary the properties of NIMs, such as using ferrites, liquid crystals, frequency-selective surfaces and hybrid-NIMs, or by manipulating their lattice structures.

Figure 2 shows the typical characteristics of a medium that explains the properties of natural and artificially engineered composite material.[1] The third quadrant describes the properties of a left-handed medium that posses NIM characteristics. The evanescent-mode energy

Making the Connection in Millimeter Waves for 25 Years!
S10MS-A
mmW Test Equipment
Oleson Microwave Labs
Visit us at www.oml-mmw.com
microwave JOURNAL
Millimeter Wave Measurement Solutions for Gigabit Wireless (50-110 GHz)
The Connection to your Next Solution
Innovation in Millimeter Wave Solutions
www.omlinc.com
(408) 779-2698
OML

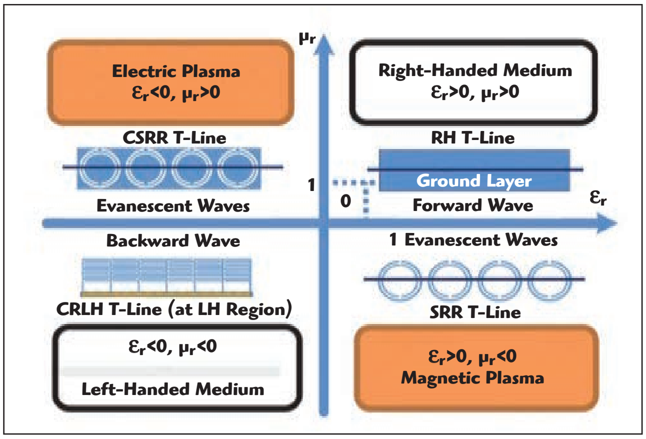

▲ *Fig. 2 Typical representation of a medium; the third quadrant explains NIM properties.*

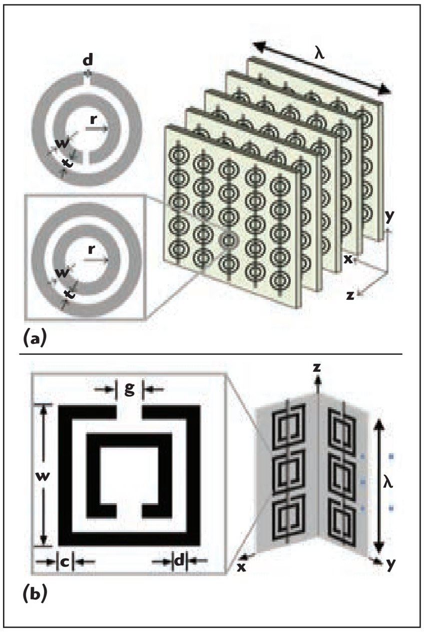

▲ *Fig. 3 Typical SRRs and NIM construction with closed SRR wire structure: circular split ring (a) and rectangular split ring (b).*

storage and resonance characteristics of the third-quadrant material enables potential applications in electronics, medical, space and optics. Hence, it is important to understand its fundamental EM dynamics for the design of NIMS resonator based electronic signal sources. It is important to note that exact characterization of ε and μ of a NIM structure is a challenging task for wideband frequency operation.

While it is possible to characterize NIMs in terms of n and normalized impedance (z), this does not provide meaningful information. The ongoing effort by research scientists is to categorize a NIM structure by its effective constitutive parameters: $\varepsilon_r = n/z$, $\mu_r = n \times z$. This gives a direct and an understandable interpretation of a NIM based element.

In addition to this, the justification for using effective constitutive parameters (ε < 0, μ < 0) provides a convenient means to understand the behavior of the artificially engineered NIM structures without considering, in detail, the local EM-field distribution. To establish faithful values for these parameters, numerous methods have been reported, but none of them provide exact solutions because of hypotheses concerning the NIM's tiny size, and they neglect coupling. The general isotropic medium model assumes that the induced electric and magnetic dipoles are mutually independent, but in reality this is not always the case. NIMs are intrinsically anisotropic and sometimes bi-anisotropic because of the geometry and orientations of their structures.

For example, split rings (SR) as shown in ***Figure 3***, typically used in NIMs, exhibit simultaneous electric and magnetic responses; i.e., their corresponding dipoles are coupled.[5] This leads to cross coupling between the electric and magnetic field in SR inspired NIM structures. Therefore, it is not recommended to discount the magneto-electric coupling that depends on the shape of inclusions, wave polarizations, excitation and orientation of NIM structures. To account for both asymmetric reflection and magneto-electrical coupling, the bi-anisotropic medium model can be used.

Figure 3 shows typical NIM circular and square split ring structures. Their sizes and the distances between them are kept smaller than a wavelength (λ). Under these conditions, an SR-NIM structure may present bulk properties that can be characterized by a macroscopic model, with parameters ε and μ. The expression n is given by

$$n = \pm\sqrt{(\pm\epsilon)(\pm\mu)} = \pm\sqrt{\mu\epsilon} \qquad (1)$$

From (1), a positive sign is used for n when ε, μ > 0, whereas a negative sign is used when ε, μ < 0. The assumption of positive index (n > 0) implies that the index n is a scalar, and does not depend on frequency. But in reality, this is not always true. The energy of the field (W), where W $=\varepsilon E^2+\mu H^2$, would be a negative value when ε and μ are negative, and this is not possible; hence ε and μ are bound to depend on frequency and fall into complex domain.[2] The unified expression of energy W can be described by

$$W = \frac{\partial(\omega\varepsilon)}{\partial\omega}E^2 + \frac{\partial(\omega\mu)}{\partial\omega}H^2 \qquad (2)$$

where $\varepsilon(\omega) = \varepsilon'(\omega) + j\varepsilon''(\omega)$ and

$\mu(\omega) = \mu'(\omega) + j\mu''(\omega)$

From (2), the electrodynamics of negative index materials (n < 0; ε< 0 and μ < 0) provide a positive W value for a very broad class of dispersive materials characterized by ε (ω) and μ(ω), exhibit dependency on frequency.

Any material supporting a single propagating mode at a known frequency usually exhibits well-defined n, whether the material is homogeneous/continuous or not. But it is not easy to assign z to a non-homogeneous material, because z strongly depends on the surface termination and overall size of the material.[1] The classical homogenization theories are typically valid when the unit-cell size is insignificant with respect to wavelength (the zero frequency limits) and thus might be expected to result in a poor description of negative index materials. The key supposition is, if the wavelength of the incident wave is much larger than the size and spacing between the NIM's unit cell elements then it is possible to perform homogenization, and to obtain a value of z within an acceptable range of error.[2,3]

Assuming the size of a NIM structure is much smaller than λ/10, the homogenization theory can be applied to topology inspired Möbius strips. The averaging of Maxwell's equations over small volumes (with respect to a wavelength) can be performed to obtain an analogous uniform continuous harmonized medium described by effective constitutive parameters (ε and μ). It is possible to retrieve values for the complex n and z of inhomogeneous periodic negative index Möbius strips (NIMS) structures with prior information about the termination of the NIM unit cell, and the phases and amplitudes of the waves

transmitted/reflected from the NIMS sample. The challenge is that if the NIMS structures are not symmetric along the wave propagation direction, two different values of z are retrieved corresponding to two incident directions of propagation. This ambiguity in the computation of z leads to a fundamental ambiguity in the definitions of ε and μ, which increases as the ratio of unit cell dimension to wavelength increases.

The simplest theoretical formulation of a SR inspired NIM can be deduced from an equivalent circuit model that gives insight into the relationship between the physical properties and geometric parameters of SRRs as shown in ***Figures*** 3 and ***4***. Analytical values of the constitutive parameters (ε_{zz}, μ_{yy}, ξ0) are given by [5, 13, 17]

$$\varepsilon_z = 1 + \frac{1}{\varepsilon_0 a^3} \left\{\varepsilon_0 \frac{16}{3} r_{ext}^3 + 4 d_{eff}^2 r_0^2 C_{pul}^2 L \left(\frac{\omega^2}{\omega_0^2 - \omega^2 - i\omega\gamma}\right)\right\} \quad (3)$$

$$\mu_y = 1 + \frac{\mu_0}{a^3}\left\{\frac{\pi^2 r_0}{L}\left(\frac{\omega^2}{\omega_0^2 - \omega^2 - i\omega\gamma}\right)\right\} \quad (4)$$

$$\xi_0 = -i\sqrt{\frac{\mu_0}{\varepsilon_0 a^3}} \left\{-2 i r_0^3 d_{eff} C_{pull} \frac{\omega_0^2}{\omega}\left(\frac{\omega^2}{\omega_0^2 - \omega^2 - i\omega\gamma}\right)\right\} \quad (5)$$

where $d_{eff}=c+s$, $\gamma=\frac{R}{L}$, $r_0=r+c+s/2$ and $r_{ext}=r+2c+s$; L and C_{pull} are the total inductance of the SRR and the capacitance between the rings respectively.

From the equivalent circuit model, RR behaves as a resonant LC circuit, and that the frequency of the resonance is given by

$$\omega_0^2 = \frac{1}{\left(\frac{1}{2}\pi r_0 C_{pull} + C_{gap}\right) L} \quad (6)$$

L and C_{pull} can be calculated from the analytical equations reported by Marques et al.[17] C_{gap} is the capacitance of the gap, if the gap is narrow, its capacitance can be analytically written as[18]

$$C_{gap} = \frac{\varepsilon_0 c h}{g} + C_0 \text{ with} \quad (7)$$
$$C_0 = \varepsilon_0 (h + c + g)$$

From Marques et al.,[17] L = 3.9287 × 10^{-9} H, C_{pul} = 1.6806 × 10^{-11} F, C_{gap} = 4.1557 × 10^{-15} F and R = 0.4901 Ω at the frequency of resonance. The poor accuracy of the analytical method for constitutive parameter calculation given in (3) through (7) and the deficiency in complex modeling of thicker structures limits its validation. The alternative approach is a retrieval technique based on the extraction of S-parameters. The advantage of the retrieval method is that it can be used for simulated and measured S-parameter data; thin samples (in the propagation direction) are preferred to minimize the errors.

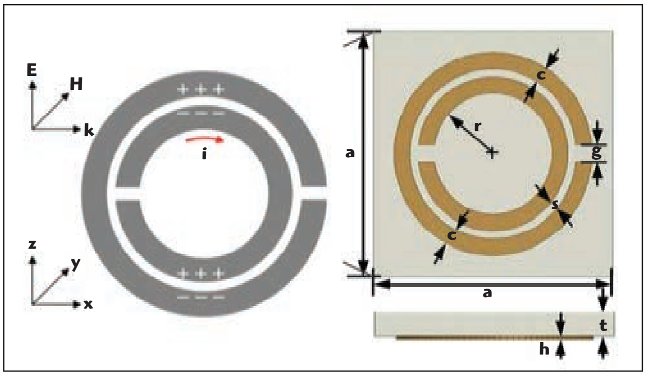

▲ *Fig. 4 Typical SRR unit cell showing the inner and outer asymmetric rings.*

In general there are three methods used for the determination of effective constitutive parameters based on applications and acceptable errors.[3] The first method is to numerically calculate the ratios of the EM field inside NIM structure. This approach is good for numerical simulations, but not appropriate for experimental measurement.[4] The second method calculates the effective constitutive parameters by using analytical models of NIM structures including the numerical averaging of fields; but, this technique is not suitable for complex NIM structures.[5] The third method is a retrieval technique based on the inversion of scattering data (S-parameters) of a finite slab, called the Nicolson–Ross–Weir (NRW) procedure.[6,7]

The NRW method was developed for the measurement of complex permittivity and permeability of natural materials and recently applied to NIMs.[1-20] The problem with NRW method arises in cases where topology-driven NIM structures undergo asymmetric reflections. Smith et al.,[2] reported a modified approach to resolve this issue of asymmetric reflections by using averaged values of reflection coefficients. The isotropic medium model cannot duplicate this property, as it is intrinsically symmetric, hence it is important to understand the EM dynamics of SR inspired NIM media that inherently possess reflection asymmetric structures ($S_{11} \neq S_{22}$).[21]

EM DYNAMICS OF MEDIA

The fundamental equations describing EM waves in a biaxial anisotropic medium (or simply called biaxial) are more complex than the isotropic equations. Isotropic materials have a single permittivity ε. In an isotropic media, the constitutive relations that relate the electric flux density $\bar{D}$ to the electric field intensity $\bar{E}$ and the magnetic flux density $\bar{B}$ to the magnetic field intensity $\bar{H}$ are given by

$$\bar{D} = \varepsilon\bar{E} = \varepsilon_o \varepsilon_r \bar{E}\ ;\ \bar{B} = \mu\bar{H} = \mu_0 \mu_r \bar{H} \quad (8)$$

From (8), ε describes the medium's electrical properties and μ describes its magnetic properties. The time-harmonic forms of Maxwell's equations for isotropic media are given by

$$\nabla \times \bar{E} = -i\omega\mu\bar{H} \quad (9)$$
$$\nabla \times \bar{H} = i\omega\varepsilon\bar{E} + \bar{J} \quad (10)$$
$$\nabla . \bar{D} = \rho_V \quad (11)$$
$$\nabla . \bar{B} = 0 \quad (12)$$

A medium is called electrically anisotropic if $\bar{D} = \bar{\bar{\varepsilon}} \cdot \bar{E}$, where $\bar{\bar{\varepsilon}}$ is the permittivity tensor. A medium is magnetically anisotropic if $\bar{B} = \bar{\bar{\mu}} \cdot \bar{H}$, where $\bar{\bar{\mu}}$ is the permeability tensor, note that $\bar{B}$ and $\bar{H}$ are no longer parallel. A medium can be both electrically and magnetically anisotropic. In the electrically anisotropic case, $\bar{D}$ and $\bar{E}$ are no longer parallel, and $\bar{\bar{\varepsilon}}$ is given by

$$\bar{\bar{\varepsilon}} = \begin{pmatrix} \varepsilon_{xx} & \varepsilon_{xy} & \varepsilon_{xz} \\ \varepsilon_{yx} & \varepsilon_{yy} & \varepsilon_{yz} \\ \varepsilon_{zx} & \varepsilon_{zy} & \varepsilon_{zz} \end{pmatrix} \quad (13)$$

For example, crystals, in general, are described by a symmetric permittivity tensor; there always exists a coordinate transformation that transforms the symmetric matrix $\bar{\bar{\varepsilon}}$ to a diagonal matrix as given by

$$\bar{\bar{\varepsilon}} = \begin{pmatrix} \varepsilon_{xx} & 0 & 0 \\ 0 & \varepsilon_{yy} & 0 \\ 0 & 0 & \varepsilon_{zz} \end{pmatrix} \quad (14)$$

From (14), the new coordinate system is called the principal system, and the three coordinate axes are called the principal axes. For a cubic crystal where $\varepsilon_{xx}=\varepsilon_{yy}=\varepsilon_{zz}=\varepsilon$, the crystal is isotropic.

$$\bar{\bar{\varepsilon}} = \begin{pmatrix} \varepsilon & 0 & 0 \\ 0 & \varepsilon & 0 \\ 0 & 0 & \varepsilon \end{pmatrix} \quad (15)$$

For tetragonal, hexagonal and rhombohedra crystals two of the three ε are equal; such a crystal is called uniaxial. Uniaxial anisotropic materials have two different permittivity values. They have the same permittivity along two dimensions and a different permittivity along the third dimension. An unrotated uniaxial permittivity tensor can be written as

$$\bar{\bar{\varepsilon}} = \begin{pmatrix} \varepsilon & 0 & 0 \\ 0 & \varepsilon & 0 \\ 0 & 0 & \varepsilon_{zz} \end{pmatrix} \quad (16)$$

From (16), the principal axis that is different (exhibits anisotropy) is called the optical axis (z-axis is the optical axis), and there exists a two dimensional degeneracy. If $\varepsilon_{zz}>\varepsilon$, the medium exhibits positive uniaxial behavior, and if $\varepsilon_{zz}<\varepsilon$, the medium shows negative uniaxial characteristics.

If $\varepsilon_{xx}\neq\varepsilon_{yy}\neq\varepsilon_{zz}$, the crystal is biaxial. Examples of biaxial crystals are orthorhombic, monoclinic, and triclinic. The defining property of electrically biaxial media is the permittivity tensor $\bar{\bar{\varepsilon}}$.

If the medium is biaxial anisotropic, the permittivity and permeability of medium take on a tensor form. From (8), the set of matrix equations can be described by

$$\vec{D} = \bar{\bar{\varepsilon}} \cdot \vec{E} = \varepsilon_o \bar{\bar{\varepsilon}}_r \cdot \vec{E}\ ;\ \vec{B} = \bar{\bar{\mu}} \cdot \vec{H} = \mu_0 \bar{\bar{\mu}}_r \cdot \vec{H} \quad (17)$$

where $\bar{\bar{\varepsilon}}_r$ and $\bar{\bar{\mu}}_r$ are relative permittivity and permeability tensors, respectively. From (17), the change in constitutive relations also affect Maxwell's equations (9)-(12) in the medium,

$$\nabla \times \vec{E} = -i\omega\bar{\bar{\mu}}\vec{H} \quad (18)$$

$$\nabla \times \vec{H} = i\omega\bar{\bar{\varepsilon}}\vec{E} + \vec{J} \quad (19)$$

$$\nabla . \vec{D} = \rho_V \quad (20)$$

$$\nabla . \vec{B} = 0 \quad (21)$$

The NIM exhibits properties of a bi-anisotropic medium, provide coupling between electric and magnetic fields. The constitutive relations for a bi-anisotropic medium are given by

$$\vec{D} = \bar{\bar{\varepsilon}}.\vec{E} + \bar{\bar{\xi}}.\vec{H} \quad (22)$$

$$\vec{B} = \bar{\bar{\mu}}.\vec{H} + \bar{\bar{\xi}}.\vec{E} \quad (23)$$

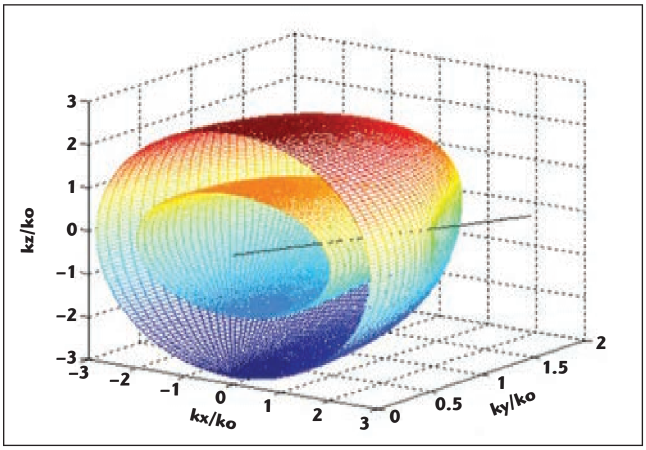

▲ *Fig. 5 Wave vector surface: unrotated biaxial medium (ε_x, ε_y, ε_z) = (2, 8, 4), plotted over 0 ≤ θ ≤ π and 0 ≤ φ ≤ π.*

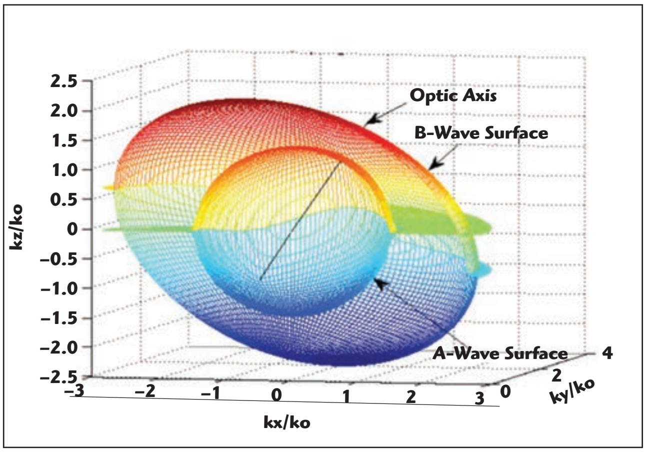

▲ *Fig. 6 Wave vector surface: rotated biaxial medium (ε_x, ε_y, ε_z) = (2, 8, 4), rotated by (ψ_1 ψ_2) = (30°, 75°).*

A bi-anisotropic medium placed in an electric or magnetic field becomes both polarized and magnetized. Almost any medium in motion becomes bi-anisotropic. The first cases of bi-anisotropic materials were indeed moving dielectrics and magnetic materials in the presence of electric or magnetic fields. The topics of moving NIMs and their constitutive relations are the subject of relativistic electromagnetic theory, and can lead to Casimir effect (anti-gravity).[15] The permittivity described in (16), represents an unrotated uniaxial medium with its optic axis along the z-direction.

Biaxially anisotropic materials have three unique values in the permittivity tensor and they have two optic axes. An unrotated biaxial permittivity tensor is given by

$$\bar{\bar{\varepsilon}} = \begin{pmatrix} \varepsilon_x & 0 & 0 \\ 0 & \varepsilon_y & 0 \\ 0 & 0 & \varepsilon_z \end{pmatrix} \quad (24)$$

where $\varepsilon_x \neq \varepsilon_y \neq \varepsilon_z$. From (8), principal axes of a biaxial medium are aligned with the Cartesian coordinate system.

For a better understanding, ***Figure 5*** shows the plots of the unrotated biaxial medium; the inner surface is called the "a-wave vector surface" and the outer surface is the "b-wave vector surface". The intersecting line is one of the optic axes, it can be seen from Figure 5 that the optic axis intersects the wave vector surfaces at some point and the "b-wave wave vector surface" is at a local minimum at the point of intersection.[10] If the biaxial medium is arbitrarily oriented with respect to the coordinate system, the permittivity tensor representation would be complex and not as simple described in (8).

The evaluation of the tensor for an arbitrarily oriented biaxial medium is given by applying rotations to the tensor in (8); the wave vector surfaces are shown in ***Figure 6***. Studying the wave vector surfaces of the unbounded region shown in Figures 5 and 6 give insight into how the wave influences the important parameters (ε, μ, n, z) in the composite NIM structures, which are intrinsically anisotropic and sometimes bi-anisotropic due to geometry and structural orientations.

CONSTITUTIVE EFFECTIVE PARAMETERS

Most of the NIMs presented over the past several years are artificially engineered SR-inspired periodic structures.[1-27] It is convenient to extract the parameters from a unit cell of periodic structures through numerical approaches. It has been demonstrated that under the condition of long wavelength, a material with a periodic structure can be viewed as a homogeneous medium and its properties can be described by the effective medium parameters. The properties of a periodic structure can be determined from the transfer-matrix (T) associated with the fields of a unit cell.

NIM structures fall into the category of anisotropic and bi-anisotropic (cross-coupling exists between electric and magnetic fields in bi-anisotropic) due to their orientation and special geometric structures. When computing the effective parameters of NIM structures, magneto-electric coupling is a critical parameter. The simplified approach to retrieve the coupling

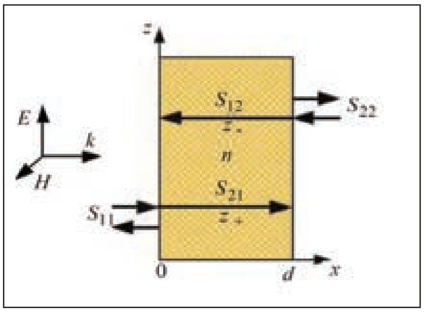

▲ *Fig. 7 Plane wave incident in the x direction into a bi-anisotropic slab.[13]*

parameter of a bi-anisotropic material from S-parameters is based on transfer-matrix method. The transfer-matrix method has been used to retrieve the effective EM parameters of homogeneous and non-homogeneous materials.[1,2]

Figure 7 shows a typical of bi-anisotropic slab of thickness d placed in air, illustrating the direction of S-parameters. For a material consisting of periodic structures, there is a phase advance per unit cell, which can be defined by the periodicity.[13]

Chen et al.,[16] extracted effective constitutive parameters of bi-anisotropic negative index material from S-parameters for various wave polarizations using a numerical approach for a plane wave polarized in the z direction and incident in the x direction. ***Figure 8*** shows the triplet $[(\overline{k_x} - H_y, E_z]$ based on a right-handed coordinate system, containing an electric and magnetic field.

As shown in Figure 8, the plane wave polarized in z- axis propagates along the x- direction, the electric fields in the z-direction will induce magnetic dipoles and the magnetic

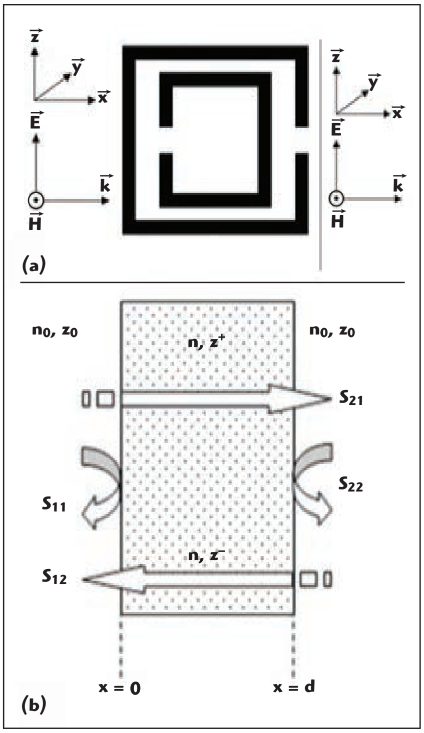

▲ *Fig. 8 Planar SRR structure (a) and homogeneous bi-anisotropic material slab suspended in air, with S-parameters used to determine forward and backward wave impedances (b).*[3]

fields in the y- direction will induce electric dipoles due to the asymmetry of the inner and outer rings. It means that electric dipoles cannot only be excited by the E-fields but also by the H-fields. Similarly, magnetic dipoles cannot only be excited by the H-fields but also by the E-fields.

Assuming that medium is reciprocal and that the harmonic time dependence is $e^{-i\omega t}$, the constitutive relationships are given by[19]

$$\vec{D} = \bar{\bar{\varepsilon}}.\vec{E} + \bar{\bar{\xi}}.\vec{H} \quad (25)$$

$$\vec{B} = \bar{\bar{\mu}}.\vec{H} + \bar{\bar{\zeta}}.\vec{E} \quad (26)$$

$$\bar{\bar{\varepsilon}} = \varepsilon_0 \begin{pmatrix} \varepsilon_{xx} & 0 & 0 \\ 0 & \varepsilon_{yy} & 0 \\ 0 & 0 & \varepsilon_{zz} \end{pmatrix}, \quad \bar{\bar{\mu}} = \mu_0 \begin{pmatrix} \mu_{xx} & 0 & 0 \\ 0 & \mu_{yy} & 0 \\ 0 & 0 & \mu_{zz} \end{pmatrix} \quad (27)$$

$$\bar{\bar{\xi}} = \frac{1}{c}\begin{pmatrix} 0 & 0 & 0 \\ 0 & 0 & 0 \\ 0 & -i\xi_0 & 0 \end{pmatrix}, \quad \bar{\bar{\zeta}} = \frac{1}{c}\begin{pmatrix} 0 & 0 & 0 \\ 0 & 0 & i\xi_0 \\ 0 & 0 & 0 \end{pmatrix} \quad (28)$$

where $\vec{E}$, $\vec{H}$, and $\vec{D}$, are electric field, magnetic field intensity, and flux density; ε_0 and μ_0 are the permittivity and permeability in a vacuum; c is the speed of light in vacuum; and the other four quantities are dimensionless and are unknowns. When a plane wave polarized in the z-direction is incident in the x-direction, only two components of EM-fields (E_z and H_y) and three EM parameters (ε_{zz}, μ_{yy}, ξ_0) are included.

The numerical formulation is done for the determination of the forward and backward wave impedances entailed by parameters ε_{zz}, μ_{yy} and ξ_0, since the unknown four quantities ε_{xx}, ε_{yy}, μ_{xx}, and μ_{zz} are not related to the bi-anisotropic structure in Figure 8b. From (18)-(19):

$$\frac{\partial^2 E_z}{\partial x^2} + k_x^2 E_z = 0, \quad \frac{\partial^2 H_y}{\partial x^2} + k_x^2 H_y = 0 \quad (29)$$

$$Z^+ = \frac{E^+}{H^+} = Z_0 \frac{\mu_{yy}}{(n + i\xi_0)} \quad (30)$$

$$Z^- = \frac{E^-}{H^-} = Z_0 \frac{\mu_{yy}}{(n - i\xi_0)}, \; Z_0 = \sqrt{\frac{\mu_0}{\varepsilon_0}} \quad (31)$$

$$z^\pm = \frac{Z^\pm}{Z_0}; \; z^+ = \frac{Z^+}{Z_0}; \; z^+ = \frac{Z^+}{Z_0} \quad (32)$$

$$k_x^2 = k_0^2(\varepsilon_{zz}\mu_{yy} - \xi_0^2), \; k_x = nk_0 \quad (33)$$

$$n^2 = \varepsilon_{zz}\mu_{yy} - \xi_0^2, \; n = \pm\sqrt{\varepsilon_{zz}\mu_{yy} - \xi_0^2} \quad (34)$$

where E_z and H_y are the z and y components of $\vec{E}$ and $\vec{H}$; k_x and k_0 are the wave number of the wave propagating in the x direction and in free-space, Z^+ and Z^- are wave impedances inside the medium for forward $(+\hat{x})$ and backward $(-\hat{x})$ propagations; z^+ and z^- are normalized (or non-dimensionalized) wave impedances in respective directions; Z_0 is the wave impedance (or intrinsic impedance) in air; and n is the refractive index of the negative index structure.

From (30),(31), bi-anisotropic NIM structure samples exhibit different values of wave impedances for forward and backward wave propagation.[2,20] The non-homogeneous periodic NIM structure does not exhibit distinct impedance values because the ratio of E/H' varies periodically throughout the structure. This variation is negligible if the NIM structure unit cell sizes are small relative to a wavelength. It is important to note that the lack of a unique definition for $z^\pm$ indicates that the values of ε and μ retrieved are not assignable but can be applied if the NIM formed by the periodic structure is always terminated in the same location of the unit cell. The surface termination has an increasing influence on the scattering properties of the structure as the scale of inhomogeneity increases relative to a wavelength.

It has been demonstrated that under the long wavelength condition, materials with periodic structures can be viewed as homogeneous and their properties can be described by the effective medium parameters. The properties of a periodic structure can be determined from the transfer-matrix (T) that is associated with the fields of a unit cell. We express the fields in the form of a vector F $=\bar{F} = (\bar{E}, \bar{H}')^T$, where $\bar{E}$ and $\bar{H}$ are the complex amplitudes of the electric and magnetic fields located on the left-hand and right-hand faces of a slab. The magnetic field is a reduced field with the normalized form $\bar{H}' = i\omega\mu\bar{H}$. The relations of fields on two sides of a slab can be expressed as

$$\bar{F}(x+d) = e^{i\alpha d}\bar{F}(x) = T\bar{F}(x) \quad (35)$$

where α is the phase advance per unit cell which relates the fields on its two sides. T is the one dimensional transfer matrix of a NIM slab

$$T = \begin{pmatrix} T_{11} & T_{12} \\ T_{21} & T_{22} \end{pmatrix} = \quad (36)$$

$$\begin{pmatrix} \cos(nk_0 d) & -\frac{z}{k_0}\sin(nk_0 d) \\ \frac{z}{k_0}\sin(nk_0 d) & \cos(nk_0 d) \end{pmatrix}$$

with k_0 being the wave number of light in free space, z being the wave impedance of a slab and n being the refractive index. From (35) and (36), the dispersion relation is given by solving

$$T_{11}T_{22} - e^{i\alpha d}(T_{11} + T_{22}) + e^{i2\alpha d} - T_{12}T_{21} = 0 \quad (37)$$

The elements of the transfer matrix can be expressed in terms of S-parameters.

$$T_{11} = \frac{(1+S_{11})(1-S_{22})+S_{21}S_{12}}{2S_{21}} \quad (38)$$

$$T_{12} = \frac{(1+S_{11})(1+S_{22})-S_{21}S_{12}}{2S_{21}} \quad (39)$$

$$T_{21} = \frac{(1-S_{11})(1-S_{22})-S_{21}S_{12}}{2S_{21}} \quad (40)$$

$$T_{22} = \frac{(1-S_{11})(1+S_{22})+S_{21}S_{12}}{2S_{21}} \quad (41)$$

Figure 9 shows the schematics of a homogeneous bi-anisotropic material slab that is placed in an open space. There are two different situations to be considered, i.e., wave incidence in the +x and −x directions. After applying the boundary continuous conditions, it is easy to obtain the expressions for the S-parameters by using the transfer matrix method.[20] When the incidence is in the +x direction as shown in Figures 7 and 9a, the corresponding reflection (S_{11}) and transmission (S_{21}) coefficients are

$$S_{11} = \frac{2i\sin(nk_0 l)\left[n^2+(\xi_0+i\mu_y)^2\right]}{\left[(\mu_y+n)^2+\xi_0^2\right]e^{-ink_0 l}-\left[(\mu_y-n)^2+\xi_0^2\right]e^{ink_0 l}} \quad (42)$$

$$S_{21} = \frac{4\mu_y n}{\left[(\mu_y+n)^2+\xi_0^2\right]e^{-ink_0 l}-\left[(\mu_y-n)^2+\xi_0^2\right]e^{ink_0 l}} \quad (43)$$

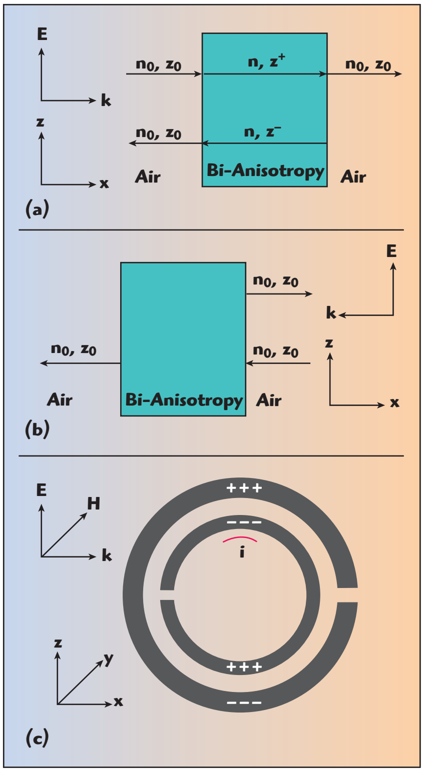

▲ *Fig. 9 Signal flow of a homogeneous bi-anisotropic slab placed in open space, for the calculation of S-parameters for plane waves incident in the +x (a) and −x (b) directions; NIM unit cell (c).*

where l is the thickness of the homogeneous bi-anisotropic material slab and k_0 is the wave number of light in free space. For the case when the incidence is in the −x direction, as shown in ***Figure 9b***, we obtain the corresponding reflection (S_{22}) and transmission (S_{12}) coefficients as

$$S_{12} = \frac{4\mu_y n}{\left[(\mu_y+n)^2+\xi_0^2\right]e^{-ink_0 l}-\left[(\mu_y-n)^2+\xi_0^2\right]e^{ink_0 l}} \qquad (44)$$

$$S_{22} = \frac{2i\,\sin(nk_0 l)\left[n^2+(\xi_0-i\mu_y)^2\right]}{\left[(\mu_y+n)^2+\xi_0^2\right]e^{-ink_0 l}-\left[(\mu_y-n)^2+\xi_0^2\right]e^{ink_0 l}} \qquad (45)$$

From (43)-(45), S_{21} is equal to S_{12}, but S_{11} is not equal to S_{22}. There are three independent equations for the three unknowns (n, μ_{yy} and ξ_0). By solving analytically (43)-(45), the expression for refractive index n is given by

$$\cos(nk_0 d) = \cos(\alpha d) = \frac{1-(S_{11}S_{22})+S_{21}^2}{2S_{21}} \qquad (46a)$$

From (36), using the condition of determinant (T)=1, and substituting (38)-(41):

$$\cos(nk_0 d) = \cos(\alpha d) = \frac{1-(S_{11}S_{22})+S_{21}^2}{2S_{21}} \qquad (46b)$$

It is understood that when S_{11} is equal to S_{22}, (46) will degenerate into a standard retrieval form.[2] The refractive index n can be obtained from the implicit expression (46), which has many solutions for n to the different branches of the inverse cosine. When solving for n from (46), one must determine one branch from many branches of solutions. For a passive medium, the n must obey the condition $n''=\mathrm{Im}(n)\geq 0$. After computing n, the other constitutive parameters are

$$\xi_0 = \left(\frac{n}{-2\sin(nk_0 l)}\right)\left(\frac{S_{11}-S_{22}}{S_{21}}\right) \qquad (47)$$

$$\mu_y = \left(\frac{in}{\sin(nk_0 l)}\right)\left(\frac{2+S_{11}+S_{22}}{2S_{21}}-\cos(nk_0 l)\right) \qquad (48)$$

$$\varepsilon_z = \left(\frac{n^2+\xi_0^2}{\mu_y}\right) \qquad (49)$$

Consequently, impedances z+ and z– can be obtained from (29)-(30). For a passive medium, the following conditions should be satisfied: $z^{+\prime}=\mathrm{Re}(z^+)\geq 0$, $z^{-\prime}=\mathrm{Re}(z^-)\geq 0$.

From (47)-(49), retrieved effective constitutive parameters can be assigned to the NIM structure; however, a variety of artifacts exists in the retrieved material parameters that are related to the NIM structure's inherent inhomogeneity. The artifacts in the retrieved material parameters are particularly severe for NIM structures that make use of resonant elements, as large fluctuations in the index and impedance can occur, such that the wavelength within the material can be on the order of or smaller than the unit cell dimension. The retrieval technique based on analyzing the S-parameter of a finite slab can suffer from unphysical anti-resonances with negative imaginary parts for some of the parameters. These anomalies could be due to periodicity of the structure and spatial dispersion.[11,12]

An example of this behavior can be seen in the retrieved imaginary parts of ε and μ, which typically differ in sign for a unit cell that has a magnetic or an electric resonance. In homogeneous passive media, the imaginary components of the material parameters are restricted to positive values. This anomalous behavior vanishes as the unit cell size approaches zero.[2] For a homogeneous or symmetric material, the value of z will be unique, while it will result in two different values for an inhomogeneous or asymmetric material. The impedance $z=\frac{E}{H}$, is an intrinsic parameter which relates the electric field to the magnetic field.

From (35), two equivalent expressions for the impedance of a slab can be obtained by

$$z = \frac{T_{12}}{e^{i\alpha d}-T_{11}} = \frac{e^{i\alpha d}-T_{22}}{T_{21}} \qquad (50)$$

from (37) and (50)

$$Z^{\pm} = \pm\frac{(T_{11}-T_{22})\pm\sqrt{(T_{22}-T_{11})^2+4T_{12}T_{21}}}{2T_{21}} \qquad (51)$$

The two roots of (51) correspond to the two propagation directions of a plane wave. Substitution of (38)-(41) into (50) leads to

$$Z^{\pm} = \pm\frac{(S_{11}-S_{22})\pm\sqrt{(1-S_{11}S_{22}+S_{12}S_{21})^2-4S_{12}S_{21}}}{(1-S_{11})(1-S_{22})-S_{12}S_{21}} \qquad (52)$$

From (51) and (52), the characteristic impedance in terms of S-parameters associated with a metamaterial having bi-anisotropic structures is obtained. For a passive medium the impedance needs to satisfy the conditions $(z^+)'\geq 0$ and $(-z^-)'\geq 0$, where ( )'denotes the real part operator.

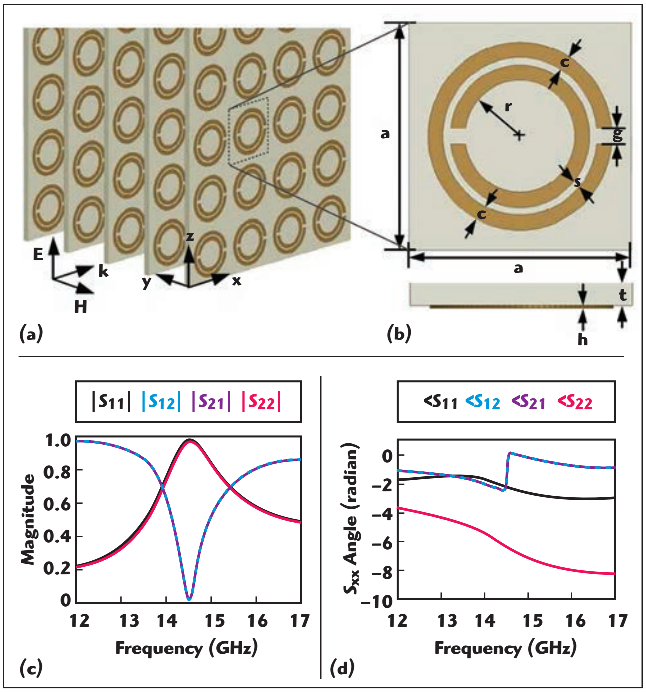

▲ *Fig. 10 A typical bi-anisotropic structure: array of SRRs printed on substrate with metallization (a) SRR unit cell (b) magnitude (c) and phase (d) of S-parameters.*[13]

For an example, a typical array of SRRs printed on substrate and unit cell is shown in ***Figure 10***. As illustrated in ***Figure 10a***, a plane wave is incident in the x direction and polarized in the z direction. The dimensions are α = 3 mm, r = 0.74 mm, c =0.2 mm, s = 0.1 mm, g = 0.2 mm, t =0.3 mm, h = 35 mm; and the substrate permittivity is ε0, for simplification.[13]

It can be seen from ***Figures 10b*** and ***10c*** that S_{12} is equal to S_{21} and the magnitudes of S_{11} and S_{22} are almost the same, while the phase of S_{11} is different with that of S_{22}. In this case, the application of the standard retrieval method[1] will lead to an inaccurate result. The discrepancy in phase of S-parameter measurements is because of the fact that the NIM's cells are not infinitely small compared to the incoming wavelength, causing spacial dispersion.

Assuming that there is a plane wave propagating in the direction of +x, polarized in the +z direction. The constitutive relationship between electric field and magnetic field can be described as


ONE PLATFORM, ZERO BARRIERS
SIMPLY SMARTER
NI AWR DESIGN ENVIRONMENT
NI AWR Design Environment™ is one platform - integrating system, circuit and electromagnetic analysis - for the design of today's advanced wireless products from base stations to cellphones to satellite communications. Its intuitive use model, proven simulation technologies, and open architecture supporting third-party solutions translates to zero barriers for your design success. Simply smarter design.
Learn more at ni.com/awr
AWR
NATIONAL INSTRUMENTS™
Microwave Office | Visual System Simulator | Analog Office | AXIEM | Analyst

$$\overline{D_z} = \varepsilon_0\varepsilon_z\overline{E_z} - ic^{-1}\xi_0\overline{H_y} \qquad (53)$$

$$\overline{B_y} = \mu_0\mu_y\overline{H_y} + ic^{-1}\xi_0\overline{E_z} \qquad (54)$$

With the substitution of (53)-(54) into Maxwell's equations (18)-(19):

$$\nabla^2\overline{E_z} + \omega^2\varepsilon_0\mu_0\left(\varepsilon_z\mu_y - \xi_0^2\right)\overline{E_z} = 0 \qquad (55)$$

From (13), the index (n) can be given by

$$n^2 = \varepsilon_z\mu_y - \xi_0^2 \qquad (56)$$

For a passive material, the roots have to be chosen properly to guarantee the condition Im(n)≥0 Otherwise, the exponentially growing solutions will occur, which violates energy conservation. The impedances of a bi-anisotropic material for wave propagation in the right-hand or left-hand directions are Z±, the values of which are given by the equations

$$Z^+ = \frac{E^+}{H^+} \text{ and } Z^- = \frac{E^-}{H^-}.$$

From Maxwell's equations (18)-(21), the formulas of the impedance and effective parameters can be obtained,

$$Z^\pm = \frac{z^\pm}{Z_0} = \frac{\mu_y}{\pm n - i\xi_0}, \; Z_0 = \sqrt{\frac{\mu_0}{\varepsilon_0}} \qquad (57)$$

$$\varepsilon_z = \frac{n + i\xi_0}{z^+} \qquad (58)$$

$$\mu_y = (n - i\xi_0)Z^+ \qquad (59)$$

$$\xi_0 = in\frac{z^- + z^+}{z^- - z^+} \qquad (60)$$

The refractive index and impedances for a bi-anisotropic medium can be obtained from (46) and (52). The expressions for the effective electromagnetic parameters (ε_z, μ_y and ξ_0) and impedance associated with the bi-anisotropic structure are obtained from (58)-(60), and can be used for designing NIMS resonators for next generation energy efficient signal sources.

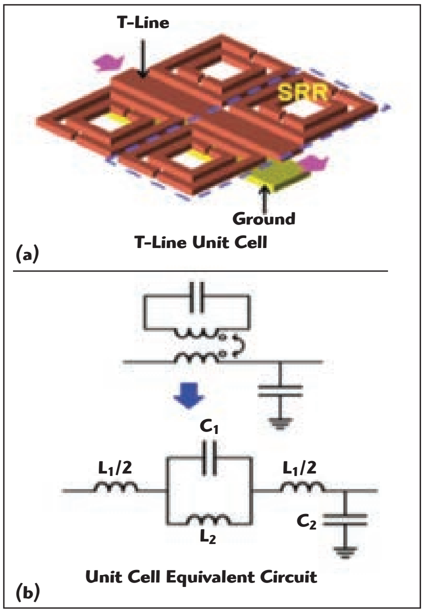

▲ *Fig. 11 SRR loaded T-line unit cell (a) and equivalent lumped LC model (b)*

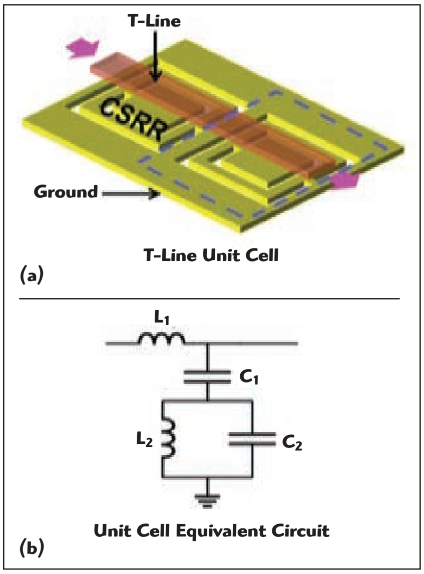

▲ *Fig. 12 CSRR loaded T-line unit cell (a) and equivalent lumped LC model (b).*

NIMS INSPIRED RESONATOR FOR OSCILLATORS

A NIMS resonator can be classified into two types: resonant type and non-resonant type: examples are the split ring resonator (SRR), and left handed (LH) transmission line (T-line). Resonant type metamaterial exhibits larger dynamic range for material parameters ($\varepsilon_r < 0$, $\mu_r < 0$), while non-resonant type metamaterial offers wide bandwidth and lower loss. Traditional metamaterial T-lines can be categorized into resonant type and non-resonant type, represented by the SRR/(complementary SRR) CSRR loaded T-line, and composite right/left handed (CRLH) T-line, with corresponding layouts shown in ***Figures 11*** and ***12***, where C and L are per-unit length capacitance and inductance that determine the T-line metamaterial properties. For a T-line loaded with an SRR (see Figure 1), L_1 and C_2 are linked with T-line, whereas C_1 and L_2 are linked to mag-

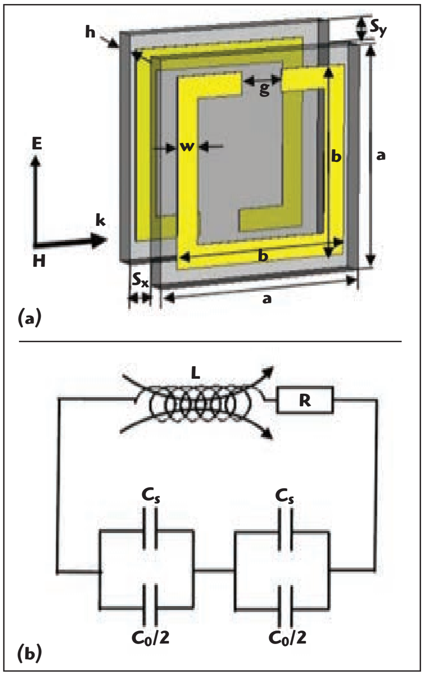

▲ *Fig. 13 Typical broadside-coupled split ring resonator (a) and equivalent lumped circuit representation (b).*[22]

netic coupling. Figure 11 shows the typical split ring resonator and NIM construction.

The physical properties in Figure 11 are given by:

$$\varepsilon = \frac{Y}{j\omega} = C_2 \text{ is} + \text{ve} \rightarrow \varepsilon > 0\ (+ve) \quad (61)$$

$$\mu = \frac{Z}{j\omega} = \frac{L_1+L_2-\omega^2 L_1 L_2 C_1}{1-\omega^2 L_2 C_1} \quad (62)$$

$$\mu < 0\ (-ve) \text{ for } \left(\frac{1}{L_2 C_1}\right)^{1/2} < \omega < \left(\frac{L_1+L_2}{L_1 L_2 C_1}\right)^{1/2} \quad (63)$$

From (61) and (63), Re (μ) is negative and Re (ε) is positive. For (ε>0, μ<0), propagating waves become evanescent waves, therefore energy cannot propagate through the resonator and is reflected back to establish a standing-wave.

As a result, the SRR loaded T-line structure stores the energy and forms a high-Q resonator tank circuit for a low phase noise oscillator application. Similarly, for a T-line loaded with a CSRR (see Figure 12), L_1 is associated with the T-line, while C_1, C_2, and L_2 account from electric coupling of the CSRR to ground.

The physical properties in Figure 12 are given by

$$\mu = \frac{Y}{j\omega} = L_1 \text{is} + \text{ve} \rightarrow \mu > 0\ (+ve) \quad (64)$$

$$\varepsilon = \frac{Y}{j\omega} = \frac{C_1(1-\omega^2 L_2 C_2)}{1-\omega^2 (C_1+C_2) L_2} \quad (65)$$

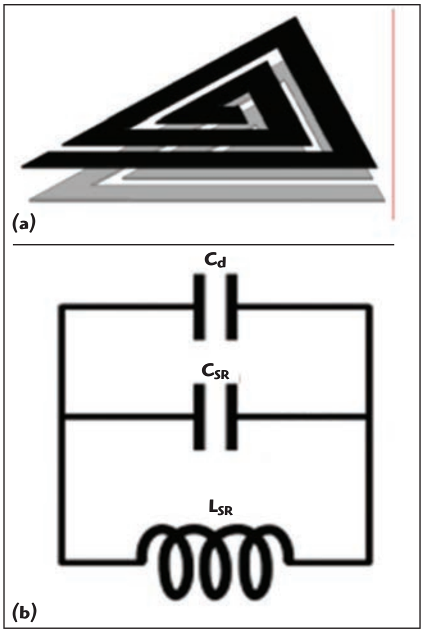

▲ *Fig. 14 Layout of the BCTSR (a) and equivalent lumped circuit (b).*

$$\varepsilon < 0\ (-ve) \text{ for } \left(\frac{1}{(C_1+C_2)L_2}\right)^{1/2} < \omega < \left(\frac{1}{L_2 C_2}\right)^{1/2} \quad (66)$$

From (64) and (66), Re (μ) is positive and Re (ε) is negative. In this case (ε < 0, μ > 0), and electric plasma is formed, where propagating waves become evanescent waves, hence, energy cannot propagate through the resonator either and is reflected back to establish a standing-wave. As a result, the CSRR loaded T-line can also be used to form a high-Q resonator.

Figure 13a shows the structure of the broadside-coupled split ring resonator, there are two relative slips S_x and S_y between the two broadside coupled rings. ***Figure 13b*** shows the corresponding equivalent circuit, where L and R are the equivalent inductance and resistance, respectively, C_0 is mutual capacitance between the two rings and C_s is the capacitance of the split. As shown in Figure 13a, the tuning can be realized with minor slips along and perpendicular to the gap direction of two broadsides coupled rings.[22] ***Figure 14a*** shows the layout of the broad coupled split ring (dark region denotes etching on the signal plane, and light region denotes broadside coupled triangular SR etched on ground plane), and ***Figure 14b*** shows the equivalent lumped circuit.

For the validation of reported research work, resonators are fabricated on low loss quartz and borosilicate material. As shown in ***Figure 15***, the metal structures are processed on top of quartz wafers (diameter D = 150 mm). The fabrication process uses a double-side coating of the substrates with a sputtered metal gold (Au) metallization. Unlike the SRR/CSRR depicted in Figure 15, the geometry of negative index Möbius strips (NIMS) is conformal, continuous, and maps one-to-one onto itself. These unique properties of NIMS permit EM coupling in such a way that a signal coupled to the loop does not encounter any obstructions when travelling around it, emulating an infinite transmission line; hence providing a large group delay and high Q-factor. In this paper, the oscillator circuit uses a negative index (ε_r <0, μ_r <0) NIMO (Negative Index Möbius Oscillator) circuit for low cost high performance solution.

EXAMPLES

Signal Source

Möbius metamaterial inspired (MMI) structures are artificially constructed media on a size scale smaller than a wavelength of the external stimuli. They can exhibit a strong localization and enhancement of fields, which may provide novel tools to significantly enhance the sensitivity and resolution of sensors, and open new degrees of freedom in sensing design.[1-10] A detailed discussion about MMI structure characteristics is given in part 1 (MWJ May 2016 Issue), this issue (part 2) presents mainly their applications in

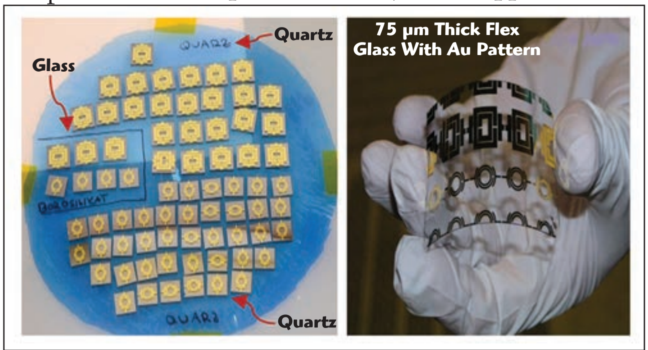

▲ *Fig. 15 Metamaterial resonators fabricated on glass and quartz.*

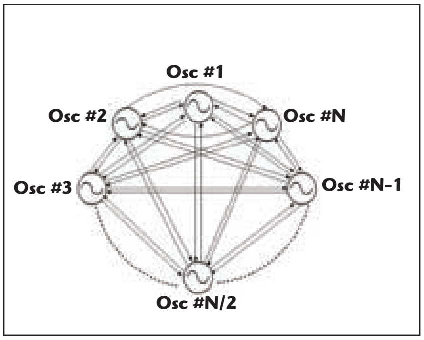

▲ *Fig. 16 A typical N-coupled N-push oscillator topology.*[29]

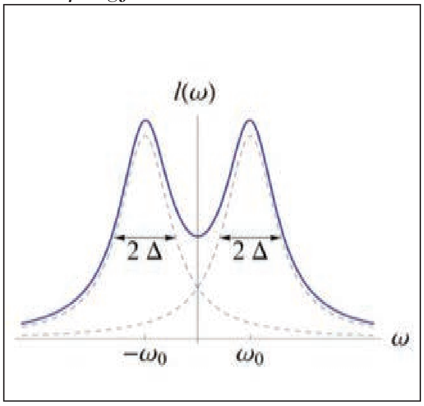

▲ *Fig. 17 Bimodal distribution consisting of the sum of two Lorentzians.*[17]

high frequency signal sources and sensors, as well as the challenges and prospects.[28]

From part 1 (MWJ May 2016 Issue, Equations 2 to 6, Ref 28), the Möbius transformation can be used for reducing the complexity of a system of N-coupled oscillators.[28] ***Figure 16*** shows the typical N-coupled N-push oscillator topology for the purpose of analysis.[29]

Globally, coupled oscillators have been used to model many diverse systems in physics, biology, chemistry, engineering, and space science. The system of coupled oscillators exhibits complex behavior because each individual unit influences the characteristics of other units. The phase dynamics of the N-coupled oscillator shown in Figure 16 is described by[29]

$$\frac{\partial\theta_i(t)}{\partial t} = \omega_i - \left[\frac{\omega_i}{2Q_i}\right] \left[\sum_{\substack{j=1\\ j\neq i}}^{N} \beta_{ij}\left(\frac{A_j(t)}{A_i(t)}\right)\sin[\theta_i(t)-\theta_j(t)+\varphi_{ij}]\right] - \left[\frac{\omega_i}{2Q_i}B_{ni}(t)\right] \quad i=1,2,3\ldots N \tag{67}$$

where $A_i(t)$, $\theta_i(t)$, ω_i, and Q_i are the amplitude, phase, free-running frequency, and Q factor of the i^{th} oscillator, B_{ni} corresponds to the phase fluctuations; and β_{ij} and φ_{ij} are the coupling parameters between i^{th} and j^{th} oscillators.

From (67),

$$\frac{\partial\theta_i}{\partial t} = \dot{\theta}_i = fe^{j\theta_i} + l + \bar{f}e^{-j\theta_i} \quad (\text{for } i = 1, 2, 3\ldots N) \tag{68}$$

where f is any smooth complex-valued 2π-periodic function of the phases $\theta_1,\ldots\theta_N$ and over bar ($\bar{f}$) is the complex conjugate.

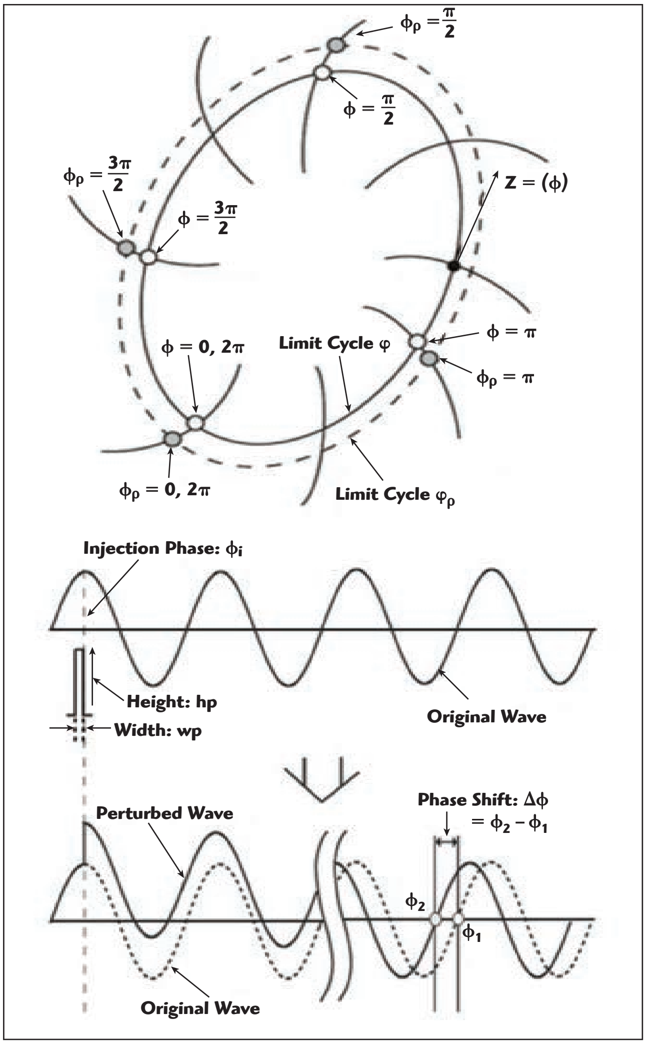

▲ *Fig. 18 Typical phase injection mechanism in a Möbius strip resonator due to perturbation at the i^{th} node.*

The coupled-oscillator system shown in Figure 16 tends to collective synchronization and lock to a common frequency, despite the difference in oscillator natural frequencies. However, an accurate solution of (67) and (68) becomes difficult due to the nonlinearity and large number of variables associated with coupled-oscillator systems.

An alternative means to solve this is by reducing the complex dynamics to phase models assuming the couplings among oscillators are sufficiently weak such that when they are uncoupled, their phases advance at constant 'velocities' (natural frequency). The functions f and l given in (68) may depend on time and on any auxiliary state variables in the system, assuming such system is sinusoidally coupled because the dependence on i occurs solely through the first harmonics $e^{j\theta i}$ and $e^{-j\theta i}$).[30] This particular class of dynamical systems (68) can be reducible by a Möbius transformation in the form.[31]

$$e^{j\theta_i(t)} = M_t[e^{j\phi_i(t)}] \quad (69)$$

for I = 1, 2, 3…N, where M_t is a one-parameter family of Möbius transformation and ϕ_j is a constant (time-independent) angle. The time-t flow map is an orientation-preserving homeomorphism that exhibits a Möbius map.

From (67) and (68), the distribution of natural frequencies for N→ ∞ is given by the sum of two Lorentzian distributions l (ω) [31]:

$$l(\omega) = \frac{\Delta}{2\pi}\left(\frac{1}{(\omega-\omega_0)^2+\Delta^2}+\frac{1}{(\omega+\omega_0)^2+\Delta^2}\right) \quad (70)$$

where Δ is the width parameter (half-width at half-maximum) of each Lorentzian and $\pm\omega_0$ are their center frequencies, as depicted in ***Figure 17***.

From (70), the challenges are the minimization of frequency detuning (proportional to the separation between the two center frequencies) and AM-PM conversion noise. For low noise oscillator applications, resonator Q-factor is important parameter. Resonator networks formed with Möbius strips are conformal, continuous, and map one-to-one onto itself; therefore, signals coupled to strips do not encounter any obstructions while travelling around them in such a way that a loop made of strips acts like an infinite transmission line. This arrangement enables a large group delay and improved Q-factor, which is promising for filter and oscillator applications. Möbius strips can have more than 1-twist (Figure 13, MWJ May 2016 Issue part 1, Ref 28). The 3-twisted Möbius strip has a trefoil knot as the boundary curve and so on. It is interesting to analyze the geometric phase of multi-knot non-orientable (Möbius) surfaces and their connection with nonlinear dynamical systems. This may provide a diagnostic analysis in abnormal neural oscillations and synchrony in schizophrenia.

Figure 18 illustrates a typical phase-injection mechanism using phase-perturbation at the ith node on a Möbius strips resonator based frequency generating electronic circuit. The Q-factor (Q_L) of the resonator is [29]

$$Q_L = \frac{\omega_0}{2}\left|\frac{d\varphi(\omega)}{d\omega}\right|_{\omega=\omega_0} = \frac{\omega_0}{2}\tau_d;\quad \tau_d = \left|\frac{d\varphi(\omega)}{d\omega}\right|_{\omega=\omega_0} \quad (71)$$

$$\tau_d = \left.\frac{d\varphi(\omega)}{d\omega}\right|_{\omega=\omega_0} = \frac{\varphi(\omega_0+\Delta\omega)-\varphi(\omega_0-\Delta\omega)}{2\Delta\omega} \quad (72)$$

where φ(ω) is the phase of the resonator impedance and τ_d is the group delay. The effective inductance of the Möbius strips varies with the current/voltage passing through them, building the evanescent field for a higher quality factor:

$$\overline{Q_m(\omega)}_{\omega\to\omega_0} = \left[\frac{\omega}{2(I_{max}-I_{min})}\int_{I_{min}}^{I_{max}} Q_m(\omega,i)\,di\right]_{\omega\to\omega_0} \quad (73)$$

where I_{min} and I_{max} are the minimum and maximum currents, and $Q_m(\omega,i)$ is the instantaneous quality factor at frequency ω and current i flowing through the Möbius strips resonator.

From Figure 18, the locking condition is given by

$$\frac{2(f-f_0)}{f} = \frac{\eta \sin(\phi)}{2+\cos(\phi)} \quad (74)$$

From (74), the locking range is restricted by the phase shift[30]

$$\Delta f = \frac{f_0}{2Q}\tan\left(\sin^{-1}\left(\frac{\eta}{2}\right)\right) \quad (75)$$

where f_0, Q, and η are the resonant frequency, quality factor of the LC tank, and the injection ratio (i_{inj}/I_{DC}) respectively.

Using Equations (71)-(75), a 25 GHz multi-knots Möbius-strips resonator based oscillator is designed and validated. ***Figure 19*** shows the circuit layout of tunable oscillator using multi-knots Möbius-strips resonators that support multi-injection nodes, thereby minimize detuning and provide a mechanism to suppress noise. The influence of phase-injection (perturbations) at different nodal points on the Möbius strips resonator are discussed for improving the tuning-range and phase noise performance of frequency generating circuits. The PCB is fabricated on an 8-mil thick Rogers substrate with a dielectric constant of 2.2.

As shown in Figure 19, the Möbius strips resonator increases evanescent mode field energy conservation due to the invariance of solutions for strips under a 2π rotation with a definite handedness. The resonator coupling coefficient β_j depends upon the geometry of the perturbation:

$$\beta_j = \left[\left(\frac{\int \varepsilon E_a \cdot E_b dv}{\sqrt{\int \varepsilon E_a^2 dv \int \varepsilon E_{bd}^2 dv}}\right)_e + \left(\frac{\int \mu H_a \cdot H_b dv}{\sqrt{\int \mu H_a^2 dv \int \mu H_b^2 dv}}\right)_m\right] \quad (76)$$

where E_a and H_a are the electric and magnetic field produced by the Möbius strip, and Eb and Hb are the corresponding fields due to perturbation of nearby adjacent resonators. The subscripts 'e' and 'm' denote electrical and magnetic coupling.

The oscillator circuit works with a DC bias of 5 Volts and 68 mA. Measured output power is typically -6 dBm. ***Figure 20*** shows measured phase noise of -109 dBc/Hz at 10 kHz offset with an output power of 6.73 dBm and 500 kHz tuning. The major drawback of this topology is limited tuning and mode-jumping.

For practical applications, output power, frequency stability, and tuning range need to be improved. These problems can be partially or fully fixed by understanding the phasor relationship between ring and Möbius strip resonator. ***Figure 21*** shows the typical representation of ring and Möbius strips resonators, and the equivalent LC representation consisting of inductors and capacitors along the transmission line. By virtue of the Möbius transformation, strips exhibit large group-delays, well suited for microwave resonator applications.

The electric currents on the ring resonator in ***Figure 21c*** can be formulated by a periodic boundary condition of the form described by

$$I_{j+k} = I_j \quad (77)$$

where I_k represents the electric current around the n^{th} closed loop on the periodic ladder structure of k-elements. The boundary condition of the general form shown in (77) governs that I_k is a conserved quantity that gives invariance to solutions under a 2π rotation with a definite handedness. The non-dissipative wave equation of the LC network for the k^{th} element is

$$I_k = A_1 e^{\left(\frac{p2\pi kM}{k}\right)} + A_2 e^{-\left(\frac{p2\pi kM}{k}\right)} \quad (78)$$

$$\left(\omega^2 - \frac{1}{LC}\right)I_k - \left(\gamma\omega^2 - \frac{1}{2LC}\right)(I_{k+1} + I_{k-1}) = 0 \quad (79)$$

$$\omega^2 = \left\{\frac{2\sin^2\left(\frac{p\pi}{k}\right)}{LC\left(1 - 2\gamma\cos\frac{2p\pi}{k}\right)}\right\} \quad (80)$$

where p is an integer specifying the normal mode and γ is the mutual coupling coefficient (mutual inductance 'M'=2γL). From (77)-(80), for even value of k, there are k-1 eigenvalues, including (k-2)/2 degenerate doublets and one singlet.

A typical ring resonator, whose eigenfunctions satisfy (17), defines a distinct inner and outer surface of the ring, shown in ***Figure 21a***. Figure 21c shows a topological transforma-

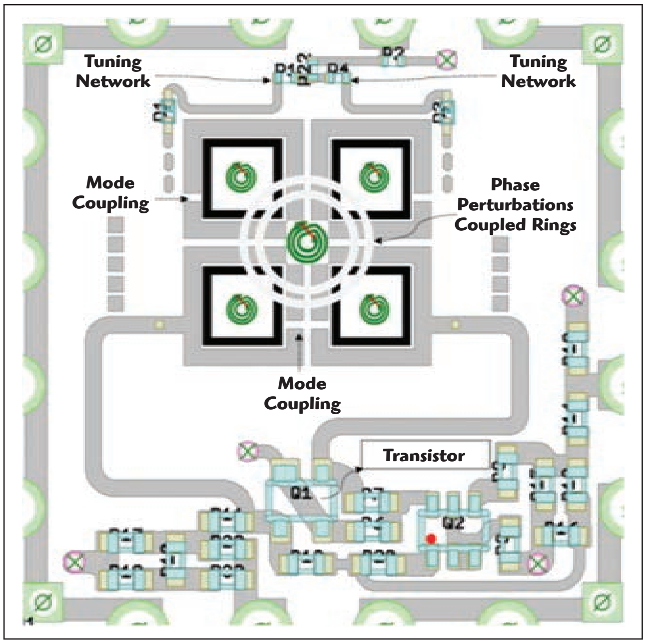

▲ *Fig. 19 Typical layout of 25 GHz oscillator using Möbius coupled resonator.*

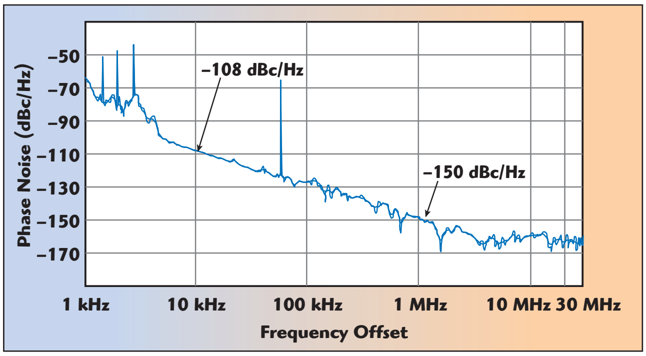

▲ *Fig. 20 Measured phase noise of the 25 GHz oscillator shown in Fig. 19.*

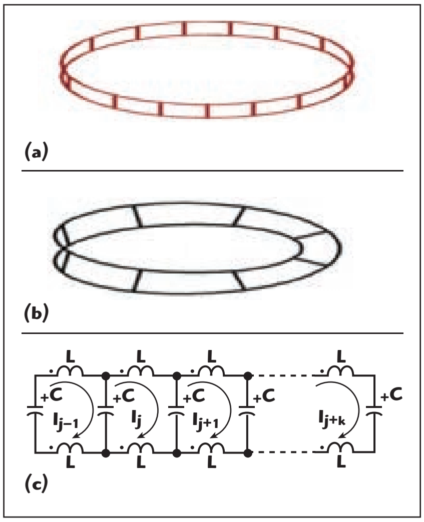

▲ *Fig. 21 Ring resonator (a) Möbius strip (b) and equivalent LC representation consisting of L and C along the transmission line (c).*

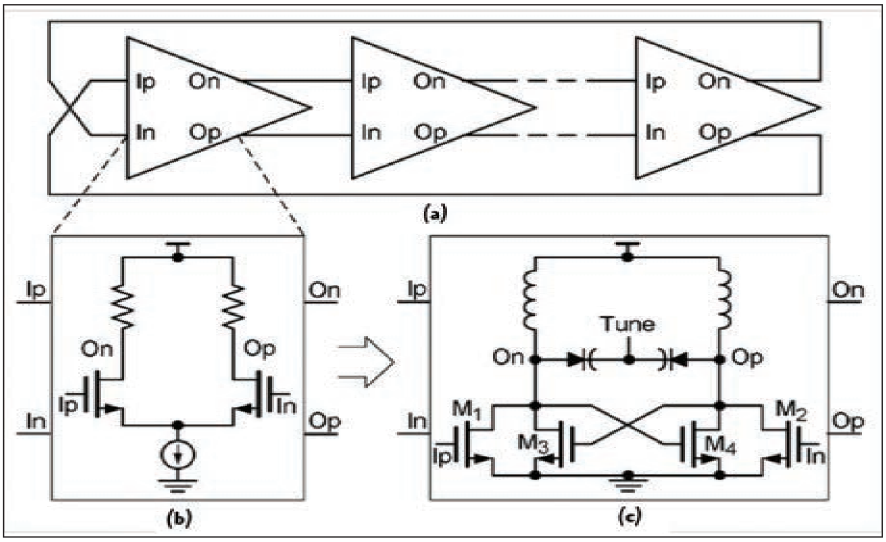

▲ *Fig. 22 Ring oscillator structure (a) active gain stage (b) and LC-boosted gain stages (c).*[32]

tion resulting in a Möbius strip resonator, whose current dynamics formulated by applying twisted boundary condition as

$$I_{j+k} = -I_j \tag{81}$$

From (81), a simple topological transformation on the resonator ring (see ***Figure 21b***) results in a sign reversal of current (I_j) upon a 2π rotation of the solutions, and a 4π rotation is now required for invariance of the eigenfunctions. Note that the eigenfunctions satisfying the condition for twisted boundary are of the same form as (77) provided that the mode indices are given half-integral values (p = 1/2, 3/2, 5/2,…(k-1)/2) relative to a ring consisting of identical components. The dispersion relation for the Möbius ring is the same as (80), however, the wave-vectors are shifted by

$$\Delta\lambda = -\left(\frac{\pi}{k}\right) \tag{82}$$

From (80)-(81), the two distinct topologies shown in Figures 21a and 21b can be considered a complementary pair related by a single transformation. The eigenfunctions of the Möbius resonator form an orthogonal basis set, presenting an interesting possibility for the design of metamaterials for multi-phase oscillator circuits. The inherent multi-phase, multi-mode nature of the Möbius strip provides additional degrees of freedom relative to traditional designs for generating multi-phase and quadrature oscillators. These are essential modules of many electronic systems, such as image rejection demodulators in wireless transceivers, half-rate clock-data-recovery (CDR) circuitry in high-speed optical receivers, phased-arrays, direct-conversion transmitters, and fractional-N frequency synthesizers.

Figures 22a and ***22b*** show a typical ring oscillator. It exhibits multi-phase but it suffers from high phase noise.[31] The LC-boosted ring oscillator shown in Figures 22a and **22c** minimizes the noise but is still inferior to a single-stage LC oscillator, largely due to the tradeoff between phase noise and phase error. Strong coupling between the gain stages (implying large-coupling MOSFETs) can minimize the phase errors; however, large coupling MOSFETs increase noise and power consumption.[31] In all multiphase LC oscillator configurations, MOSFETs play a dual role; they compensate LC tank energy loss and they couple LC tanks together to maintain a desired phase relation.[32] The second role, however, deteriorates phase noise, especially 1/f (flicker) noise upconversion.[33]

These problems can be partially, or fully, overcome by replacing the MOSFETs with metamaterial Möbius connected high order LC ring resonators in a distributed topology, as shown in ***Figure 23***. The resonant frequency of metamaterial (-ve index) LC-ring resonators increases with the number of stages N as compared to right-handed (+ve index) LC-ring resonators. Therefore, the metama-

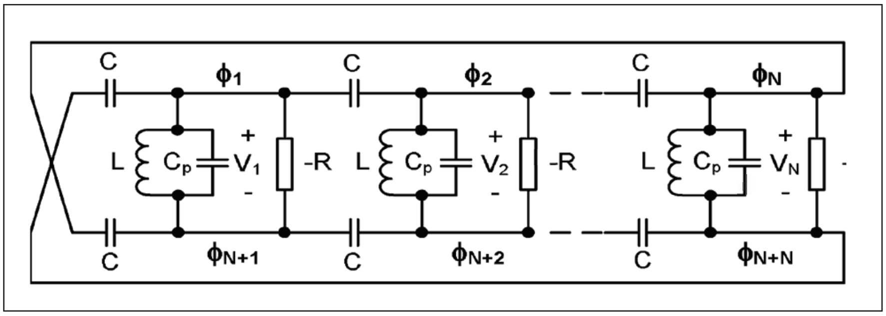

▲ *Fig. 23 Typical negative index Möbius connected LC-ring oscillator.*[33]

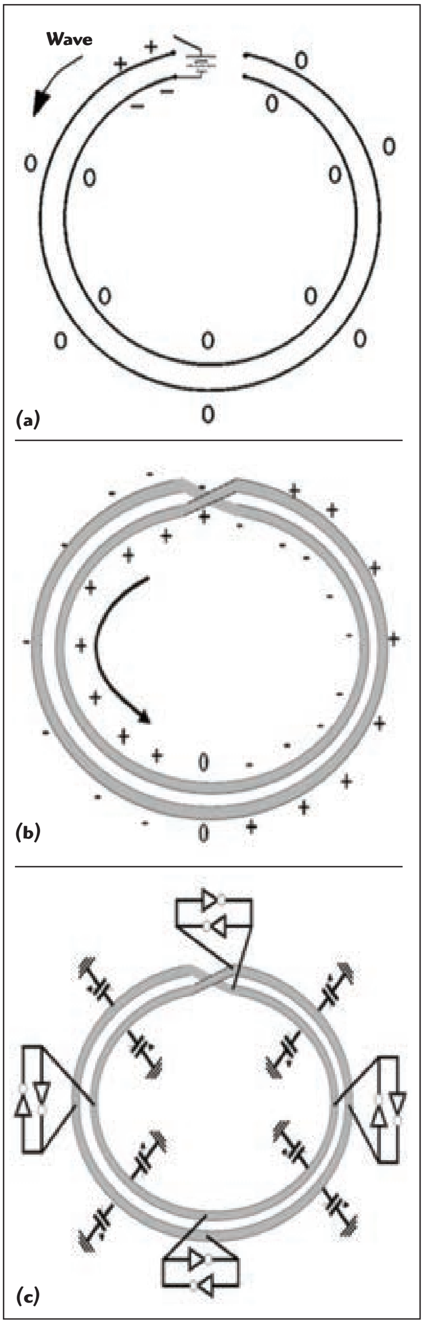

▲ *Fig. 24 Oscillation based on the Möbius effect: open loop differential ring (a) Möbius connected differential ring (b) and practical tunable Möbius connected differential oscillator circuit (c).*[37]

terial LC-ring resonator is well suited for high frequency generation. The MOSFETs act as negative resistance generating devices, needed only for compensating the losses of the LC-ring resonators, implying that current from the MOSFETs is always injected into the resonator in phase with the voltage and does not resonate with LC resonator components. For an N-stage distributed LC-ring oscillator, the phase noise scales as 1/N, while the power consumption increases linearly with N. This allows synthesizing multi-phases, while maintaining the identical figure of merit (FoM) as a 1-stage LC oscillator.[34]

The main challenges of these topologies are mode selection and maintaining desired phase relationships. In addition, the number of noise sources increases linearly with N; the total phase noise should be proportional to 1/N, but this no longer holds under large signal drive level conditions. The alternative approach is a wave-based Möbius oscillator. The energy recycling nature of Möbius strips allows very high frequency oscillation with minimal power consumption for a given class of frequency generating circuits.

Figures 24a and ***24b*** show the differential open ring and closed cross-connected ring, respectively. When the voltage source connected in Figure 24a is replaced by a cross-connection of the inner and outer conductors, it leads to a signal inversion. If there were no losses, a wave could travel on this differential ring indefinitely, providing a full clock cycle for every other rotation of ring through the Möbius effect.[35] In real applications, however, multiple anti-parallel inverter pairs are added to the line shown in ***Figure 24c*** to overcome losses and provide rotation lock in the Möbius connected differential ring.

Figure 25 shows the lumped equivalent of coupled stripline used for the

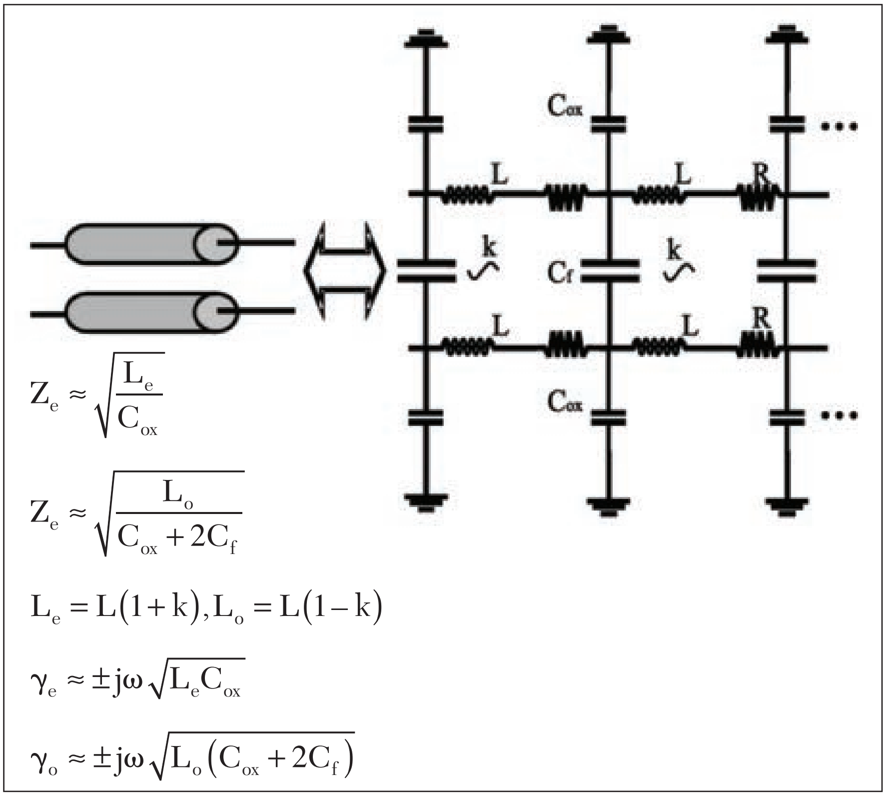

▲ *Fig. 25 Lumped representation of coupled stripline model (Z_e, Z_o are even and odd mode impedances; γ_e, γ_o are even and odd mode propagation constants; L_e, L_o are even and odd mode lengths).*[36]


TACONIC®
Finding a better way
EZ-IO
Nanotechnology Based PTFE Laminate
• DF @ 10 GHZ = 0.0012
• For emerging high speed digital and E/W frequencies
• Near FR-4 fabrication
fastRise™
Multilayer Non-Reinforced Prepreg
• DF @ 10 GHZ = 0.0014
• Low temperature thermosetting prepreg/ alternative to thermo-plastic film
• Lowest loss RF prepreg
Lowest Loss Materials for Multilayer, Power Amplifier & Rigid/Flex
RF-35TC
Thermally Conductive Low Loss Laminate
• DF @ 10 GHZ = 0.0011
• High adhesion to low profile coppers
• Diffuses heat away from transmission lines and surface mount components
TSM-DS3
Dimensionally Stable Low Loss Laminate
• DF @ 10 GHZ = 0.0011
• Enables large format high layer count PWBs
• Diffuses heat away from heat sources in PWBs
Scan for more information
www.4taconic.com
1-800-833-1805

Möbius ring described in Figure 24.[36] As shown in Figure 25, coupled lines support even and odd mode propagation. The even mode (fast wave mode) is when the two lines are excited with the same signal; as a result, the coupling capacitance C_f between the two lines has no effect on the propagation constant γ. The odd mode (slow wave mode), is obtained as the line pair is excited differentially, so the coupling capacitance between the two lines has a doubling effect on the propagation constant of this mode. For the resonator application, slow wave propagation is of interest and care must be taken to suppress even mode propagation.

Figure 26 shows the method for achieving stable oscillation. Inverters across the lines provide gain and theoretically force the line to operate differentially; varactor diodes and the center ring provide even mode cancellation.[35-37]

As shown in Figure 26, the Möbius effect enables energy harvesting (energy is not lost at each stage but re-circulates in closed path). While the benefits of Möbius connected wave-based oscillators are evident, this topology still has a limited tuning range of 10 to 20 percent. In this article, a novel approach for improving the tuning range is suggested and validated with the practical example of a 4 to 12 GHz/12 to 18 GHz oscillator based on a metamaterial Möbius strips resonator.

The phase-injections (perturbations) at different nodal points on the strips improve the tuning-range and phase noise performance of Möbius strip based frequency-generating circuits. The oscillator circuit shown in ***Figure 27*** works with a DC bias of 5 V and 35 mA; measured output power is typically 0dBm over the operating frequency band. The measured phase noise performance for a 12-18 GHz VCO is -130 dBc/Hz at 1 MHz frequency offset. It has a 6000 MHz tuning range with a phase noise variation within 3-5 dB over the operating frequency band.

The novel negative index Möbius oscillator (NIMO) circuit shown in ***Figure 28*** is built on an 8-mil thick substrate and uses a BFP740 SiGe-HBT transistor for providing negative resistance to compensate the losses of the resonator tank. The total DC power consumption is 680 mW (8 V at 85mA), including the buffer amplifier.

Figure 28 shows the typical schematic of 28.5 GHz NIMO circuit that uses a NIMS resonator as a tank network for improving evanescent mode coupled energy of the resonator tank module and a coupled SRR for mode locking and unwanted mode suppression. ***Figure 29*** shows the measured phase noise of -144dBc/Hz at 100 kHz offset with 10.56 dBm output power. The measured FOM at 1MHz is -226 dBc/Hz for 680 mW DC power consumption. The main drawback of this configuration is limited tuning (<5 percent) to compensate for frequency drift due to temperature.

For practical applications, the tuning range must be improved. The tuning capability of the NIMO circuit in Figure 28 is enhanced by incorporating phase-stabilization (manipulating the phase velocity by introducing a mode-suppression ring that allows multi-mode-phase-injection into the

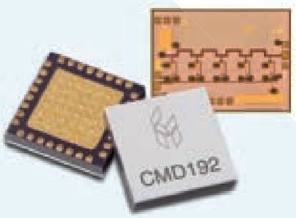

BroadRange™
Distributed Amps

- Frequency bands of DC to 20, DC to 30, and DC to 50 GHz
- OIP3 up to +38 dBm
- Gain from +9 to +20 dB
- Noise figures down to 1.9 dB

Keep pushing the limits. We'll keep pushing the range.

BroadRange Distributed Amplifiers™ from Custom MMIC provide unprecedented dynamic range for your boldest EW and SIGINT ideas. These proven MMICs come in die form or standard QFN packages and offer best-in-class performance for OIP3, gain stability, and noise figure across the broadest of bands. Several products feature a unique positive gain slope, and a positive bias, eliminating the need for equalizers and sequencing circuitry.

Download fully characterized datasheets and S-parameters, and start designing today.

CustomMMIC.com

Custom MMIC
Let Performance Drive

Mobius strips cavity). This introduces a Q-multiplier effect and an exponential rise in the Q-factor over the desired tuning range. ***Table 1*** shows several recently published papers to compare with this work based on FOM.

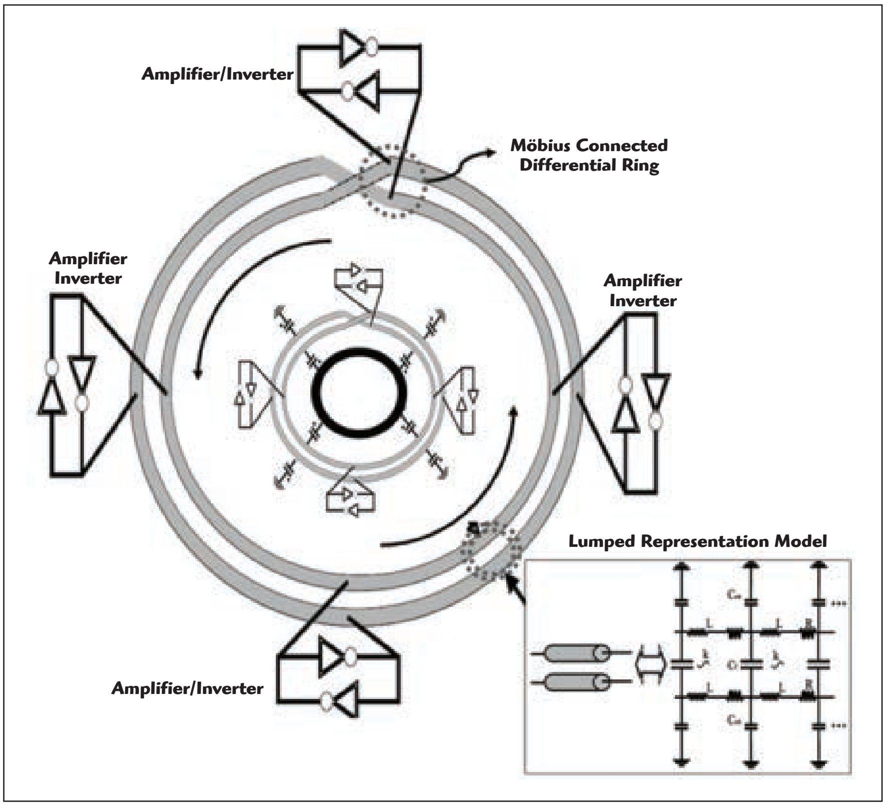

▲ *Fig. 26 Möbius connected rotary wave oscillator, with distributed coupled lines represented as the continuous limit of the multi-section lumped LC circuit.*

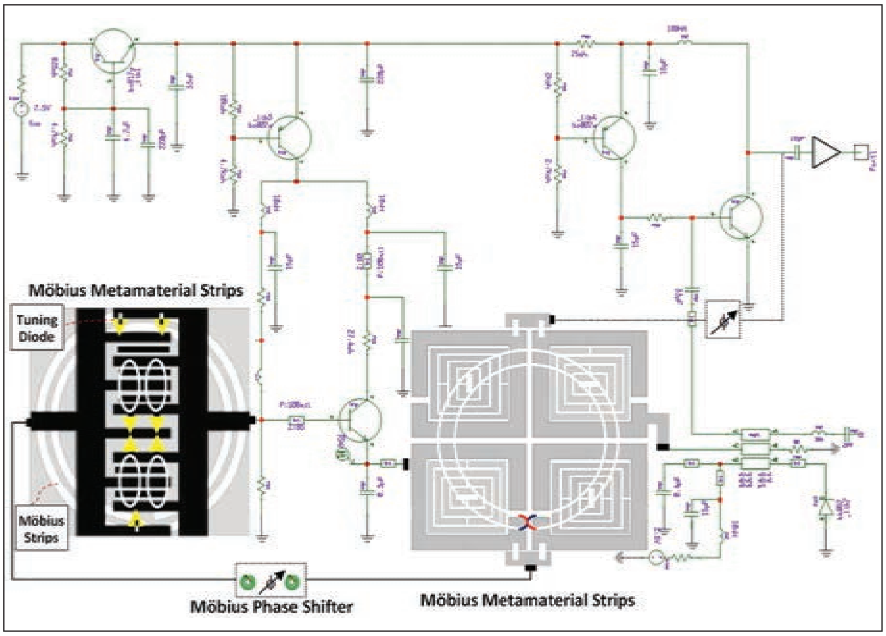

▲ *Fig. 27 Layout of a 12 to 18 GHz oscillator using an evanescent mode metamaterial Möbius strip resonator network realized using 8 mil RT/Duroid 5880 with ε_r = 2.2. The oscillator measures 0.75" × 0.75".*

Wireless and Wearable Electronics

Wireless and wearable implantable biomedical electronics are promising for the continuous real-time measurement of underlying physiological signals such as in electrocardiography,[43] electromyography,[44] and brain action potentials.[45] In these biomedical devices, wireless power and data telemetry are employed to prolong operational life with communication based on backscattering, which can run either without a battery or with just a single rechargeable battery.

Magneto-inductive telemetry is widely used in these devices for wireless power and data transfer. The typical inductive telemetry core consists of a pair of antenna/coils placed coaxially in space, one inside the device and one placed externally as part of the reader/interrogator. The external coil typically transmits data which is also harvested for its power and regulated to power up the implant circuitry. The antennas used for these telemetry systems are either loop wire coils or printed spiral coils. One of the most important design criteria is to maximize the coupling coefficient between external and implanted coils, which affects the power/data transfer efficiency significantly.

There has recently been an effort to use a metamaterial resonator for improved wireless energy transfer. Metamaterial resonators such as SRRs can exhibit strong magnetic resonance to EM waves,[46] with high Q factors. This makes them excellent candidates for near-field resonant power/data transfer. The SRR also enables sub-wavelength focusing of the incident energy at resonance in the capacitive gap of the metamaterial, which could be harvested for energy/power. Compared to a conventional antenna/coil system for power telemetry, the SRR provides a compact and low profile geometry due to an integrated antenna and resonator function built into the structure.[47]

Coupled mode theory (CMT)[48] predicts that when the resonances of both coils are matched, within the "strongly coupled regime," it results in maximal energy transfer between the coils. However, if the resonance of either of the coils deviates from one another, the power transfer efficiency drops sharply. Since the biological environment is expected to vary due to physiological changes, it is very hard to match their resonances. This issue is especially critical for metamaterial-based energy harvesters[49-50] due to their sharp narrowband resonances, thus automatic tuning of resonances is necessary. This can be done for conventional coils with tunable varac-

TechnicalFeature

tors;[51-52] however, the tuning needs precision, adds complexity in the system and may be difficult with motion artifacts. The alternative is to embed of non-foster impedance circuitry inside the SRR metamaterial to achieve optimal power transfer over a broad band without the need for any tuning.

Current wireless power transfer (WPT) technology allows power transfer only over a limited distance because, as the distance between the

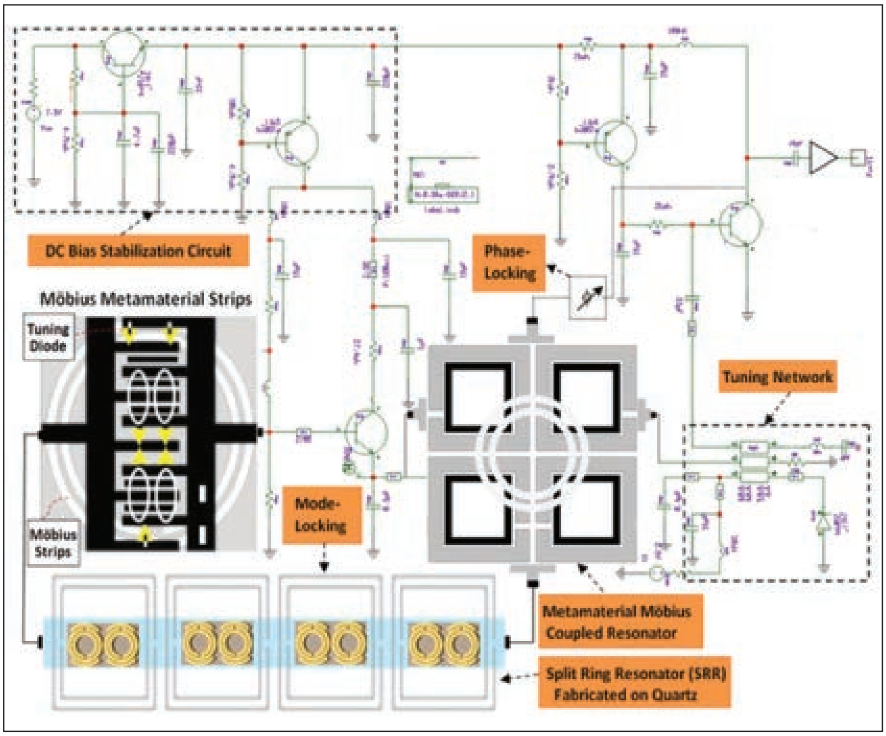

▲ *Fig. 28 28.5 GHz NIMO oscillator.*

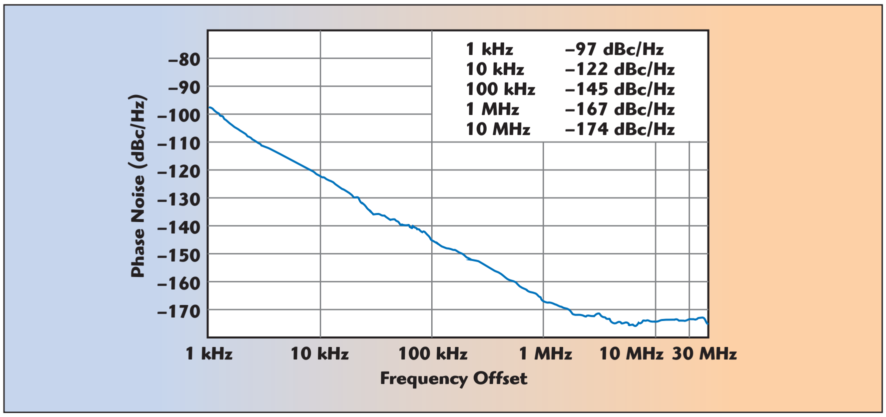

▲ *Fig. 29 Measured phase noise of the 28.5 GHz NIMO oscillator shown in Fig. 28.*

TABLE I

OSCILLATOR PERFORMANCE SUMMARY

Reference	f_0 (GHz)	P_{DC} (mW)	P_O (dBm)	Tuning (%)	L(f) (dBc/Hz)	FOM (dBc/Hz)
[38]	22.1	11	-11	20.6%	-109	-181
[39]	11.2	20	2.9	4.1%	-125	-193
[40]	12.4	30	7.0	2.5%	-122	-189
[41]	38.1	130	10.5	2.6%	-112	-183
[42]	28.3	15	0.3	-	-98.5	-176
This Work (Fig. 28)	28.5	680	10.6	1.8%	-167	-227

transmitter (Tx) and receiver (Rx) coils increases, the power transfer efficiency (PTE) decreases with a steep slope, while the electromagnetic field (EMF) leakage increases. In order to increase PTE and decrease EMF leakage simultaneously, we need a method to concentrate the magnetic fields between the Tx and Rx coils. In this article, we proposed a novel metamaterial structure to realize high efficiency and low EMF leakage. Metamaterial can confine the magnetic fields between the Tx and Rx coils by negative relative permeability, including the reduction in leakage. ***Figure 30*** shows a typical experimental setup for optimized efficiency of wireless power transfer.[53]

Artificial Gravitational Field

The generation of artificial gravitational fields with electric currents could in principle be detected through the induced change in space-time geometry that results in a purely classical deflexion of light by magnetic fields. Fuzfa 54 has proposed the experimental set-up shown in ***Figure 31*** that includes stacked large superconducting Helmholtz coils for the generation of the artificial gravitational field and the detection would be achieved by highly sensitive Michelson interferometers whose arms contain Fabry-Perot cavities to store light into the generated gravitational field. As depicted in Figure 31, the amplitude of the phase shift accumulated during the bouncing of light in the curved space-time generated by the magnetic field would reach, in a few months, the level of an astrophysical source of gravitational wave passing through ground-based GW observatories.[55] Since space-time is slightly shrunk inside the superconducting coils, light trapped inside the powered coil accumulates phase shift as round trips succeed each other. The sensitivity and dynamic range of superconducting coils can be increased by incorporating MMI superconducting coils. The ongoing research in the MMI field could open new eras in experimental gravity and laboratory tests of space-time bends based on equivalence principle of general theory of relativity.

Figure 32 illustrates the deflected trajectories of a bundle of rays of incoming parallel light from spatial infinity, these trajectories have been obtained from the numerical resolution of geodesic equations in strongly curved space-times around a loop of solenoids with extremely large magneto-gravitational coupling (CI) so that the way light is deflected can be easily shown. Deflections of trajectories are plotted with different values of solenoid length (L), radius of current loop (l) and magneto-gravitational coupling (CI) strength.[54]

MMI structures represent artificially engineered materials that can create and enable unique interactions of matter with electromagnetic and gravitational waves.

MMI Superconducting Coils

Superconductors offer unique advantages compared to ordinary metal, semiconductor and dielectric meta-atoms, namely: low loss, flux quantization and Josephson effects, quantum interactions between photons and discrete energy states in the

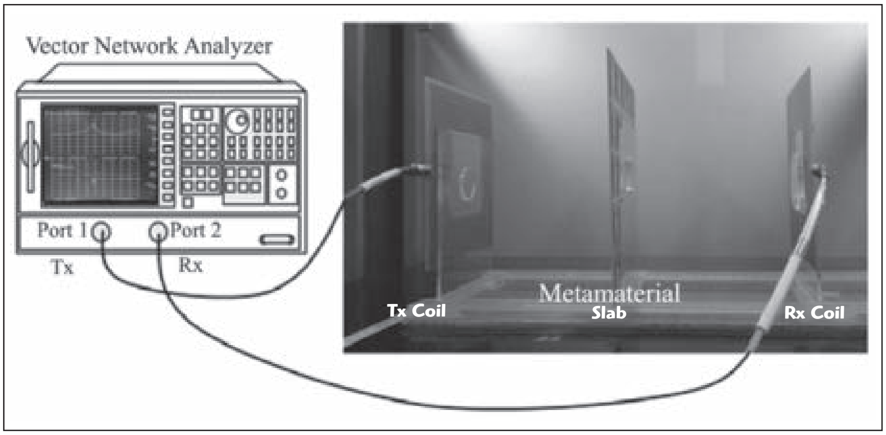

▲ *Fig. 30 Typical measurement setup for wireless power transfer efficiency.*[53]

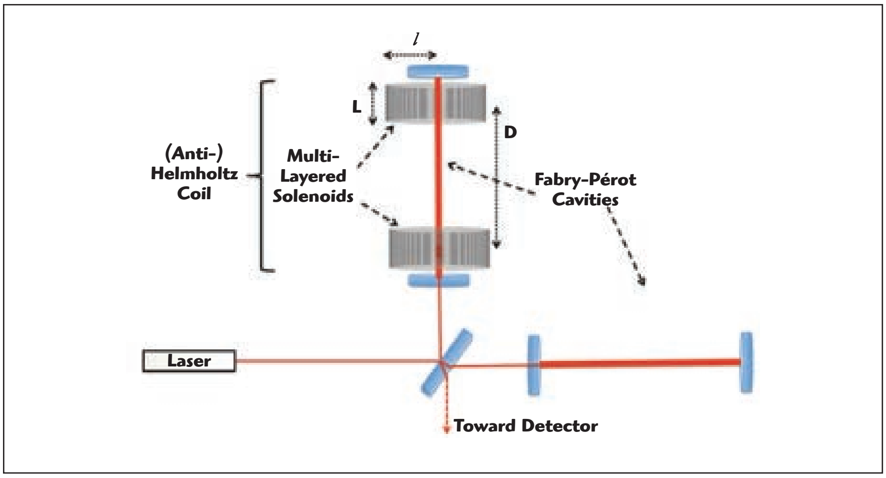

▲ *Fig. 31 Typical experimental setup for measuring gravitational waves.*[54]

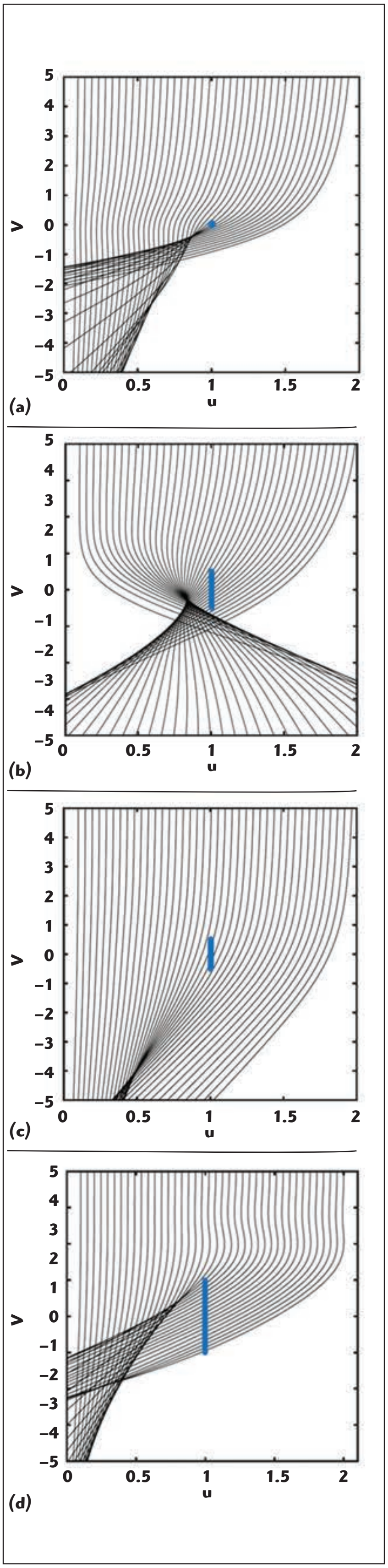

▲ *Fig. 32 Deflection of trajectories of parallel light rays coming from infinity. C_I = 10 and L >> l (a) C_I = 10 and L = 0.5l (b) C_I = 10 and L = l (c) and C_I =1 and L = 10l (d).*[54]

meta-atom, and strong diamagnetism.[56]

Figure 33 shows the typical symbolic representation of a superconducting metamaterial as a subset of meta-atoms and meta-molecules. Superconducting quantum metamaterial opens the possibility to explore collective quantum dynamics under very strong coupling between electromagnetic fields, gravitational field and artificial atoms.[57]

Metamaterial, where interaction strengths and length scales can be engineered, are a promising avenue for studying topological structure such as Möbius strips. Time-reversal broken topological metamaterial have been realized in the microwave domain via a lattice of chiral magnetic (gyrotropic) resonators.[58-59] ***Figure 34*** shows a typical Möbius metamaterial insulator, realized by connecting the left and right edges of the system with a half twist and a spin flip.[60]

As illustrated in ***Figure 34b***, "a" inductor j sites from the top of the left edge are connected to the "b" inductor at the j sites from the bottom of the right edge. The spin flip is necessary, as "up" spins propagate rightwards on the top edge but leftwards on the bottom edge.[61] Figure 34b shows the temporal dynamics of a spin-up excitation in the system; it propagates rightward along the system edge, until it reaches the other edge, is converted into a down spin, and continues its progression around the system perimeter; this cycle is repeated until the excitation is damped out by the finite system Q.

CONCLUSION

Part 2 discusses MMS resonator based topology that enables next generation energy efficient signal source solutions in integrated circuit and surface mounted planar technology. The unique features of Möbius metamaterial strips promise many future inventions, recurring in an endless loop – one could say that the future exists on a Möbius strips surface. Part 3 will follow in the July 2016 issue.■

- Amplifiers – Solid State
- Attenuators – Variable/ Programmable
- Couplers (Quadrature, 180° & Directional)
- Detectors – RF/Microwave
- DLVAs, ERDLVAs & SDLVAs
- DTOs, VCOs, PLO, DROs, & Frequency Synthesizers
- Filters & Switched Filter Banks
- Form, Fit, Functional Products & Services
- Frequency Discriminators & IFMs
- Integrated MIC/MMIC Assemblies (IMAs)
- IQ Vector Modulators
- Limiters – RF/Microwave
- Log Amplifiers
- Millimeter Wave Components (Up to 50 GHz)
- Miscellaneous Products
- Multifunction Integrated Assemblies (MIAs)
- Phase Shifters & Bi-Phase Modulators
- Power Dividers/Combiners (Passive & Active)
- Pulse Modulators (SPST)
- Rack & Chassis Mount Products
- Receiver Front Ends & Transceivers
- SDLVAs, ERDLVAs & DLVAs
- Single Side Band Modulators
- SMT & QFN Products
- Switch Matrices
- Switched Filter Banks
- Switches – Solid State
- Systems – Fly Eye Radars
- Threshold Detectors
- USB Products

Planar Monolithics Industries, Inc.

Solid State Multi-Throw Switches & Switch Matrices, DC to 50 GHz

PMI offers a full line of RF and Microwave, Solid-State Switches that range from DC to 50 GHz. A wide range of standard models with various options are available that include:

- SPST to SP128T Configurations.
- Reflective or Absorptive
- Hermetic Sealing
- High Reliability to MIL-STD-883
- Small Quantity Requirements Accepted
- Military or Stringent Screening
- Specialized Testing & Custom designs welcome!

Switch Matrix

Standard Models...

Model P20T-4G8G-80-T-515-SFF
Absorptive, SP20T PIN Diode Switch

Frequency	4.0 to 8.0 GHz
Isolation	80 dB Min - Measured 83.3 dB
Insertion Loss	4.0 dB Max - Measured 3.95 dB
VSWR In/Out	2.0:1 Max, 1.8:1 Typ
Input Power	100 mW Max CW (Hot Switchable)

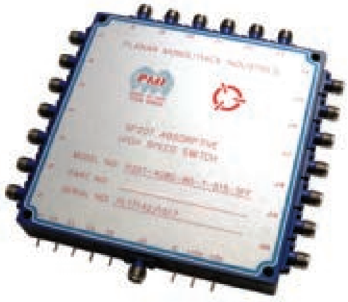

- **Package Size:** 4.0” sq x 0.63”
- **DC Voltage:** +5 VDC @ 144 mA, +15 VDC @ 160 mA
- **Switching Speed:** 100 ns Measured

Model P32T-0R5G18G-60-T-SFF
Absorptive, SP32T PIN Diode Switch

Frequency	0.5 to 18.0 GHz
Isolation	60 dB Min (0.5 - 2.0 GHz) 70 dB Min (2.0 - 18.0 GHz) - Measured 77.3 dB
Insertion Loss	9.5 dB Max - Measured 8.66 dB
VSWR In/Out	2.0:1 Max
Input Power	20 dBm CW Max (Operating)

- **Package Size:** 8.0” x 3.5” x 1.0”
- **DC Voltage:** +5 VDC @ 1470 mA, -5 VDC @ 100 mA
- **Switching Speed:** 85 ns Measured

West Coast Operation:
4921 Robert J. Mathews Pkwy, Suite 1
El Dorado Hills, CA 95762 USA
Tel: 916-542-1401
Fax: 916-265-2597

East Coast Operation:
7311-F Grove Road
Frederick, MD 21704 USA
Tel: 301-662-5019
Fax: 301-662-1731

sales@pmi-rf.com • www.pmi-rf.com

ISO9001-2008 REGISTERED

References

1. D. R. Smith, S. Schultz, P. Markos and C. M. Soukoulis, "Determination of Effective Permittivity and Permeability of Metamaterials from Reflection and Transmission Coefficients," *Physical Review B*, Vol. 65, No. 19, April 2002, pp. 195104-1-5.
2. D. R. Smith, D. C. Vier, T. Koschny, and C. M. Soukoulis, "Electromagnetic Parameter Retrieval from Inhomogeneous Metamaterials," *Physical Review E*, Vol. 71, No. 3, March 2005, pp. 36617-1-11.
3. U. C. Hasar and J. J. Barroso, "Retrieval Approach for Determination of Forward and Backward Wave Impedances of Bianisotropic Metamaterials," *Progress In Electromagnetics Research*, Vol. 112, 2011, pp. 109–124.
4. J. B. Pendry, A. J. Holden, D. J. Robbins and W. J. Stewart, "Low Frequency Plasmons in Thin-Wire Structures," *Journal of Physics: Condensed Matter*, Vol. 10, No. 22, June 1998, pp. 4785–4809.
5. R. Marqués, F. Medina and R. Rafii-El-Idrissi, "Role of Bianisotropic in Negative Permeability and Left-Handed Metamaterials," *Physical Review B*, Vol. 65, No. 14, April 2002, pp. 144440-1-6.
6. A. M. Nicolson and G. Ross, "Measurement of the Intrinsic Properties of Materials by Time-Domain Techniques," *IEEE Transactions on Instrumentation and Measurement*, Vol. 19, No. 4, November 1970, pp. 377–382.
7. W. B. Weir, "Automatic Measurement of Complex Dielectric Constant and Permeability at Microwave Frequencies," *Proceedings of the IEEE*, Vol. 62, No. 1, January 1974, pp. 33–36.
8. V. Milosevic, B. Jokanovic and R. Bojanic, "Effective Electromagnetic Parameters of Metamaterial Transmission Line Loaded With Asymmetric Unit Cells," *IEEE Transactions on Microwave Theory and Techniques*, Vol. 61, No. 8, August 2013, pp. 2761–2772.
9. L.D. Landau, L. P. Pitaevskii and E.M. Lifshitz, *Electrodynamics of Continuous Media*, 2nd ed. Oxford, U.K.: Pergamon, 1984.
10. J. W. Graham, "*Arbitrary Oriented Biaxial Anisotropic Media: Wave Behaviors and Microstrip Antennas*," Ph.D. Dissertation, Syracuse University, May 2012.
11. T. Koschny, P. Markoš, E. N. Economou, D. R. Smith, D. C. Vier, and C. M. Soukoulis, "Impact of Inherent Periodic Structure on Effective Medium Description of Left-Handed and Related Metamaterials," *Physical Review B: Condensed Matter*, Vol. 71, No. 24, June 2005, pp. 245105-1-22.
12. A. Alù, "Restoring the Physical Meaning of Metamaterial Constitutive Parameters," *Physical Review B, Condensed Matter*, Vol. 83, No. 8, February 2011, pp. 081102-1-4.
13. L. Chen, Z. -Y. Lei, R. Yang, X. -W. Shi and J. Zhang, "Determining the Effective Electromagnetic Parameters of Bianisotropic Metamaterials with Periodic Structures," *Progress In Electromagnetics Research M*, Vol. 29, 2013, pp. 79–93.
14. X. Chen, T. M. Grzegorczyk, B. -I Wu, J. Pacheco, Jr. and J. A. Kong, "Robust Method to Retrieve the Constitutive Effective Parameters of Metamaterial," *Physical Review E*, Vol. 70, No. 1, July 2004, pp. 16608-1-7.
15. U. L. Rohde and A. K. Poddar, "Möbius Metamaterial Inspired Next Generation Circuits and Systems," *Microwave Journal*, Vol. 59, No. 5, May 2016.
16. X. Chen, B. -I. Wu, J. A. Kong and T. M. Grzegorczyk, "Retrieval of the Effective Constitutive Parameters of Bianisotropic Metamaterial," *Physical Review E*, Vol. 71, No. 4, April 2005, pp. 046610.
17. R. Marqués, F. Martín, M. Sorolla, *Metamaterial with Negative Parameters: Theory, Design and Microwave Applications*, Wiley, 2008.
18. O. Sydoruk1, E. Tatartschuk1, E. Shamonina1 and L. Solymar, "Analytical Formulation for the Resonant Frequency of Split Rings," *Journal of Applied Physics*, Vol. 105, No. 1, January 2009, pp. 14903.
19. X. Chen, T. M. Grzegorczyk and J. A. Kong, "Optimization Approach to the Retrieval of the Constitutive Parameters of a Slab of General Bianisotropic Medium," *Progress In Electromagnetics Research*, Vol. 60, 2006, pp. 1–18.
20. Z. Li, K. Aydin and E. Ozbay, "Determination of the Effective Constitutive Parameters of Bianisotropic Metamaterials from Reflection and Transmission Coefficients," *Physical Review E*, Vol. 79, No. 2, February

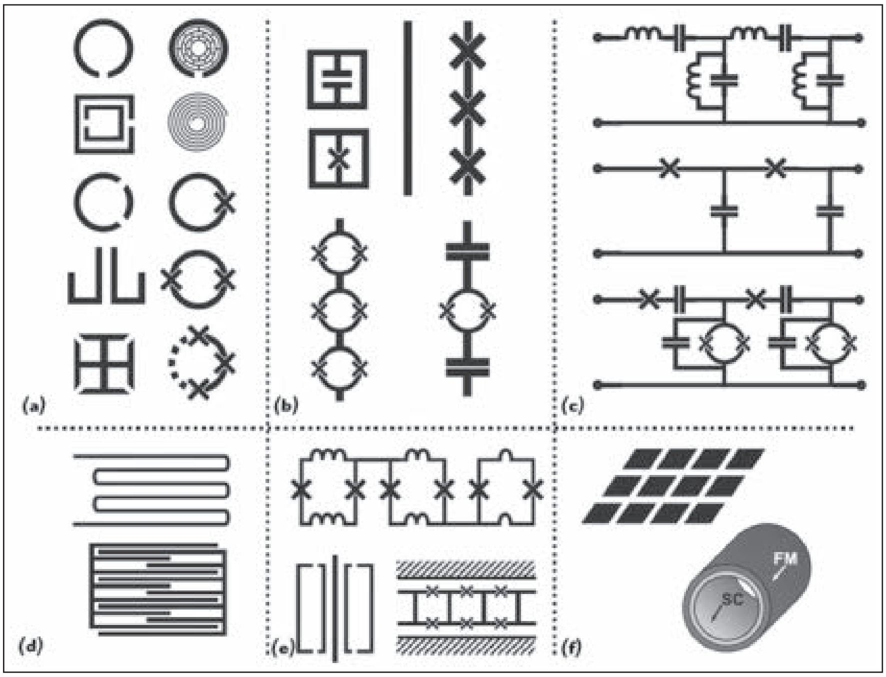

▲ *Fig. 33 Typical symbolic representation of a superconducting metamaterial as a subset of meta-atoms and meta-molecules: magnetically active meta-atoms (a) electrically active meta-atoms (b) transmission line metamaterials (c) lumped element meta-atoms (d) various meta-molecule realizations (e) and DC magnetic cloak structures (f).*[57]

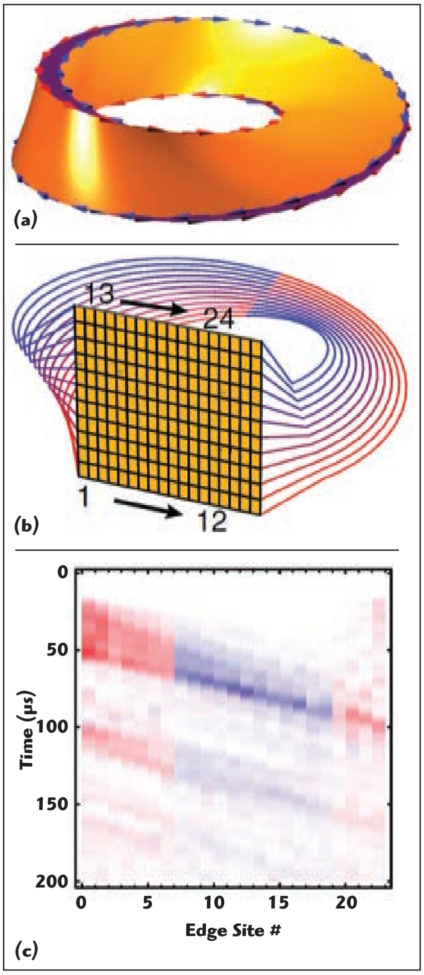

▲ *Fig. 34 Typical topological Möbius metamaterial insulator: Möbius TI, with the arrow indicating the edge propagation direction, color the spin state (a) connectivity of the Möbius TI, with metamaterial PCB and external connections generating the topology indicating spin on traversing the edge (b) and spin-resolved detection of edge transport after excitation of ↑. ↑ and ↓ intensities are plotted in the red and blue channels, respectively, showing the conversion from ↑ to ↓ when the excitation moves from one edge to the other (c).*

2009, pp. 026610-1-7.
21. U. C. Hasar, "Procedure for Accurate and Stable Constitutive Parameters Extraction of Materials at Microwave Frequencies," *Progress In Electromagnetics Research*, Vol. 109, 2010, pp. 107–121.
22. J. Wang, S. Qu, J. Zhang, H. Ma, Y. Yang, C. Gu and X. Wu, "A Tunable Left-Handed Metamaterial Based on Modified Broadside-Coupling Split-Ring Resonators," *Progress In Electromagnetics Research* Letters, Vol. 6, 2009, pp. 35-45.
23. T. Nakamura, T. Masuda, N. Shiramizu, A. Nakamura and K. Washio, "A 11.1-V Regulator-Stabilized 21.4-GHz VCO and a 11.5% Frequency-Range Dynamic Divider for K-Band Wireless Communication," *MTT-Transactions*, Vol. 60, No. 9, September 2012, pp. 2823–2832.
24. Z. Chen, W. Hong, J. Chen and J. Zhou, "Design of High-Q Tunable SIW Resonator and its Application to Low Phase Noise VCO," *IEEE Microwave and Wireless Components Letters*, Vol. 23, No. 1, January 2013, pp. 43–45.
25. A. Collado, F. Mira and A. Georgiadis, "Mechanically Tunable Substrate Integrated Waveguide (SIW) Cavity Based Oscillator," *IEEE Microwave and Wireless Components Letters*, Vol. 23, No. 9, September 2013, pp. 489-491.
26. C. -L. Chang, C. -H. Tseng and H. -Y. Chang, "A New Monolithic Ka-Band Filter-Based Voltage Controlled Oscillator Using 0.15um GaAs PHEMT Technology," *IEEE Microwave and Wireless Components Letters*, Vol. 24, No. 2, February 2014, pp. 111–113.
27. Y. Chen, K. Mouthaan and F. Lin "Design of X-band and Ka-band Colpitts oscillators Using a Parasitic Cancellation Technique," *IEEE Transactions on Circuits and Systems-I*, Vol. 57, No. 8, August 2010, pp. 1817–1828.
28. Ulrich L. Rohde and Ajay K. Poddar, "Möbius Metamaterial Inspired Next Generation Circuits and Systems," *Microwave Journal*, Vol. 59, No. 5, May 2016.
29. A. Poddar, Slow Wave Resonator Based Tunable Multi-Band Multi-Mode Injection-Locked Oscillator, Habil Thesis, BTU Cottbus, Germany, 2014.
30. S. A. Marvel, R. E. Mirollo and S. H. Strogatz, "Identical Phase Oscillators with Global Sinusoidal Coupling Evolve by Möbius Group Action," *Chaos: An Interdisciplinary Journal of Nonlinear Science*, Vol. 19, No. 4, December 2009, pp. 043104-1-4.
31. E. Martens, "*Cooperative Behavior in Networks of Coupled Oscillators*," Ph.D. Diss., Faculty of the Grad School of Cornell University, May 2009.
32. A. Rofougaran, J. Rael, M. Rofougaran and A. Abidi, "A 900 MHz CMOS LC Oscillator with Quadrature Outputs," *IEEE International Solid State Circuits Conference Digest*, February 1996, pp. 392–393.
33. L. Guansheng, E. Afshari, "A Low Phase Noise Multi-Phase Oscillator Based on Left-Handed LC-Ring," *IEEE Journal of Solid State Circuits*, Vol. 45, No. 9, September 2010, pp. 1822–1833.
34. L. Romano, A. Bonfanti, S. Levantino, C. Samori and A. L. Lacaita, "5-GHz Oscillator Array with Reduced Flicker Up-Conversion in 0.13-um CMOS," *IEEE Journal of Solid State Circuits*, Vol. 41, No. 11, November 2006, pp. 2457–2467.
35. J. Wood, T. C. Edwards and Steve Lipa, "Rotary Travelling-Wave Oscillator Arrays: a New Clock Technology," *IEEE Journal of Solid State Circuits*, Vol. 36, No. 11, November 2001, pp. 1654–1665.
36 . H.T. Ahn and D. J. Allstot, "A 0.5-8.5-GHz Fully Differential CMOS Distributed Amplifier," *IEEE Journal of Solid State Circuits*, Vol. 37, No. 8, August 2002, pp. 985–993.
37. D. Ham and W. Andress, "A Circular Standing Wave Oscillator," *IEEE Solid State Circuits Conference Digest*, Vol. 1, February 2004, pp. 380–533.
38. T. Nakamura, T. Masuda, N. Shiramizu, A. Nakamura and K. Washio, "A 1.1-V Regulator-Stabilized 21.4-GHz VCO and a 11.5% Frequency-Range Dynamic Divider for K-Band wireless communication", *IEEE Transactions on Microwave Theory and Techniques*, Vol. 60, No. 9, September 2012, pp. 2823-2832.
39. Z. Chen, W. Hong, J. Chen and J. Zhou, "Design of High-Q Tunable SIW Resonator and its Application to Low Phase Noise VCO," *IEEE Microwave and Wireless Components Letters*, Vol. 23, No. 1, January 2013, pp. 43–45.
40. A. Collado, F. Mira and A. Georgiadis, "Mechanically Tunable Substrate Integrated Waveguide (SIW) Cavity Based Oscillator," *IEEE Microwave and Wireless Components Letters*, Vol. 23, No. 9, September 2013, pp. 489–491.
41. C. -L. Chang, C. -H. Tseng and H. -Y Chang, "A New Monolithic Ka-Band Filter-Based Voltage Controlled Oscillator Using 0.15um GaAs PHEMT Technology," *IEEE Microwave and Wireless Components Letters*, Vol. 24, No. 2, February 2014, pp. 111–113.
42. Y. Chen, K. Mouthaan and F. Lin "Design of X-Band and Ka-Band Colpitts Oscillators Using a Parasitic Cancellation Technique," *IEEE Transactions on Circuits and Systems-I*, Vol. 57, No. 8, August 2010, pp. 1817–1828.
43. J. Riistama, E. Aittokallio, J. Verho and J. Lekkala, "Totally Passive Wireless Biopotential Measurement Sensor by Utilizing Inductively Coupled Resonance Circuits," *Sensors and Actuators A: Physical*, Vol. 157, No. 2, February 2010, pp. 313-321.
44. D. J. Young, "Wireless Powering and Data Telemetry for Biomedical Implants," International Conference of the *IEEE Engineering in Medicine and Biology Society*, September 2009, pp. 3221–3224.
45. W. Biederman, D. J. Yeager, N. Narevsky, A. C. Koralek, J. M. Carmena, E. Alon and J. M. Rabaey, "A Fully-Integrated, Miniaturized (0.125 mm^2) 10.5 μW Wireless Neural Sensor Solid-State Circuits," *IEEE Journal of Solid State Circuits*, Vol. 48, No. 4, April 2013, pp. 960–970.
46. V. G. Veselago, "The Electrodynamics of Substances with Simultaneously Negative Values of ε and μ," Sov Phys Uspekhi, Vol. 10, No. 4, 1968, pp. 509–514.
47. R. A. Shelby, D. R. Smith and S. Schultz, "Experimental Verification of a Negative Index of Refraction," *Science*, Vol. 292, No. 5514, April 2001, pp. 77-79.
48. A. Kurs, A. Karalis, R. Moffatt, J. D. Joannopoulos, P. Fisher and M. Soljačić, "Wireless Power Transfer via Strongly Coupled Magnetic Resonances," *Science*, Vol. 317, No. 5834, July 2007, pp. 83–86.
49. A. M. Hawkes, A. R. Katko S. A. Cummer, "A Microwave Metamaterial with Integrated Power Harvesting Functionality," *Applied Physics Letters*, Vol. 103, No. 16, October 2013, p. 163901.
50. O. M. Ramahi, T. S. Almoneef, M. Alshareef and M. S. Boybay, "Metamaterial Particles for Electromagnetic Energy Harvesting," *Applied Physics Letters*, Vol. 101, No. 17, October 2012, p. 173903.
51. J. M. Wilson, R. Bashirullah, D. P. Nackashi, D. A. Winick, B. E. Duewer and P. D. Franzon, "Design of Rotating MEMS Tunable Capacitors for use at RF and Microwave Frequencies," *Proceedings of the SPIE*, Vol. 4593, 2001, pp. 186–197.
52. A. S. Y. Poon and M. Taghivand, "Supporting and Enabling Circuits for Antenna Arrays in Wireless Communications," *Proceedings of the IEEE*, Vol. 100, No. 7, July 2012, 2207–2218.
53. Y. Cho, J. J. Kim, D. -H. Kim, S. Lee, H. Kim, C. Song, S. Kong, H. Kim, C. Seo, S. Ahn and J. Kim, "Thin PCB-Type Metamaterial for Improved Efficiency and Reduced EMF Leakage in Wireless Power Transfer Systems," *IEEE Transactions on Microwave Theory and Techniques*, Vol. 64, No. 2, February, 2016 pp. 353-364.
54. A. Fuzfa, "How Current Loops and Solenoids Curve Space-Time," *Physical Review D*, V3, December 2015.
55. W. Chaibi, R. Geiger, B. Canuel, A. Bertoldi, A. Landragin and P. Bouyer, "Low Frequency Gravitational Wave Detection With Ground Based Atom Interferometer Arrays," *Physical Review D*, January 2016.
56. S. M. Anlage, "The Physics and Applications of Superconducting Metamaterials," *Journal of Optics*, Vol. 13, No. 2, April 2010.
57. P. Jung, A. V. Ustinov and S. M. Anlage, "Progress in Superconducting Metamaterials," *Superconductor Science Technology*, Vol. 27, May 2014.
58. Z. Wang, Y. D. Chong, J. D. Joannopoulos and M. SoljaSoljačić, "Reflection-Free One-Way Edge Modes in a Gyromagnetic Photonic Crystal," *Physical Review Letters*, Vol. 100, No. 1, February 2008.
59. Z. Wang, Y. Chong, J. D. Joannopoulos and M. Soljacic, "Observation of Unidirectional Backscattering-Immune Topological Electromagnetic States," Vol. 461, No. 7265, October 2009, pp. 772–775.
60 J. Ningyuan, C. Owens, A. Sommer, D. Schuster and J. Simon, "Time- and Site-Resolved Dynamics in a Topological Circuit," *American Physical Society*, Vol. 5, No. 2, June 2015.
61. L. T. Huang and D. H. Lee, "Topological Insulators on a Mobius Strip," *Physical Review B*, Vol. 84, No. 19, November 2011.

INVITED PAPER

In-Device Coexistence Interference

Abinash Sinha, Reiner Stuhlfauth and Fernando Schmitt
Rohde & Schwarz, Munich, Germany

An emerging trend in mobile communications is the parallel usage of multiple radio technologies in mobile devices, tablets and other communications modules. In order to support this parallel operation, the devices are equipped with multiple radio transceivers, which are located extremely close to each other. When the different radio technologies operate simultaneously these transceivers interfere with each other resulting in in-device coexistence (IDC) interference. This article describes the IDC interference problem involving LTE (Band 7) and WLAN (2.4 GHz) technology and evaluates the performance of two different mitigation techniques used to reduce the interference effect.

With the increasing demand to have ubiquitous and seamless data connectivity to several wireless networks, modern day devices are designed to support different radio access technologies (RAT). These devices, e.g., mobile phones, tablets and various other communications modules are capable of supporting different cellular as well as non-cellular communications standards at the same time. For instance, a mobile phone might be connected to a wireless local area network (WLAN)[1] router for Internet access in parallel to an established long term evolution (LTE)[2] call.

Due to the small size of these devices, the transceivers of different radio technologies are located very close to each other. As a result, when these collocated radio transceivers operate concurrently in the same or adjacent frequency bands, it leads to potential interference between their operations known as in-device coexistence interference. IDC interference affects the receiver sensitivity, thereby degrading the quality of the wanted signal or resulting in the loss of data.

This article discusses the challenge of reducing IDC interference while multiple RATs are operating simultaneously. Reducing IDC interference would prevent degradation of the signal quality without disconnecting the interfering radio signal. The article highlights the coexistence scenario between LTE and WLAN, where LTE Band 7 uplink affects the WLAN 2.4 GHz channels, and discusses possible solutions to mitigate IDC interference. First, the cause of IDC interference is described then the different frequency bands where IDC interference occurs are considered, along with the different RATs involved.

Next, the methodology for calculating the desensitization value is discussed, including a description of a possible test setup required to carry out the measurements. After that, it analyzes the use of two different mitigation techniques in order to reduce IDC interference for

The Smart Choice for Small Spaces

Coilcraft is the brand engineers trust most when specifying tiny inductors for wearable technology

Boost the performance and battery life of your wearable products with these tiny RF and power inductors from Coilcraft:

- Wirewound chip inductors as small as 0201 size for wireless communications
- Shielded power inductors as thin as 0.71 mm for power management
- Coupled inductors as small as 2.2 x 1.45 mm for LED display drivers

You can get started by using our suite of web tools to quickly locate the perfect inductors for your design. Compare and analyze multiple parts based on your true operating conditions, and then order free evaluation samples with just a click.

Learn why we're the biggest name in ultra-miniature inductors. Visit us at **www.coilcraft.com.**

Coilcraft®

WWW.COILCRAFT.COM

coilcraftdirect.com
No min order. Next day delivery.

the different LTE-WLAN use case scenarios and assesses the measurement results. Finally, the article's contribution is summarized along with some further possible enhancements and future applications of this work.

IN-DEVICE COEXISTENCE PROBLEM AND SCENARIOS

As the term 'in-device' suggests, such interference arises due to the proximity of transceivers of different radio technologies that are situated on the same platform. Consequently, when these different RATs operate simultaneously in the same or adjacent frequency bands, the transmitter of one technology acts as the aggressor/interferer and affects the other technology's receiver, which behaves as the victim. There are three main causes of this adverse effect:

- Need of multiple radio technologies for ubiquitous connectivity and limited spectrum availability that leads to concurrent operation of these different radio technologies in close frequency range.
- Undesirable emissions such as spurious emissions, out-of-band emissions, spectral harmonics and intermodulation products from the aggressor transmitter[3] that fall in the frequency range of the victim receiver.
- Inability of the filters at the transceivers of different RATs to properly filter out the unwanted signal due to the overlapping of transition bands of the different radio technologies.[4]

Eventually, all these effects add up to increase the noise level of the victim receiver, thus reducing receiver sensitivity and leading to receiver blocking or desensitization. ***Figure 1*** illustrates an example of IDC interference where LTE, global positioning system (GPS), Bluetooth (BT) and WLAN transceivers are situated on the same device. When the LTE transmitter is operating it affects the GPS, BT and WLAN receivers and similarly, the BT and WLAN transmitters affect the LTE receivers due to the proximity of the transceivers and operation in the same or adjacent frequency range.

The IDC interference scenario has gradually spread in the field of wireless communications and users are inadvertently experiencing such interference while using their communications devices. Some common day-to-day scenarios where the users might experience this interference include usage of LTE and WLAN portable routers, LTE and WLAN offloading, LTE voice over Internet protocol (VoIP) calls, multimedia and other possible applications such as Bluetooth headsets, etc.

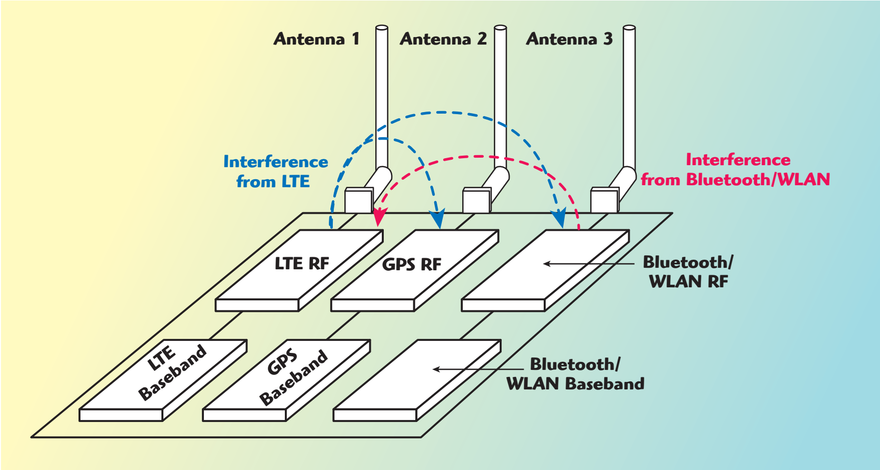

▲ *Fig. 1 The close proximity of LTE, Bluetooth, WLAN and GPS radios makes the device vulnerable to coexistence interference.*[5]

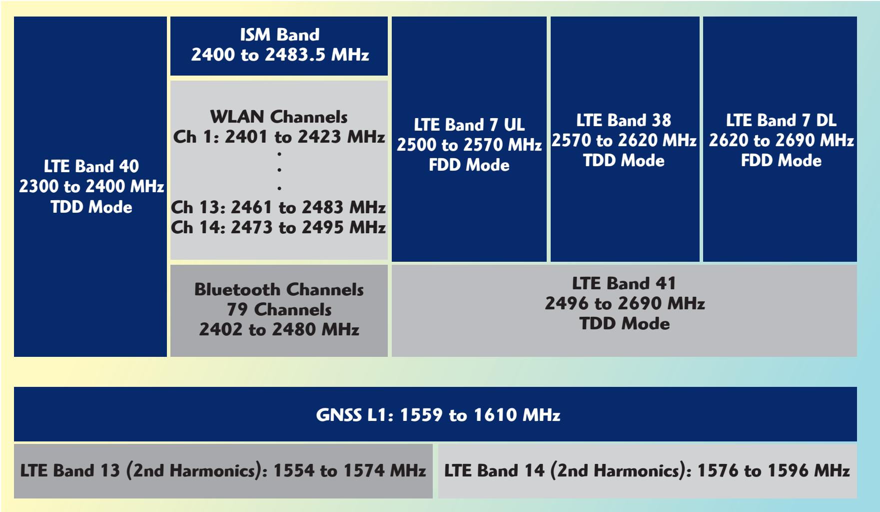

▲ *Fig. 2 3GPP frequency bands surround the ISM band used for WLAN and Bluetooth.*

As mentioned, one of the main reasons for IDC interference is limited availability of frequency spectrum for simultaneous operation of several RATs. Such a situation can be observed in the 2.4 GHz industrial, scientific and medical (ISM) frequency bands lying in between the 3GPP frequency bands, resulting in adjacent operational frequencies with small or no guard band between various RATs.[5]

As illustrated in ***Figure 2***, WLAN and Bluetooth technologies operate in the ISM Band, where the lower boundary of this band is adjacent to LTE Band 40 operating in TDD mode and the upper boundary is near the uplink frequency region of LTE Band 7 (operating in FDD mode), with a band gap of approximately 20 MHz.[5] Since LTE Band 40 is working in TDD mode, the transmitter of LTE Band 40 affects WLAN and Bluetooth receiver operation and similarly, the WLAN and Bluetooth transmitters affect the functionality of the LTE band 40 receiver.

Likewise, the uplink frequency of LTE Band 7 affects WLAN and Bluetooth reception since the Band 7 uplink is situated close to the ISM band. Another coexistence scenario occurs between the navigation satellite system and LTE frequency Bands 13 and 14 as shown in Figure 2, where the receivers of the navigation system are affected by the 2nd harmonics of LTE Bands 13 and 14 uplink frequen-

Leading Global Communications

PP10-10/-11 0.1µm Power pHEMT

- 0.1µm high performance power / low noise process
- 50µm and 100µm thickness are standard
- Useable gain to 110GHz
- 4V operation - Psat > 800mW/mm, > 50% PAE, and 13dB Gain at 29GHz

PP10 Transfer Curve

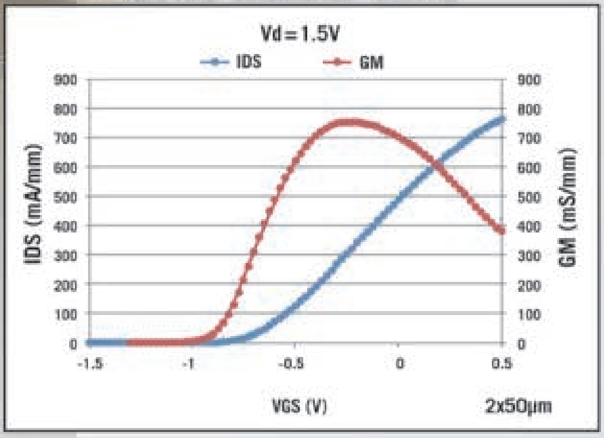

PP10 I-V Curves

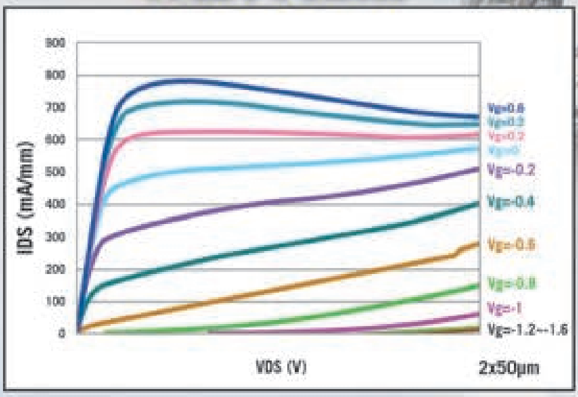

PP10 Load Pull Data

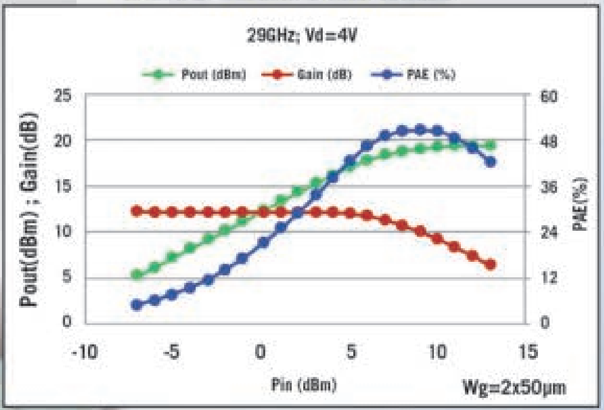

PP10 Max Gain

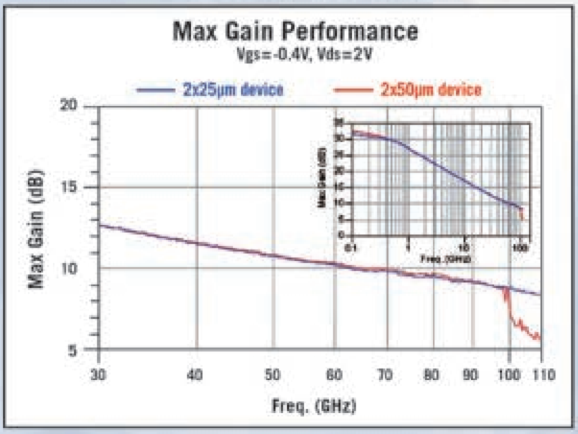

WIN SEMICONDUCTORS CORP. Tel:+886-3-397-5999 Fax:+886-3-397-5069 http://www.winfoundry.com

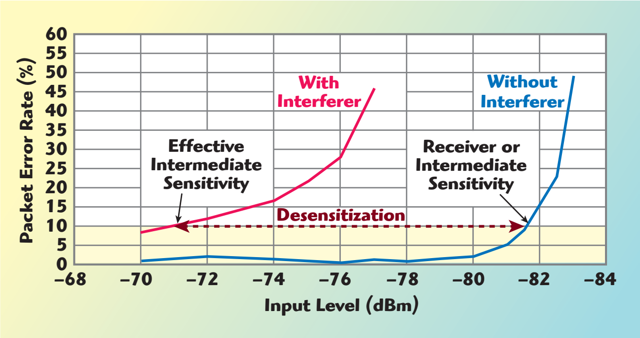

▲ *Fig. 3 Packet error rate measurement, with and without interfering signal.*

cies. The uplink frequencies of LTE Bands 13 and 14 operate in the range of 777 to 787 MHz and 788 to 798 MHz respectively, and the 2nd harmonics of these LTE Bands fall in the operational frequency range of global navigation satellite system (GNSS) receivers being used for commercial civil purposes,[4,5] thereby causing interference.

METHODOLOGY AND TEST SETUP

The influence of IDC interference on the operation of different RATs can be analyzed using the desensitization value of the receiver being affected. This desensitization value is based on the receiver's sensitivity performance, which is measured first in the absence of the interfering signal and then again in the presence of the interfering signal as shown in ***Figure 3***.

It illustrates a packet error rate (PER) measurement scenario where the x-axis represents the power level being received at the receiver in dBm and the y-axis represents the PER value in percentage. As the power level is reduced, the PER value starts increasing, which is shown by the gradual increase in the slope of the curves or the knee of the curves, and the power level at which the PER value reaches 10 percent is defined as the sensitivity of the receiver. Using this receiver's sensitivity, two different types of receiver power levels or sensitivity terms can be defined – receiver or intermediate sensitivity and effective intermediate sensitivity, which can be used later to determine the desensitization value of the receiver as depicted in Figure 3.

Receiver or intermediate sensitivity is the receiver power level that corresponds to the 10 percent PER value measured in the absence of any interfering signal. Similarly, the power level corresponding to the 10 percent PER value measured in the presence of an interfering signal is known as effective intermediate sensitivity. Finally, the difference between these two receiver sensitivity parameters defines the desensitization value as shown in the following equation:[6]

Desensitization Value = Effective Intermediate Sensitivity Level - Intermediate Sensitivity Level

A prototype test setup for IDC interference measurement and analysis can be put together using the test setup shown in ***Figure 4***. Since most radiocommunications in a real-world scenario takes place over the air (OTA), the IDC interference analysis and measurements were carried out OTA. The wideband radio communication tester was used to generate two different radio signals, i.e. WLAN and LTE signals on different RF channels as required and interfering signals. The DUT was placed in an isolated environment, e.g., inside a shield box in order to isolate the device from any external interfering signals.

The two radio signals were combined using a coupler and fed to the antenna coupler board of the RF shield box using RF cables. The radio links established via the communication tester were bidirectional in order to generate the victim and aggressor radio signals and to measure not only the DUT receiver characteristics of the victim technology but also the DUT transmitter quality of the aggressor technology.

The entire setup was controlled using a sequencer software tool, which was installed on a laptop or PC and managed the operations of wideband radio communication tester via SCPI commands. In order to control the DUT placed inside the shield box, a USB connection was established between the DUT and the controller laptop that enabled the software to manage the DUT's operation using Android Debug Bridge (ADB) commands.

MITIGATION TECHNIQUES AND RESULTS

In order to analyze the IDC interference effect of LTE Band 7 uplink on WLAN, the first and foremost step was to establish a proof of concept. To implement such a concept, most of the RAT parameters were selected in a way so as to simulate a severe interference scenario between the two radio technologies. The following approaches were considered:

- The two RATs, i.e., LTE acting as the aggressor technology and WLAN as the victim technology, were placed as close as possible to each other in the frequency domain.
- The RAT causing interference was configured to transmit at maximum power level.

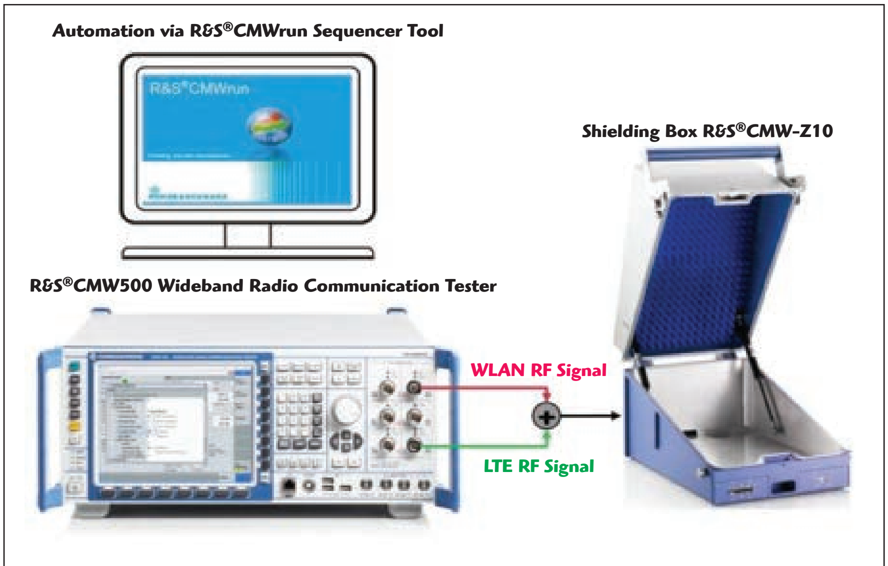

▲ *Fig. 4 One test setup for performing in-device coexistence interference measurements.*

TABLE 1
LTE AND WLAN PARAMETERS (LTE THE AGGRESSOR)

LTE Parameters	Values	WLAN Parameters	Values
Frequency Band	Band 7	Frequency Channel	13
Operational Mode	FDD	Frequency	2472 MHz
Cell Bandwidth	20 MHz	Transmit Burst Power	–45 dBm
RS EPRE (dBm/15 KHz)	–85 dBm	Operating Mode	SISO AP
Downlink Frequency	2630 MHz	Standard	802.11g/n
# RB on Downlink	100	Modulation Scheme	16 QAM ¾
Uplink Frequency	2510 MHz	Data Rate	36 Mbps
# RB on Uplink	100		
Connection Type	Test Mode		
Scenario	Single-Input-Single-Output (SISO)		
Uplink Power Control	Closed Loop		
Maximum Uplink Transmit Power	23 dBm		

TABLE 2
PARAMETERS FOR WLAN PER MEASUREMENT

Parameter	Values
Modulation Scheme	16 QAM ¾
Data Rate	36 Mbps
Number of Packets	1000
Payload Size (Bytes)	1000
Interval Between Packets (ms)	10

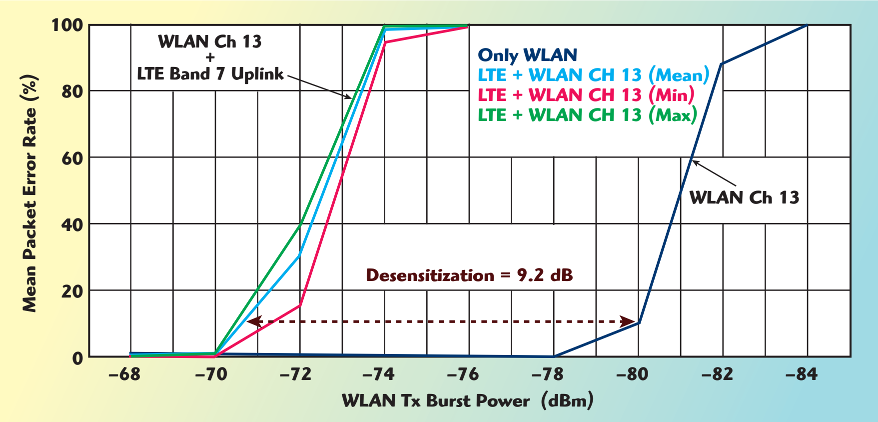

▲ *Fig. 5 WLAN Channel 13 (f_C = 2472 MHz) desensitization by LTE Band 7 uplink (f_C = 2510 MHz), with an uplink transmit power of 23 dBm.*

- Continuous or heavy traffic was generated by the interfering RAT.

First, the WLAN connection was set up using the parameters in ***Table 1*** and the PER value was measured as a factor to determine the sensitivity performance of the DUT's WLAN receiver. The details of the parameters used for the PER measurement are in ***Table 2***. The WLAN receiver inside the DUT was able to receive most of the packets efficiently as sent by the WLAN access point (AP), even when the transmit power of the AP was low at around -80 dBm as illustrated by the 'Only WLAN' curve in ***Figure 5***.

The LTE connection was then established as per the parameters defined in Table 1, and the WLAN PER measurements were carried out once more in order to study the effect of the interference. When the PER measurements were carried out again in the presence of the LTE signal, the error value showed a sudden increment at a much higher transmit power of the WLAN AP at around -71 dBm, illustrated by the 'LTE + WLAN Ch 13 (mean)' curve shown in Figure 5. Finally, the desensitization of the WLAN receiver caused by the IDC interference from LTE Band 7 uplink was measured using the difference in sensitivity level of the two PER curves, and calculated as shown in the following equation.

Desensitization Value = Effective Intermediate Sensitivity Level – Intermediate Sensitivity Level

= (-70.64 dBm) – (-79.84 dBm)

= 9.2 dB

Once the IDC interference effect between LTE and WLAN was detected, the next step was to analyze the various possible mitigation techniques that might help in reducing the interference effect. One way to avoid IDC interference is to increase the band gap between the aggressor technology and the victim radio technology.[4,5,7] In other words, the victim radio technology is moved away from the interfering radio technology or vice-versa, to another frequency range that lies a certain band gap away. Due to an increment in the band gap between the two radio technologies, the transition bands of these technologies do not overlap even if these two RATs are operating at the same time.

As a result, the RF filters are able to properly distinguish between the wanted and unwanted signals, thereby

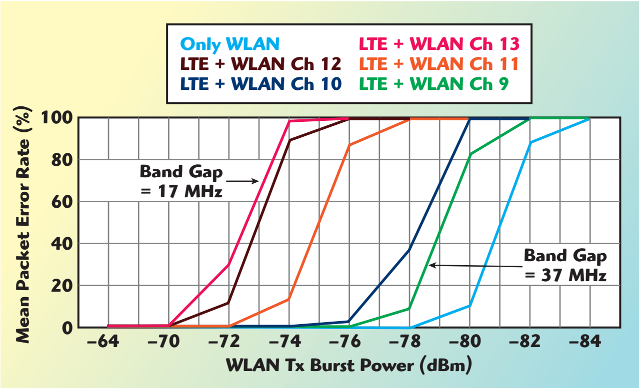

▲ *Fig. 6 WLAN frequency shifting with the LTE Band 7 uplink (f_C = 2510 MHz with 23 dBm transmit power) acting as the aggressor.*

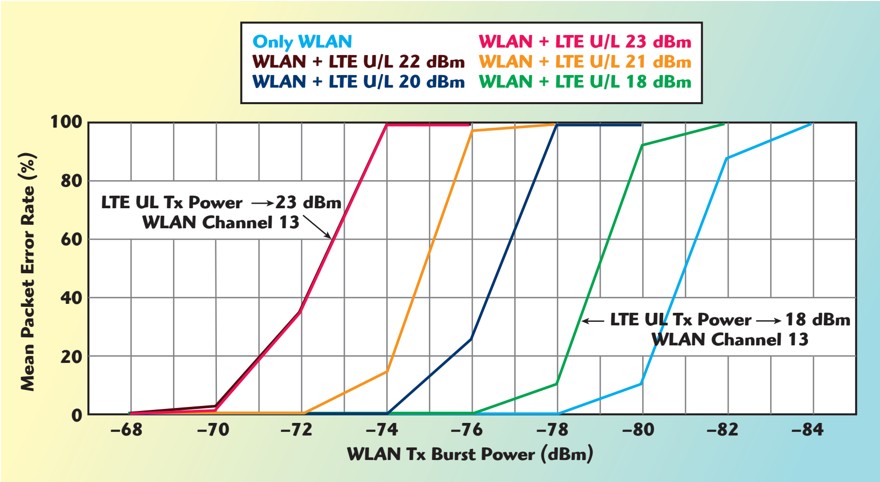

▲ *Fig. 7 LTE transmit power control with LTE Band 7 uplink (f_C = 2510 MHz) acting as the aggressor for WLAN Channel 13 (f_C = 2472 MHz).*

reducing the impact of IDC interference. ***Figure 6*** illustrates this mitigation technique, where the various colored curves represent the different frequency channels of WLAN operating simultaneously with the LTE Band 7 uplink signal. As the WLAN frequency channel is gradually shifted away from the LTE uplink carrier frequency, the band gap increases between the LTE and WLAN signals, leading to a comparatively reduced interference effect.

IDC interference can also be suppressed by reducing the signal strength of the interfering signal. Unwanted transmitter emissions such as out-of-band emissions, intermodulation products and spurious emissions are directly related to the transmit power, i.e. the higher the transmit power, the higher the magnitude of these emissions, resulting in more interference. Furthermore as mentioned earlier, these unwanted emissions from the interfering RAT reduce the sensitivity of the victim RAT's receiver, leading to suppression of the wanted signals or loss of data at the receiver end. In order to reduce the effect of IDC interference, one possible solution is to reduce the transmit power of the aggressor technology.

Figure 7 represents an IDC interference scenario where LTE Band 7 uplink acts as the main source of interference for the WLAN receiver. The IDC interference effect can be reduced by decreasing the LTE uplink power, eventually reducing unwanted emissions. The various colored curves in Figure 7 depict the different power levels of the LTE Band 7 uplink signal operating concurrently with WLAN receiver operations. As the LTE uplink power level is reduced, the unwanted emissions from the LTE end also decrease, resulting in comparatively less interference.

In addition to the mitigation techniques mentioned above, there are a few more approaches that might reduce the IDC interference effect. One possible technique is to distribute or schedule the operational time between LTE and WLAN in such a way that the transmission time of one technology does not coincide with the reception time of another technology. In this way, even if these two technologies were operating in the same or adjacent frequency bands, they would not interfere with each other.[4,5,7] Another method is to shift the resource blocks (RB) allocated to the UE for LTE uplink data transmission to a frequency range away from the WLAN technology. In other words, the RBs that are situated far away from the operational frequency of WLAN are used for data transmission on the LTE uplink and downlink. This increases the band gap between LTE and WLAN, thereby improving the filtering performance of the RF filters.

The aforementioned techniques offer a promising effect in mitigating IDC interference between LTE and WLAN, yet these mitigation techniques have their own limitations. The selection of a particular mitigation technique depends upon the combinations of the RATs, which defines the RAT acting as the aggressor or interferer technology and the RAT acting as the victim technology. It also

Need to speed up your testing ?
Try our Push- and Slide-Ons !

The products mate with any standard SMA, N, TNC, 7/16

Spectrum
Elektrotechnik GmbH

when Quality is needed

80905 Munich, Germany **P.O. Box 450533**
Telephone: +49-89-3548-040 **Facsimile: +49-89-3548-0490**
www.spectrum-et.com **Email: sales@spectrum-et.com**

depends on the ease of implementation of these techniques considering the state-of-the-art features of the two technologies. Techniques such as reducing the transmit power reduces the interference effect by reducing the LTE uplink power level. However, the LTE uplink power is high only when the channel quality is bad, for example the UE might be inside a tunnel, in the basement of a building or at the cell edge.

Subsequently, reducing the uplink transmit power in order to reduce the IDC interference effect might actually result in the LTE call being dropped or a reduction in data throughput. The frequency shifting technique reduces the interference effect by increasing the band gap between the two radio technologies. However, the biggest challenge lies in the availability of frequency spectrum as there might be a scenario where no frequency range is free or where all the frequency channels are experiencing interference from another radio technology. Similarly, modifying the relative position of RB in the allocation grid or scheduling the operational time of different RATs could also be used to reduce the interference effect.

However, the implementation of these techniques would depend upon the availability of the subcarriers for shifting the RB and on data throughput plus the delay restrictions while scheduling the operational time.

CONCLUSION

The growing number of wireless devices equipped with multiple RAT transceivers is being driven by the increasing user demand and the stringent requirements of new applications and services that necessitate the operation of several RATs in parallel. Simultaneous operation of these collocated RAT transceivers in the same or adjacent frequency bands results in IDC interference and loss of useful data. This article discussed different techniques that might help mitigate this interference effect. However, these techniques have some drawbacks and are still being discussed in 3GPP before being implemented in the LTE protocol layers.

Analysis of IDC interference and possible solutions to mitigate such interference would be quite instrumental in manufacturing wireless chipsets and devices, the innovative Internet of Things (IoT) scenario – especially machine-to-machine (M2M) communications, the automotive industry and futuristic communications technologies that would involve using multiple RATs in the same communications channel.

NOTE:

1. The IDC measurement results shown in this article are device-specific and may vary from one device to another.
2. All the measurements were executed five times in order to obtain an average value.
3. The PER measurements were carried out with a receiver power step size of 2 dB, thereby resulting in sharp edges of the PER measurement curves. A higher granularity of power steps would have resulted in a longer measurement time. ■

References

1. IEEE Standards Association, "IEEE 802.11TM: Wireless LANs," October 2015, www.standards.ieee.org/about/get/802/802.11.html.
2. 3GPP A Global Initiative, "LTE Technology Overview," October 2015, www.3gpp.org/technologies/keywords-acronyms/98-lte.
3. ITU-R Radiocommunication Sector of ITU, "Unwanted Emissions in the Spurious Domain," Recommendation ITU-R SM.329-12, 09/2012.
4. Zhenping Hu, R. Susitaival, Zhuo Chen, I-Kang Fu, P. Dayal and S.K. Baghel, "Interference Avoidance for In-device Coexistence in 3GPP LTE-Advanced: Challenges and Solutions," *IEEE Communications Magazine*, Vol. 50, Issue 11, pp. 60–67, November 2012.
5. 3GPP, Technical Specification Group Radio Access Network, Evolved Universal Terrestrial Radio Access Network (E-UTRA), "Signaling and Procedure for Interference Avoidance for In-device Coexistence," Release 11, 3GPP TR 36.816 v11.2.0 (2011-12).
6. Detlev Liebl and Bernard Schulz, "LTE and Bluetooth In-device Coexistence with WLAN," Application Note, 1MA255, Rohde & Schwarz, 2015.
7. S.K. Baghel, M.A. Ingale and G. Goyal, "Coexistence Possibilities of LTE with ISM Technologies and GNSS," National Conference on Communications 2011 (NCC), pp. 1–5.
8. Abinash Sinha, Prof. Dr. Wolfgang Kellerer, Reiner Stuhlfauth, Fernando Schmitt, and Thomas Feddersen, "Master's Thesis: Analysis of In-Device Coexistence Interference," Rohde & Schwarz and Technische Universität München, October 2015.

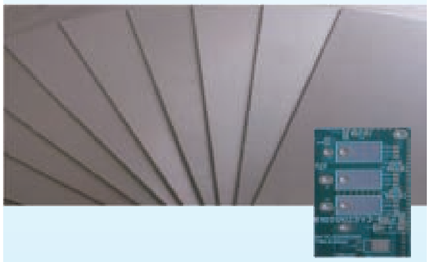

INVITED PAPER

Solving Mobile Radar Measurement Challenges

Dingqing Lu
Keysight Technologies, Santa Rosa, Calif.

Modern radar systems are exceptionally complex, encompassing intricate constructions with advanced technologies from multiple engineering fields. Accurately detecting moving targets in these multifaceted environments is difficult, given the detrimental effects of interference on precision measurements. The adoption of a simulation technique provides a design-oriented value proposition of shortening the development period, saving time and money by avoiding unnecessary field tests. This measurement solution promises lower product risk, reduced cost, higher system performance, customization and ease of use. The following discussion examines an alternative simulation method that allows for better cross-domain modeling in a single framework, to capture the complete effects of modern radar system performance.

INCREASING ACCURACY, DECREASING COST

The interference involved in mobile radar measurements poses a large challenge for radar designers and operators. Any form of interference in the radar system floods the receiver with irrelevant and distracting noise or false information. This overload of unwanted data makes it impossible to analyze and measure the desired data. The system is essentially overrun with irrelevant information, and no essential data may be collected. In order to properly address these issues in mobile radar measurement, it is optimal to create a simulation of the scenario.

The use of a simulation allows for elimination of interference, guaranteeing accurate measurements. The scenario framework simulation (SFS) technique can be easily implemented, lessening the difficulties involved in testing. The use of the SFS technique presents a solution to the problems faced during the performance of mobile radar measurements. Expenditures are decreased, while accuracy and efficiency are boosted. Any scenario may be modeled, measured and accurately understood, enabling superior performance in the physical application of the scenario. The advantages of the SFS are:

- Models any system, including monostatic ground-based systems, more complex multistatic systems and phased arrays
- Supports motion of radar transmission and receiving platforms and targets
- Eliminates field testing costs, increasing efficiency and reducing test times.

Designing advanced radar systems is a challenge when one considers the complexity of the operating environment and the fact that these systems are becoming less reliant on tra-

ditional RF design and pushing more functionality in baseband signal processing and digital signal processing (DSP). The ability to model the complexity of the operating environment while accounting for the interaction between baseband, DSP, RF and antenna systems can be a real challenge with existing system-level engineering methodologies.

Further, it is vital that new systems capable of providing operational differentiation and advantages be deployed quickly. Not only does this provide tactical advantages, it also delivers economic advantages to the companies who can deploy systems most quickly and with the highest performance and capability. Radar designers demand a platform for testing radar receiver processing algorithms with the capability to handle complex operational environments. Simulation fulfills these demands and moves testing into the lab. The extensive expenses involved in field testing places a burden on the tester. The use of simulation promises not only the most accurate results, but also the least expensive and most expedient path to accurate data.

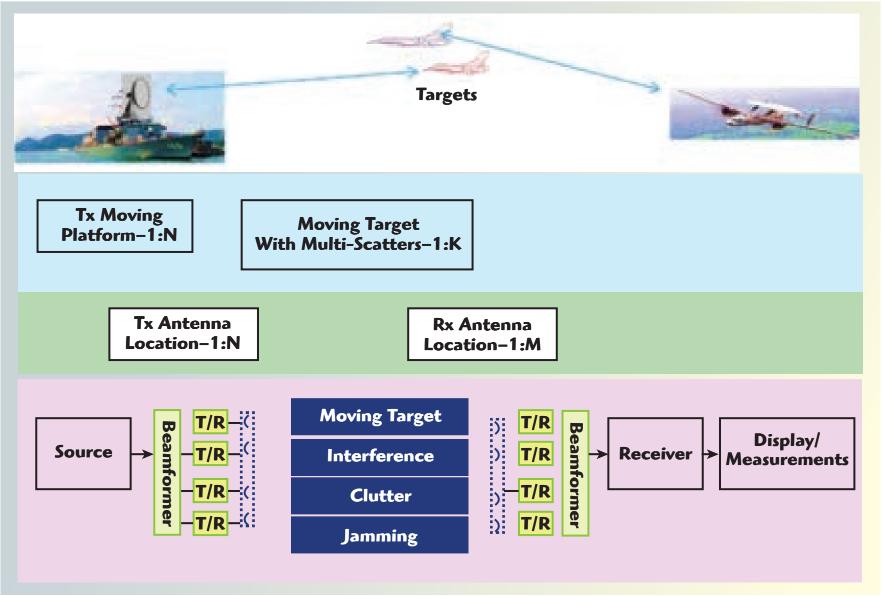

▲ *Fig. 1 Scenario framework simulation using SystemVue software. Simulation replicates any radar scenario, eliminating the need for costly field testing.*

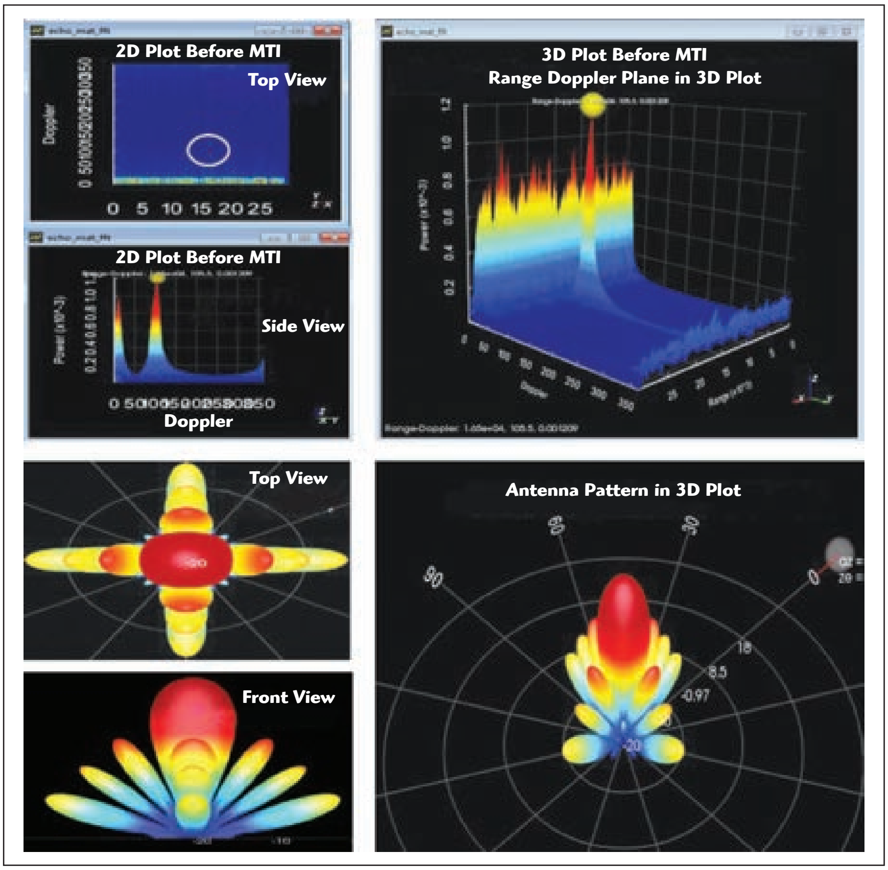

▲ *Fig. 2 SystemVue simulation supports advanced measurements, including detection and false alarm probabilities. The program can account for interference and remove it from the data and results.*

SCENARIO FRAMEWORK SIMULATION

To better understand the importance of implementing this simulation technique, an explanation of how it functions is beneficial. Given the number of different radars, and the inconsistencies between them, a generalized simulation tool is essential to accurately model all scenarios. A standardized simulation uses the basic assumptions involved when testing radars: no matter what type of radar, the signals are always transmitted from some radar system and received by themselves or by other radar systems. When using the SFS, this standardized simulation is implemented.

While setting up the simulation framework in the testing device, there are three layers to consider: the trajectory layer, the antenna layer and the signal layer (see ***Figure 1***). The trajectory layer locates all receivers and transmitters in 3D position, velocity and acceleration spaces. A radar platform model and radar target trajectory model are used to compute the trajectories. The antenna layer tracks the rotational attitude (i.e., pitch, yaw and roll) and beam forming directions. The azimuth angle and elevation angle of the targets in the antenna frame are computed to calculate the final antenna gain. The signal layer measures the traditional baseband signal processing paths, using MATLAB, HDL and RF models. The signals are delayed, attenuated and amplified by the antenna and transmit/receive (Tx/Rx) chains.

The signals received by radar systems are the signals from transmitters and the echoes from targets or the


RF-LAMBDA
THE LEADER OF RF BROADBAND SOLUTIONS
ITAR & ISO9000
Registered Manufacture
ITAR
PIN DIODE, GaAs
AND GaN CONTROL PRODUCTS
SWITCH IN PIN DIODE, GaAs AND GaN TECHNOLOGY
UP TO 67GHZ
PN: RFSP4TA5M43G
FULL BAND 0.05-43.5GHZ SP4T
SWITCH 50NS SPEED
PN: RFSP2TRDC18G
HIGH POWER 10W DC-18GHZ HOT
SWITCHABLE SP2T SWITCH
PN: RFSP2TR5M06G
HIGH POWER 100W DC-6GHZ HOT
SWITCHABLE SP2T SWITCH
RF-Lambda
RFSP8TA0018G
F:0.02-18GHz
PN: RFSP8TA0018G
HIGH IP3 50DBM 0.02-18GHZ
SP8T PIN DIODE SWITCH
DIGITAL AND VOLTAGE CONTROL PHASE SHIFTER
UP TO 40GHZ
RF-LAMBDA
PN: RFPSHT1826N6
DIGITAL CONTROL PHASE SHIFTER 360
DEGREE 64 STEP 18-26GHZ
PN: RFPSHT0618N6
DIGITAL CONTROL PHASE SHIFTER
360 DEGREE 64 STEP 6-18GHZ
PN: RVPT0818GBC
VOLTAGE CONTROL PHASE
SHIFTER 360 DEGREE 8-18GHZ
PN: RVPT0408GBC
VOLTAGE CONTROL PHASE
SHIFTER 360 DEGREE 4-8GHZ
DIGITAL AND VOLTAGE CONTROL ATTENUATOR
UP TO 50GHZ
PN: RFDAT0040G5A
DIGITAL STEP ATTENAUTOR
0.1-40GHZ 5 BITS 31DB
PN: RFVAT0218A30
VOLTAGE CONTROL ATTENUATOR
2-18GHZ 30DB IP3 50DBM
PN: RFVAT0050A17V
VOLTAGE CONTROL ATTENUATOR
0.01-50GHZ 17DB
RF-Lambda
RFDAT0018G8A
F:0.1-18GHz
PN: RFDAT0018G8A
DIGITAL STEP ATTENUATOR 0.1-18GHZ
8 BITS 128DB IP3 50DBM
www.rflambda.com
sales@rflambda.com
1-888-976-8880
1-972-767-5998
Plano, TX, US
San Diego, CA, US
Ottawa, ONT, Canada

different scatters of targets. The distances between transmitters and targets, and between targets and the receiver, determine the delay values of each sample of echoes, which finally determine the magnitude attenuation and Doppler frequency. In addition to the above parameters, the position between the transmitter and the target and the direction of the antenna main lobe relative to the antenna carrier determine the transmitter antenna gain. The same is true for the receiver antenna gain. Given this basic framework, one can model any number of radar systems.

Once the various layers of the simulation are set up, one can begin to make many different types of advanced radar measurements, ranging from basic spectrum or signal-to-noise ratio (SNR) to detection and false alarm probability. ***Figure 2*** illustrates several plots that can be generated to

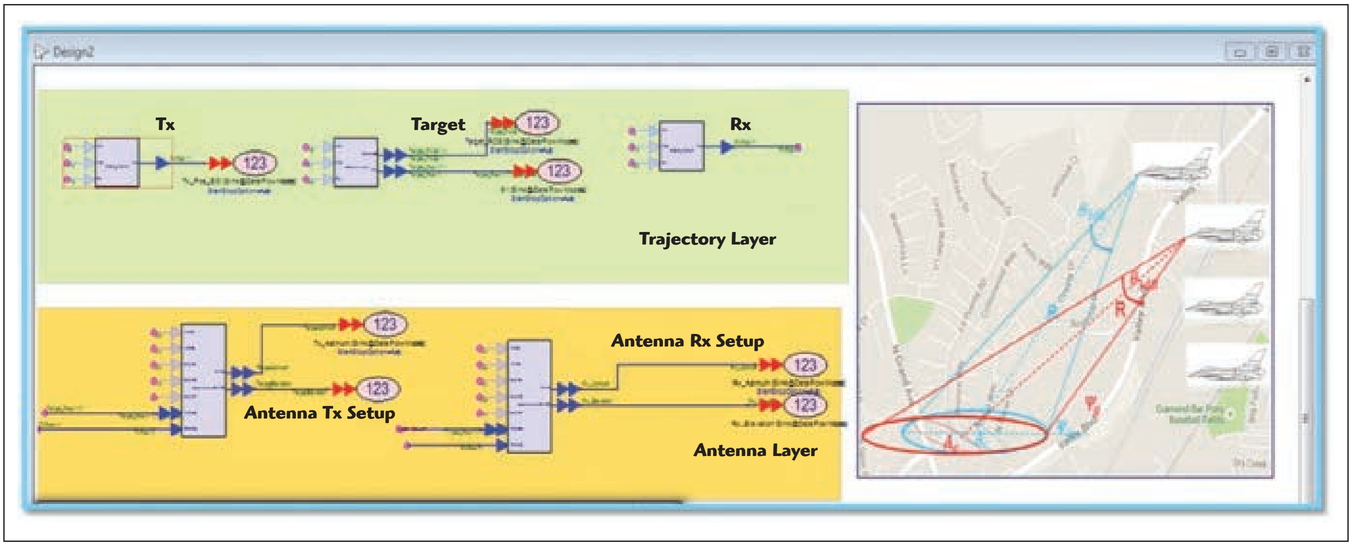

▲ *Fig. 3 Trajectory and antenna layer setup.*

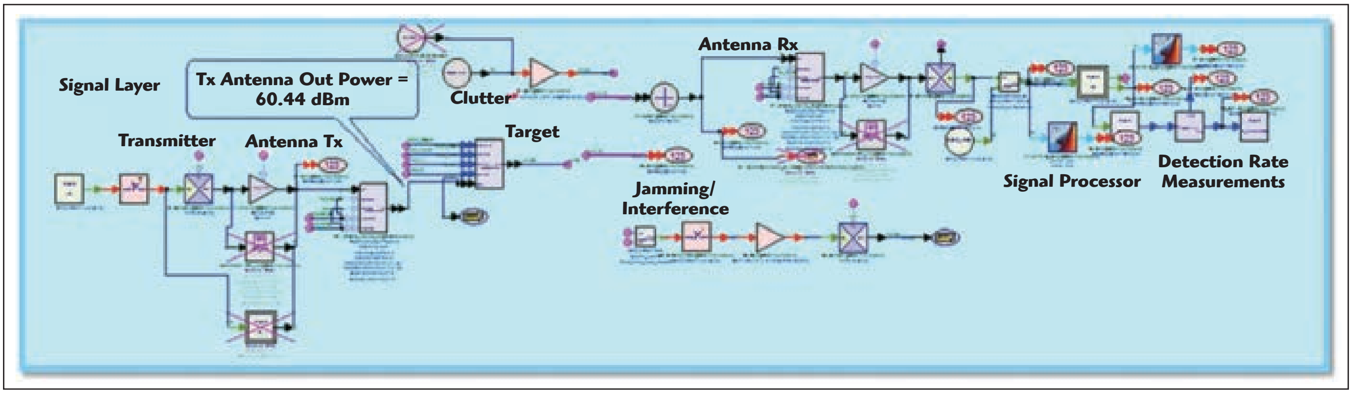

▲ *Fig. 4 Signal layer setup.*

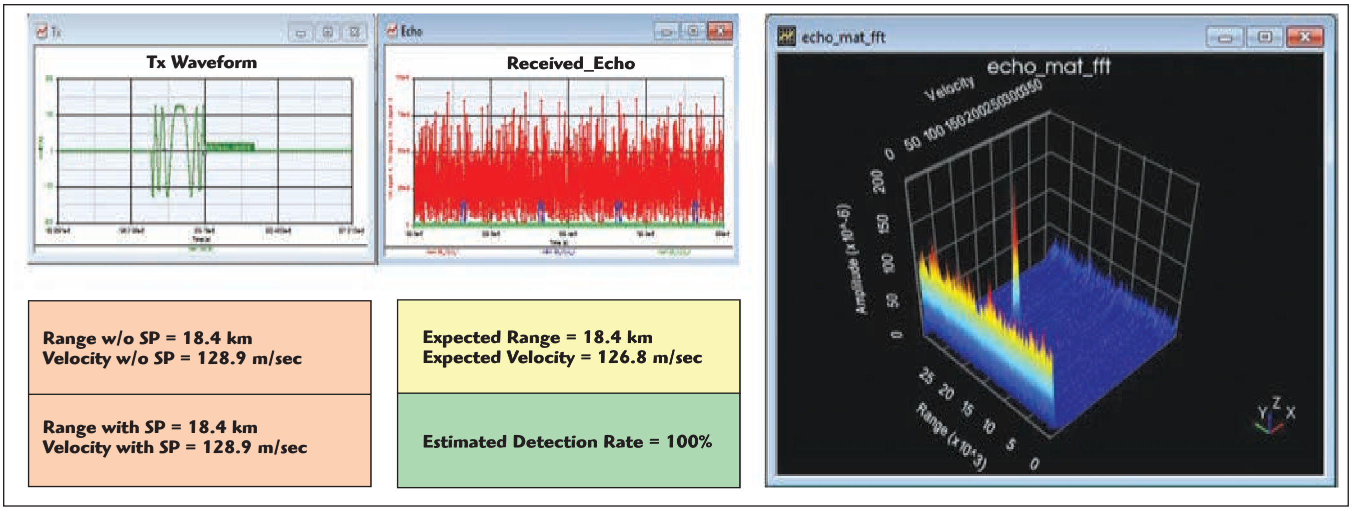

▲ *Fig. 5 With the platform setup, the user can adjust and measure all forms of interference.*

provide a detailed visual of the simulation.

Now that the basic system set up and functionality of this simulated approach are clear, a specific example is presented to demonstrate the capability this scenario has of solving difficulties associated with mobile radar measurements.

OVERCOMING INTERFERENCE

The advantages of implementing an SFS technique are underscored when applying its capabilities to a specific model, such as an airborne radar in lookdown mode with surface clutter, where the operator wishes to simulate a moving platform that is also tracking a moving target. In this scenario, there are several considerations to be addressed to fully and accurately simulate the setting: surface clutter, target RCS and any jamming/deception techniques used by an opposing threat. When performing measurements, there is much interference. One of the main issues faced in moving radar measurements is clutter. Surface clutter essentially refers to any area-based clutter that can exist on both land and sea and typically becomes an issue in airborne radars in the lookdown mode. To adequately account for clutter and all other forms of interference, several measurements must be performed precisely to obtain accurate results:

- Waveform and spectrum calculation of detection probability
- Creation of 3D plots of the range-Doppler plane
- Estimation of range and Doppler effects.

The first step in setting up the simulation is to construct the three layers previously discussed. For the platform setup, assume the airplane is flying with a certain velocity VT and the initial location in LLA is longitude R, latitude R and altitude R. Using the radar platform model, Tx, the Tx and Rx platforms in the trajectory layer are specified as seen in ***Figure 3***, with the same for the target model. Target location and speed can be set using the radar target model. If the user wants volume target, this model also allows specifying multi-scatters in one target.

Once the signal layer has been set up, as shown in ***Figure 4***, the physical layer setup is considered. A linear FM (LFM) signal is used by default. Custom waveforms such as nonlinear FM (NLFM) or coded signals can also be used. Under the "RF Transmitter" parameter, there are several options with which the data can be formed, including analog/digital and cross-domain simulation. Phased array models are available. Detection environments such as target RCS, clutter, jamming/deception have been considered. A radar signal processing algorithm, such as MTI or MTD, is put in the radar receiver. Once the layers have been set up, many measurements can be used to characterize the different elements of the scenario (see ***Figure 5***).

To summarize, the three layers were set up, the physical layer was formed, the detection environment (clutter) was considered, and now appropriate measurements may be performed. All forms of interference may be accounted for and accurately modeled in this system framework. This simplistic approach to airborne radar measurements demonstrates not only its power but also the ease of use. This example may be modeled on any number of different radar scenarios; the universal quality of the SFS enables testing of all kinds of radar signals and situations. Once the basic framework has been achieved, any environmental interference may be easily accounted for within the calculations of the software, guaranteeing accurate results. Radar scenario simulations can be challenging to design and test, especially when they are airborne. The new simulation approach successfully addresses these challenges.

To save development time and reduce cost, simulation of different radar scenarios is paramount. These scenarios can include radar signal generation and processing, as well as environmental effects and simulated platform and target hardware specific parameters. The capability to simulate the full deployment environment enables exceptional development speed and provides rapid prototyping capabilities for any radar system development. By moving testing into the lab and away from the field, time and money are saved, while measurement accuracy is improved. ■

Tektronix Expands USB Spectrum Analyzer Line

Tektronix
Beaverton, Ore.

Tektronix has expanded its line of USB-based real-time spectrum analyzers with four new higher performance models targeting design, spectrum management and wireless transmitter installation and maintenance applications. The RSA500 and RSA600 series of analyzers offer frequency coverage from 9 kHz to 7.5 GHz with 40 MHz acquisition bandwidth, a measurement dynamic range from -161 dBm/Hz displayed average noise level (DANL) and +30 dBm maximum input. The RSA500 and RSA600 build on the design approach of the 6.2 GHz RSA306 USB-based real-time spectrum analyzer introduced last year, which has been updated with the RSA306B, offering 10 dB better spurious performance, improved amplitude accuracy and a longer (three year) warranty.

The new RSA500 and RSA600 series feature higher instrument performance levels and analysis capabilities, compact packaging and aggressive pricing. Designed for use with a laptop or tablet PC, the RSA500 is intended for field applications, is battery operated and features a rugged package. Keeping a compact profile, the RSA600 is intended for laboratory use, is housed in a laboratory package and is powered by line voltage. Both instruments offer an optional tracking generator with an integrated internal bridge for basic device, cable and antenna testing.

Compared to traditional spectrum analyzers, Tektronix USB-based instruments offer comparable performance at lower price points. Through a standard USB 3.0 connection, the instruments are operated from

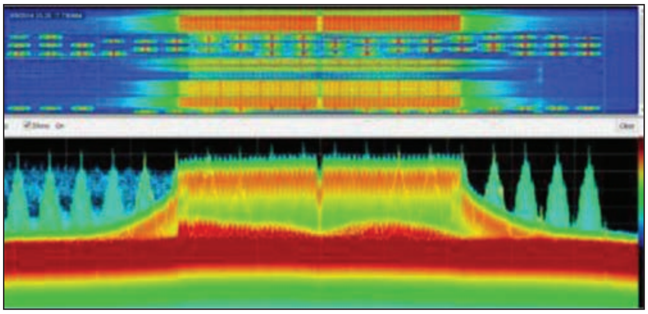

▲ *Fig. 1 DPX spectrogram display available in the RSA500/600 shows every instance of an interfering signal.*

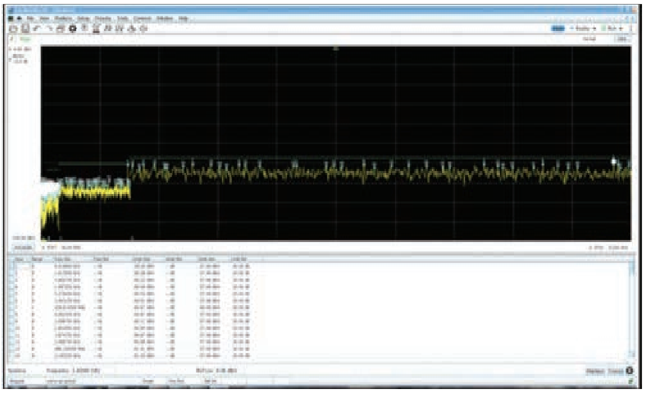

▲ *Fig. 2 The RSA500/600 can test to FCC Part 15 "Limit Lines for Radiated Emissions."*

a desktop PC, laptop or tablet using an updated version of the included SignalVu-PC software suite that provides 17 measurements, real-time DPX signal processing and a range of application-specific, add-on modules for in-depth analysis. Lower price is just one of the advantages of USB-based instruments. In the field, operators no longer have to hold a heavy instrument during use; instead, they can hold a lightweight tablet PC for analysis, which is needed for data logging in any case. Another advantage is the ability to record and play the entire 40 MHz RF bandwidth through software. Traditionally, complete I/Q RF bandwidth record/playback systems have been prohibitively expensive. However, with a PC or tablet equipped with a solid-state drive (SSD), the I/Q data can simply be written to the hard drive, making record/playback an affordable option. Applications include interference hunting, where users can capture RF interferers in action, or designers can record the first turn-on of a new radio device and analyze the event in detail later.

FEATURES AND APPLICATIONS

The RSA500 series of portable spectrum analyzers offers features and performance normally found in benchtop instruments, bringing lab performance levels to the field for fast, cost-effective spectrum management, interference hunting and network troubleshooting. The series includes the 3 GHz RSA503A and the 7.5 GHz RSA507A. These battery-powered instruments are qualified to MIL-STD 28800 Class 2 for shock and vibrations and rated IP52 for water ingress. Additional features and capabilities facilitate field applications, including a GPS receiver with locked frequency accuracy up to ±0.025 ppm and an available tracking generator for cable and antenna testing, enabling measurements like return loss and the distance to a fault.

As a real-time spectrum analyzer, the RSA500s allow spectrum managers to see very short duration signals for fast identification of problem or interfering signals. With 40 MHz of real-time bandwidth, a DPX spectrogram exposes every instance of an interfering or unknown signal down to 100 µs duration. ***Figure 1*** shows a WLAN transmission, in green and orange; the narrow signals that repeat across the screen are Bluetooth access probes. The spectrogram shown in the upper part of the screen separates these signals in time to show any signal collisions.

The RSA600 series includes the 3 GHz RSA603A and the 7.5 GHz RSA607A. They match the performance levels of the portable units but are designed to use line-cord power and have a desktop form factor. These analyzers handle a wide range of design applications, such as Internet of Things (IoT) modules and components. Using SignalVu-PC measurement packages, the analyzers can test everything from Bluetooth low energy (LE) to Bluetooth enhanced data rate (EDR) and WLAN standards through 802.11ac. Antenna and gain/loss testing capabilities speed system integration. The RSA600 is well suited to compliance testing, such as EMI pre-compliance tests to the limits of CISPR and other standards (see ***Figure 2***).

SIGNALVU-PC UPDATE

In conjunction with the new spectrum analyzers, Signal Vu-PC has an updated user interface with several new options and capabilities: expanded support for signal classification, channel navigation and mapping. Floating licenses are now available in addition to node-locked licenses, to give organizations more flexibility deploying the software and USB spectrum analyzers. Recording and playback of long signals is also available.

Engineers who need programming access to their instrument can choose either the SignalVu-PC programmatic interface or the included application programming interface (API), which provides a rich set of commands and measurements. The real-time processing capability provided by SignalVu-PC when using the recommended PC hardware is about 1,000 times faster than spectrum analyzers from other major suppliers.

PRICING AND AVAILABILITY

The U.S. suggested retail price for the RSA500 and RSA600 series of USB spectrum analyzers starts at $5,900 for the 3 GHz models and $9,900 for the 7.5 GHz models. The price of the RSA600 is 30 percent lower than that of the nearest traditional instrument and is about one-third the price of a Wi-Fi capable (40 MHz bandwidth) instrument. The RSA500 and RSA600 series are available through the global network of Tektronix distributors and partners.

Tektronix
Beaverton, Ore.
tek.com/usb-spectrum-analyzer

Modular Multi-Channel RF-Biased HTOL Test System

Accel-RF Instruments Corp. has released an 80 channel RF, high temperature operational life (HTOL) measurement system to help GaN technology move from research novelty to market reality. Test requirements for RF power amplifier devices and modules are moving beyond basic qualification and compliance standards to more stringent RF-biased HTOL testing. Accel-RF's RF, HTOL platforms can identify device wear-out and performance degradation to end-of-life (EOL) expectations, usually measured in millions of hours. Their platform is the only available instrument that complies with aerospace, government and commercial RF semiconductor burn-in standards.

The genesis of the RF HTOL measurement system was Accel-RF's highly developed and field-proven automated accelerated reliability test system (AARTS). Accel-RF's systems deliver a plug and play platform with performance over a wide range of RF frequencies and power levels. AARTS is a turnkey system that incorporates all of the capability needed for accelerated aging and parametric testing of RF semiconductor devices. System capacity is expandable from 16 to 80 channels with features that can be adapted to device package type, power level and frequency range. The platform includes powerful software for data acquisition, storage and presentation. Customers can choose system features to meet their technical needs and capital budgets. In addition to reducing cost, Accel-RF's modular solutions accelerate time-to-market, saving months of product development.

Accel-RF is a leader in supplying equipment for high temperature RF reliability testing on compound semiconductors such as GaN and SiC. The company offers the world's only line of modular, fully integrated and completely automated accelerated life test systems, designed to service a wide range of semiconductor technologies. These systems have supported the technology development, product launch and industry adoption of GaN transistors and integrated ICs for space, military and commercial wireless markets.

Accel-RF Instruments Corp.
San Diego, Calif.
www.accelrf.com

Multi-Function CPRI and RF PIM Site Analyzer

High-speed data acquisition in today's global mobile communication networks demands high efficiency of the network infrastructure. Passive Intermodulation (PIM) in a network can cause serious interference and significantly degrade the network quality and impact KPI figures. The cause of PIM is very complex and uncertain. It can result from low-grade transmission line components or loose connectors, dirty surfaces, magnetic materials or the surrounding environment.

Rosenberger produces a wide range of PIM analyzers, including rack types and desktop models but it is the portable PIM analyzer sector where the company is having a significant impact with the introduction of the PIM Site Analyzer α.

This new CPRI and RF PIM multi-functional instrument is claimed to be the first analyzer for mobile network infrastructure with copper or fiber interface and exchangeable filter units. This portable equipment is ultra-broadband and presents various options for test and measurement functionality: CPRI PIM, RF PIM, RF return loss/VSWR, isolation and the most accurate distance to fault on the market.

PLUG-AND-PLAY

The site analyzer's plug-and-play modular and broadband design from 698 to 2700 MHz with exchangeable band filter units ensures high flexibility and is future-proof, catering for all existing and upcoming bands.

Portable, with a rugged design and sunlight readable 12 inch touch screen the PIM Site Analyzer α offers a continuous wave signal (no pulse), antenna isolation measurement, DTF measurement (VSWR versus distance, PIM versus distance) and VSWR/return loss measurement. It provides increased safety and simplified handling in the workplace and a cancellation function shows potential improvement of PIM values.

The standard 698 to 2700 MHz PIM Site Analyzer α broadband base unit comes complete with a Tablet for recording and processing results, a power unit and a filter unit (e.g. 900 MHz). Optional accessories include a battery unit, CPRI software option (HW ready) and a carry bag.

Rosenberger
Fridolfing, Germany
www.rosenberger.com

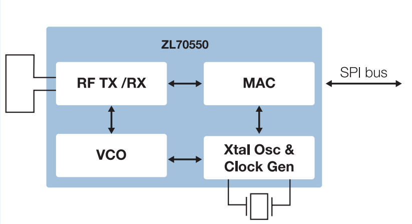

Low Power ISM Transceiver for Secure IoT Applications

Microsemi has developed a low power, sub-GHz RF transceiver for industrial, security and medical (ISM) applications. The ZL70550 is highly integrated, with a small footprint and best-in-class power dissipation. The IC is well-suited for wireless applications operating on coin-cell batteries or energy harvesters, such as electronic shelf labels, retail asset tracking, process control, wearable monitoring and medical diagnostics. To operate for years on small batteries, these applications require a transceiver with much lower power dissipation than Wi-Fi, Bluetooth and Zigbee provide.

The ZL70550 operates in the 779 to 965 MHz unlicensed ISM band and handles data rates up to 200 kbps. The transceiver consumes 2.8 mA, while transmitting at –10 dBm output, and 2.5 mA during receive. The "sleep state" current is only 10 nA, believed to be the industry's lowest and optimum for low duty cycle applications. The operating voltage range is 1.7 to 3.6 V. For applications requiring extended range, the transmitter output power, receiver input sensitivity and data rate can be adjusted to increase receive sensitivity to –107 dBm, with a slight increase in power consumption. In a 3 × 2 mm chip scale package, the ZL70550 is highly integrated: other than the antenna and, in some cases, its matching network, only a crystal, resistor and two coupling capacitors are required for operation.

The transceiver includes an advanced media access controller (MAC) that performs most link support functions, received signal strength indications (RSSI), clear channel assessment, sniff, preamble and synchronization, packetization, whitening and forward error correction (FEC). Microsemi offers an application development kit (ADK) and a wireless sensor network evaluation kit to speed hardware and software development. The ADK provides all the necessary hardware and software to demonstrate the performance of the ZL70550. The optional Microsemi Z-Star protocol enables rapid product development and offers a full star configuration to deploy a full network.

Microsemi Corp.
Aliso Viejo, Calif.
www.microsemi.com/zl70550

FIVE DAYS
THREE CONFERENCES
ONE EXHIBITION
EUROPEAN MICROWAVE WEEK 2016
EXCEL LONDON, UK
3 - 7 OCTOBER 2016
EuMW 2016
Microwaves Everywhere
EUROPEAN MICROWAVE WEEK
LONDON, UK
3-7 OCTOBER 2016
www.eumweek.com
EUROPEAN MICROWAVE WEEK 2016
REGISTRATION INFORMATION
EUROPE'S PREMIER MICROWAVE, RF, WIRELESS AND RADAR EVENT
EuMA
European Microwave Association
Official Publication:
Microwave Journal
Organised by:
horizon house
Supported by:
IET
Co-sponsored by:
MTT-S
Co-sponsored by:
IEEE
EuMIC 2016
The 11th European Microwave Integrated Circuits Conference
Co-sponsored by:
GAAS
46TH EUROPEAN MICROWAVE CONFERENCE 2016
The 46th European Microwave Conference
Co-sponsored by:
EuRAD 2016
The 13th European Radar Conference
Co-sponsored by:
AESS
Register online at
www.eumweek.com

EUROPEAN MICROWAVE WEEK
LONDON, UK
3-7 OCTOBER 2016
www.eumweek.com
EuMW 2016
Microwaves Everywhere

EUROPEAN MICROWAVE WEEK 2016
THE CONFERENCES

Don't miss Europe's premier microwave conference event. The 2016 week consists of three conferences and associated workshops:

- **European Microwave Integrated Circuits Conference (EuMIC) 3rd – 4th October 2016**
- **European Microwave Conference (EuMC) 4th – 6th October 2016**
- **European Radar Conference (EuRAD) 5th – 7th October 2016**
- **Plus Workshops and Short Courses (From 3rd October 2016)**
- **In addition, EuMW 2016 will include the 'Defence, Security and Space Forum' on 5th October 2016**

The three conferences specifically target ground breaking innovation in microwave research through a call for papers explicitly inviting the submission of presentations on the latest trends in the field, driven by industry roadmaps. The result is three superb conferences created from the very best papers. For a detailed description of the conferences, workshops and short courses please visit www.eumweek.com. The full conference programme can be downloaded from there.

FAST TRACK BADGE RETRIEVAL

Register online and print out your badge in seconds onsite at the Fast Track Check In Desk

CONFERENCE PRICES

There are TWO different rates available for the EuMW conferences:

- **ADVANCE DISCOUNTED RATE** – for all registrations up to and including 3rd September
- **STANDARD RATE** – for all registrations made after 3rd September

Please see the Conference Registration Rates table on the back page for complete pricing information. All payments must be in £ Sterling – cards will be debited in £ Sterling.

Online registration is open now, up to and during the event until 7th October 2016

DELEGATES

Registering for the Conference

- Register online at **www.eumweek.com**
- Receive an email receipt with barcode
- Bring your email, barcode and photo ID with you to the event
- Go to the Fast Track Check In Desk and print out your delegate badge
- Alternatively, you can register onsite at the self service terminals during the registration opening times below:

  - Sunday 2nd October (16:00 - 19:00)
  - Monday 3rd October (08:00 – 17.00)
  - Tuesday 4th October (08:00 – 18.00)
  - Wednesday 5th October (08:00 – 17.00)
  - Thursday 6th October (08:00 – 17.00)
  - Friday 7th October (08:00 – 10.00)

Once you have collected your badge, you can collect the conference proceedings on USB stick and delegate bag for the conferences from the specified delegate bag area by scanning your badge.

CONFERENCE REGISTRATION INFORMATION
EUROPEAN MICROWAVE WEEK 2016, 3rd - 7th October, London, UK

Register Online at www.eumweek.com
ONLINE registration is open from 1st June 2016 up to and during the event until 7th October 2016.
ONSITE registration is open from 16:00 on 2nd October 2016.
ADVANCE DISCOUNTED RATE (up to and including 3rd September) STANDARD RATE (from 4th September & Onsite)

Reduced rates are offered if you have society membership to any of the following*: Eu*M*A, GAAS, IET or IEEE.

Eu*M*A membership fees: Professional £19/year, Student £11/year.

If you register for membership through the EuMW registration system, you will automatically be entitled to discounted member rates.

Reduced Rates for the conferences are also offered if you are a Student/Senior (Full-time students 30 years or younger and Seniors 65 or older as of 1st August 2016).

ADVANCE REGISTRATION CONFERENCE FEES (UP TO AND INCLUDING 3RD SEPT.)

CONFERENCE FEES	ADVANCE DISCOUNTED RATE			
	Society Member (*any of above)		Non Member	
1 Conference	Standard	Student/Sr.	Standard	Student/Sr.
EuMC	£355	£100	£500	£140
EuMIC	£270	£90	£380	£130
EuRAD	£240	£80	£340	£120
2 Conferences				
EuMC + EuMIC	£500	£190	£710	£270
EuMC + EuRAD	£480	£180	£680	£260
EuMIC + EuRAD	£410	£170	£580	£250
3 Conferences				
EuMC + EuMIC + EuRAD	£610	£270	£860	£390

STANDARD REGISTRATION CONFERENCE FEES (FROM 4TH SEPT. AND ONSITE)

CONFERENCE FEES	STANDARD RATE			
	Society Member (*any of above)		Non Member	
1 Conference	Standard	Student/Sr.	Standard	Student/Sr.
EuMC	£500	£140	£700	£200
EuMIC	£380	£130	£540	£190
EuRAD	£340	£120	£480	£170
2 Conferences				
EuMC + EuMIC	£710	£270	£1,000	£390
EuMC + EuRAD	£680	£260	£950	£370
EuMIC + EuRAD	£580	£250	£820	£360
3 Conferences				
EuMC + EuMIC + EuRAD	£860	£390	£1,210	£560

WORKSHOP AND SHORT COURSE FEES (ONE STANDARD RATE THROUGHOUT)

FEES	STANDARD RATE			
	Society Member (*any of above)		Non Member	
	Standard	Student/Sr.	Standard	Student/Sr.
Half day WITH Conference registration	£75	£60	£100	£75
Half day WITHOUT Conference registration	£100	£75	£130	£100
Full day WITH Conference registration	£105	£80	£135	£100
Full day WITHOUT Conference registration	£135	£105	£180	£130

THE EUMW CRUISE ON THE RIVER THAMES - 5th Oct 16

Tickets for the cruise are limited and are available on a first-come -first-served basis at the price of £25.00 for EuMW Delegates and £36.00 for guests.

Proceedings on USB Stick

All papers published for presentation at each conference will be on a USB stick, given out FREE with the delegate bags to those attending conferences. For additional USB sticks the cost is £50.

International Journal of Microwave and Wireless Technologies (8 issues per year)

International Journal combined with Eu*M*A membership: £50 for Professionals or £43 for Students.

Partner Programme and Social Events

Full Details and contacts for the Partner Programme and other Social Events can be obtained via the EuMW website **www.eumweek.com**

SPECIAL FORUMS & SESSIONS						
Date	**Time**	**Title**	**Location**	**No. of Days**	**Fee**	
Wednesday 5th October	11:20 - 19:00	Defence, Security & Space Forum	Rooms 8 to 11	1	£10 for delegates (those registered for EuMC, EuMIC or EuRAD)	£40 for all others (those not registered for a conference)

Web & Video Update

Electromagnetic Safety Products

VENDORVIEW

AR RF/Microwave Instrumentation is proud to offer a wide range of electromagnetic safety products for measuring exposure levels of a variety of products and systems such as industrial ovens, RF medical devices, power plants, ground transport systems, wireless telecommunications and more. In this video at: http://bit.ly/ARsafetyvideo, AR applications engineer Flynn Lawrence discusses AR's electromagnetic field safety products. For more information on AR electromagnetic safety products, visit http://bit.ly/ARElectroMagneticSafety.

AR RF/Microwave Instrumentation
www.arworld.us

RF Power Amplifier Design

VENDORVIEW

Take 30 seconds to watch Keysight's latest video announcing a series of five RF power amplifier (PA) design videos intended to provide engineers with the building blocks to design more complex PA classes (i.e., A, AB, B, FE, E and J). While PAs are used everywhere, their large signal nonlinear nature makes designing them difficult. Designers can download the PA workspaces used in the videos to start their own design with a solid circuit topology. Find the video at: https://youtu.be/YfIuG3ELhG0.

Keysight Technologies Inc.
www.keysight.com

Datasheets at Your Fingertips

VENDORVIEW

SAGE Millimeter has launched a new website featuring over 800 downloadable datasheets with measured data and full specifications. SAGE Millimeter's complete product offering can now be browsed in "photo" view (pictured here) or in "sortable table" view, which allows users to sort by their most critical performance specifications. Products can be added to the RFQ cart with a few clicks and submitted directly to the sales team for speedy pricing.

SAGE Millimeter Inc.
www.sagemillimeter.com

New Website Launch

VENDORVIEW

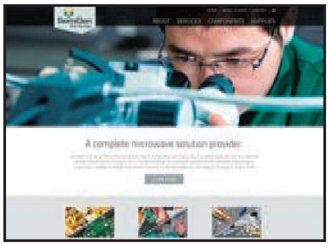

SemiGen's new website features updated RF/microwave testing/assembly/design, PCB assembly, semiconductor upscreening, and RF/microwave module repair pages with detailed parameter and specification listings. The site also offers downloadable datasheets of all components ranging from super thin chip capacitors, spiral inductor coils and limiter diodes. If you're looking for supplies, the site now features a large selection of sizes of adhesives, bonding tools, wires and ribbon, and epoxy preforms available for purchase. The new SemiGen website can be easily viewed and fully navigated on any device.

SemiGen Inc.
www.semigen.net

Low-PIM Switches and EasyDocks

VENDORVIEW

Measurement processes are easy to automate with low PIM switches and EasyDocks from SPINNER. This video shows a practical example of how to calibrate measurement paths and measure VSWR and PIM with these products. The benefits are obvious: major cost savings and more efficient testing of mobile communication components. SPINNER manufactures RF components for broadcast, mobile communication, test & measurement, and radar & satellite systems. Check out the video at: youtube.com/user/SPINNERGMBH.

SPINNER GmbH
www.spinner-group.com

Microwave/RF Assembly Calculator

The GORE™ Microwave/RF Assembly calculator is an online tool used to calculate insertion loss, VSWR and other parameters of GORE® Microwave/RF Assemblies for different cable types. The main calculator section enables the user to select a market (A&D, Spaceflight, T&M) and category (such as general purpose, ruggedized and phase stable, etc.) from the dropdowns to view cable types and specs. The online interface features a responsive design, making it equally usable on PCs, tablets and smartphones using any major browser.

W. L. Gore & Associates Inc.
tools.gore.com/gmcacalc

eLEARNING center

Presented by: Microwave Journal

June Short Course Webinars

Technical Education Training
Expanding the Possibilities of Cellular Wireless Infrastructure with GaN
Sponsored by: Qorvo
Live webcast: 6/7/16

Technical Education Training
Practical Antenna Design for Advanced Wireless Products
Sponsored by: National Instruments
Live webcast: 6/14/16

Technical Education Training
Sponsored by: National Instruments
Live webcast: 6/16/16

Technical Education Training
Faster Analysis of Complex RF Signals
Sponsored by: Boonton (Wireless Telecom Group)
Live webcast: 6/23/16

Technical Education Training
Radar Signal Generation with up to 2 GHz Bandwidth for Single-Channel and Multichannel Receiver Testing
Sponsored by: Rohde & Schwarz
Live webcast: 6/28/16

Register to attend at mwjournal.com/webinars

Past Webinars On Demand

Technical Education Training Series
- Designing Next-Gen Cellular and Wi-Fi Switches Using RF SOI Technology
- Improving Reliability and Efficiency with Solid State Spatial Combining Technology
- Introduction to Radar
- Effect of Conductor Profile Structure on Propagation in Transmission Lines
- Minimize Your Y-Factor Noise Figure Measurement Uncertainty
- Doherty at Eighty
- Millimeter Wave and E-Band Vector Network Analyzer Solutions
- Making Noise Work for You
- RF and Microwave Heating Simulation and Application Design
- Critical Aspects of Dielectric Constant Properties for High Frequency Circuit Design
- Demystifying MIMO Radar and Conventional Equivalents

RF/Microwave Training Series
Presented by: Besser Associates
- RF and Microwave Filters
- Mixers and Frequency Conversion

CST Webinar Series
- Hybrid Simulation for Electrically Large Aerospace Platforms
- Simulation of Implanted Medical Devices

Innovations in EDA
Presented by: Keysight Technologies
- Advances in High Power RF Design
- 5G Physical Layer Modeling: A Communication System Architect's Guide
- Designing X-Band PAs Using SMT Plastic Packaged GaN Transistors

Keysight Technologies Webcast
- LTE in the Unlicensed Spectrum
- Using a Multi-Touch UI to Streamline Signal Analyzer Measurements
- Testing Voice Over LTE on Your Device

Keysight RF and Microwave Basics Education Series
- Simulating, Generating and Analyzing Custom-Modulated Satellite Signals

Keysight FieldFox Series
- Wireless Site Survey, Spectrum Monitoring and Interference Analysis

Scan page using layar app

NEW PRODUCTS

FOR MORE NEW PRODUCTS, VISIT WWW.MWJOURNAL.COM/BUYERSGUIDE
FEATURING VENDORVIEW STOREFRONTS

COMPONENTS

Thin Film Resistors

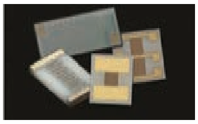

For years customers asked the company to bring its short lead times, outstanding customer service and quality focus to the thin film resistor industry. Compex announced that it now offers a full line of wire-bondable and edge-terminated resistors built to its customer's exact specifications. Available alternatives include single, dual, center-tap, array and custom configurations. Compex would be happy to provide samples to ensure you have the right parts for your needs.

Compex Corp.
www.compexcorp.com

Integrated Mixer

The new MX6000L integrated mixer from DS Instruments combines a cutting-edge active-core wideband mixer with a programmable LO and OLED display. This innovative new stand-alone device is completely USB powered and provides its own precision reference clock for the LO. Covering an RF range up to 6 GHz and an IF output to 600 MHz makes the MX6000L a powerful down-converter and general purpose RF mixing tool for any RF engineer.

DS Instruments
www.dsinstruments.com

Programmable Attenuators

Fairview Microwave Inc. released their new digitally controlled programmable attenuators with performance up to 40 GHz and up to 60 dB attenuation range with 0.03 dB minimum step size. These programmable attenuators are commonly used in electronic warfare, military and space communication systems, radar, and test and measurement applications. Fairview's digitally controlled attenuators perform the important function of adjusting the amplitude of signal levels in RF, microwave and millimeter wave systems.

Fairview Microwave Inc.
www.fairviewmicrowave.com

Digital Step Attenuators

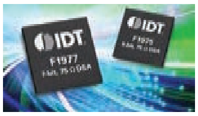

Integrated Device Technology Inc.® (IDT®) expanded its RF portfolio with the addition of a new family of digital step attenuators (DSA) optimized for the demanding requirements of the broadband and CATV markets. The ultra-high-linearity 75 ohm DSAs feature IDT's industry-first Glitch-Free™ technology for enhanced performance. The F1975 and F1977 deliver very low insertion loss and distortion, and offer higher power handling with pinpoint attenuation accuracy than competing devices, giving customers the performance needed to achieve higher data rates in their system.

Integrated Device Technology Inc.
www.idt.com

MCV Helical Filters
VENDORVIEW

MCV helical filters feature small bandwidth, custom design and reliably tunable center frequency in UHF, VHF and SHF frequency range. MCV helical filters are silver plated in a through-hole package to offer higher Q and low insertion loss. Toko helical filter (5HW, 5HT, 7HW, 7HT, 5CHW, 5CHT, 5CHLW, CBT13, CBW13 series) replacements are available in a pin-to-pin footprint match through-hole package.

MCV Microwave
www.mcv-microwave.com

Microwave/Millimeter Wave 2-Way Power Dividers
VENDORVIEW

2-Way, 30 W Wilkinson power dividers are optimized for excellent performance across all microwave and millimeter wave bands from 6 to 40 GHz in (2.92 mm). Resistive 2-way splitters cover DC to 26.5 GHz (2.92 mm). Also available are attenuators, isolators, terminations and couplers. Their rugged construction makes them ideal for telecommunications, aerospace & test equipment systems. Made in the U.S. and 36-month warranty.

MECA Electronics Inc.
www.e-MECA.com

Coaxial Limiter
VENDORVIEW

These coaxial limiters feature wideband, 20 to 4000 MHz, low insertion loss 0.36 dB typ., fast recovery time, 33 nsec typ., excellent VSWR 1.2:1 typ. and low output power, 12 dBm typ. Applications include: military, hi-rel applications, stabilizing generator outputs, reducing amplitude variations and protects low noise amplifiers and other devices from ESD or input power damage.

Mini-Circuits
www.minicircuits.com

UltraCMOS® Mixers

The UltraCMOS PE41901 and PE41902 are high-frequency mixers that operate from 10 to 19 GHz. The PE41901 is an up-conversion mixer with an integrated LO coupler, and the PE41902 is a down-conversion mixer with an integrated LO combiner and RF coupler.

These complete MMIC mixer solutions are ideal for test and measurement systems and Ku-Band earth terminals such as VSAT and point-to-point communication systems. These mixers encompass the key UltraCMOS technology strengths of high isolation and high linearity, while providing a robust and reliable solution for frequency-mixing applications.

Peregrine Semiconductor
www.psemi.com

Suspended Substrate Lowpass Filter
VENDORVIEW

PMI model no. 7LP6G-6175-CD-TNC is a suspended substrate lowpass filter with TNC female connectors in/out.

This model offers very high Q with broadband performance in a silver plated CNC machined housing. This unit has very low loss and is ideal for eliminating broadband harmonics.

Planar Monolithics Industries Inc.
www.pmi-rf.com

8-Way Power Divider

The PS8-53-454-4S is an 8-way power divider that covers a frequency range of 10 to 40 GHz. It offers an insertion loss of 2.5 dB and isolation of 12 dB. Amplitude balance is 0.8 dB and phase balance is 12 degrees. VSWR is 1.90:1. Power handling is 10 W. Connectors are 2.92 mm female. Outline dimensions are 4" × 2"× 0.4".

Pulsar Microwave Corp.
www.pulsarmicrowave.com

SP4T Switch
VENDORVIEW

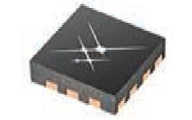

RFMW Ltd. announced design and sales support for Skyworks' dual-band, internally matched, SP4T switch developed for Wi-Fi applications in the 2.4 and 5 GHz ISM bands. The Skyworks SKY13575-639LF supports access points and CPEs along with WLAN test

and measurement equipment. Frequency coverage is from 100 MHz to 6 GHz with a maximum insertion loss of 1.4 dB. Isolation ranges from 26 to 40 dB and the SKY13575-639LF can handle up to 32 dBm of input power for demanding applications. Processed using SOI technology, this Skyworks switch consumes less than 10 mA.

RFMW Ltd.
www.rfmw.com

Switches

RLC Electronics introduced SP7T and SP8T switches with N connectors. These switches operate up to 6 GHz, and are designed for both low power and high power applications (500 W cW at 6 GHz, 2000 W cW at < 500 MHz). In addition to long life, the switch also features extremely low insertion loss (0.1 dB to 4 GHz and 0.3 dB to 6 GHz, typically) and VSWR over the entire frequency range, while maintaining high isolation (>80 dB). The switch can be provided in latching or failsafe modes, which is standard on all RLC switches.

RLC Electronics Inc.
www.rlcelectronics.com

71 to 76 GHz Waveguide Bandpass Filter

VENDORVIEW

Model SWF-74305350-12-B1 is an E-Band, waveguide bandpass filter that is used to pass

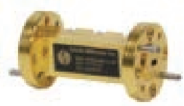

the frequency range of 71 to 76 GHz, while rejecting the frequency range of DC to 67 GHz and 81 to 90 GHz. The nominal insertion loss of the bandpass filter is 2 dB and the typical rejection is 50 dB. The standard interface offers WR-12 waveguides with UG-387/U flanges.

SAGE Millimeter Inc.
www.sagemillimeter.com

BPSK Modulator

The SBM-K5 is a compact bi-phase modulator

(BPSK) designed for high modulation speeds. The carrier frequency band operates from 1000 to 1650 MHz and modulation bandwidth can range from up to approximately 100 to 165 MHz. The device can be driven with external complementary drivers capable of sourcing and sinking up to 20 mA. The typical amplitude unbalance is 0.4 dB and phase error is ± 4 degrees. The compact package measures 0.31" × 0.25"× 0.21".

Synergy Microwave Corp.
www.synergymwave.com

CABLES & CONNECTORS

Type N Female Bulkhead Precision Adapters

Type N female bulkhead precision adapters feature: frequency range: DC to 18 GHz (Mode

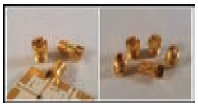

FREE), electrical: 50 ohm, low VSWR and low insertion loss, VSWR: 1.15:1 max at 18 GHz (Typical VSWR 1.05:1 through 18 GHz), O-Ring seal captivated within the flange body groove, Materials: Passivated 303 stainless steel or nickel plated brass available and dielectrics fluorocarbon (PTFE). They are available for immediate delivery — same day shipping for all stock items.

SGMC Microwave
www.sgmcmicrowave.com

AMPLIFIERS

High Gain Limiting Amplifier

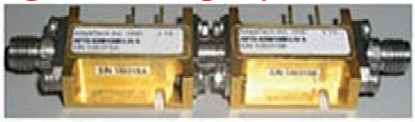

The APT55-02001800-7016-66-LMS is an example of a wideband, high gain medium power limiting amplifier with +20 dBm saturated output power for which AmpliTech is sole-source supplier. It is designed mainly for IFM EW airborne applications where multiple signals are present at the input and low harmonic distortion is required to preserve the two-tone ratio at the output under limiting conditions. The input signals can be as large as +10 dBm.

AmpliTech
www.amplitech.com

Solid-State Power Amplifier Modules

VENDORVIEW

AR's line of 0.7 to 6 GHz hybrid power module products (HPM) offer the ultimate in performance over this wide frequency range in one compact connectorized housing. This design meets the stringent requirements of today's military systems, and can also be price competitive to be used in various wireless applications. Both Class A and Class AB versions are available with output power levels up to 50 W CW.

AR RF/Microwave Instrumentation
www.arworld.us/html/11200_hybrid_modules.asp

Digital Variable Gain Amplifier

VENDORVIEW

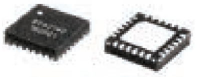

BeRex announced the BVA2140, a highly linear 0.25 W digital variable gain amplifier (DVGA) that integrates a 6-step digitally controlled step attenuator and 50 ohm matched, input/output gain block amplifiers in a single 4 mm × 4 mm package that consumes only 150 mA of current. Designed primarily for W-CDMA/LTE wireless infrastructure equipment, satellite radio and other high end wireless applications, the BVA2140 offers a controlled variable gain range of 31.5 dB in 0.5 dB steps with high attenuation accuracy.

BeRex Corp.
www.berex.com

Wideband Low Noise Amplifier

The ALN-33144030-01 is a wideband low noise amplifier operating across the entire Ka-Band (26.5 to 40 GHz). It provides ultra-flat

small signal gain of over 30 dB, with a typical 4 dB noise figure. The amplifier operates from a single bias supply of +8 to +12 VDC with an internal voltage regulator and bias sequencing circuitry. The amplifier is ideal for communication or radar systems that need broadband low noise operation.

Ducommun Inc.
www.ducommun.com

Ultra Broadband High Power Solid-State Amplifiers

VENDORVIEW

With a linear GaAsFET hybrid, Class AB design to achieve maximum output the AMP3033 amplifier module delivers 7 W CW typical output power from 24 to 31 GHz (4 W, min 24 to 25 GHz and 6 to 7 W min across the rest of the band). These amplifiers are suitable for a number of applications including EMI/EMC susceptibility testing, millimeter component testing and EW.

Exodus Advanced Communications
www.exoduscomm.com

RF Power LDMOS Transistor

VENDORVIEW

Richardson RFPD Inc. announced the availability and full design support capabilities for a new LDMOS transistor from NXP Semiconductors. The MRF8VP13350NR3 is a 350 W CW transistor designed for industrial, scientific and medical (ISM) applications in the 700 to 1300 MHz frequency range. It is capable of 350 W CW or pulse power in narrowband operation. The new device is internally input matched for ease of use, and it can be used single-ended or in a push-pull configuration. It is qualified up to a maximum of 50 VDD operation and includes integrated ESD protection.

Richardson RFPD Inc.
www.richardsonrfpd.com

Low Noise Amplifier

Model ABL0150-02-2916 is a high dynamic range PIN diode limiter protected PHEMT

transistor based low noise amplifier module offering 29 dB of linear gain and 1.6 dB noise figure over the frequency range from 30 MHz to 1.5 GHz. The maximum input no damage RF power can be as high as 30 dBm at RF input port. The unit has a built in voltage regulator, and a reverse polarity protection diode. It operates with a single DC power supply voltage from +10 to +15 V. The package size of the amplifier is 1.2" × 0.85" × 0.375".

Wenteq Microwave
www.wenteq.com

New**Products**

SOURCES

Pulse Generator
VENDOR**VIEW**

Berkeley Nucleonics Corp. (BNC) offers optical outputs to trigger, delay, gate and sync multiple devices for use in high EMI and RFI environments. Optical outputs allow distribution over longer distances while maintaining the precision timing and coherence between channels. Model 577, BNC's latest digital delay/pulse generator, provides the ability to select timing references for each channel. In addition to this the unit allows control of both the delay and width of each channel and independent channel amplitudes and polarities.
Berkeley Nucleonics
www.berkeleynucleonics.com

Dual Frequency Phase-Locked DRO
VENDOR**VIEW**

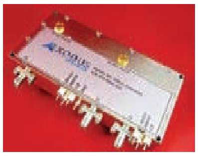

Exodus Dynamics introduced EDPLO-2200 series ultra low noise, dual frequency phase locked DRO. The unit locks to a single reference frequency of 30 to 200 MHz and generates two single frequencies from 100 MHz to 45 GHz. The EDPLO-2200 uses a single supply of +12 or +15 VDC, with an output power up to +25 dBm at -40° to +85°C operating temperature.
Exodus Dynamics
www.exodusdynamics.com

Coaxial Packaged Noise Sources
VENDOR**VIEW**

Pasternack has greatly expanded their lines of coaxial packaged noise sources covering frequency bands up to 60 GHz. Various types of noise source design configurations are available including octave band and broadband noise sources, amplified noise sources, noise sources with integral isolators and precision calibrated instrumentation grade noise sources. Pasternack's new noise sources might generally be used as a reference source to measure system level noise figure for test and measurement applications.
Pasternack
www.pasternack.com

ASIC-Based OCXOs

Rakon's patented Mercury™ technology enables ASIC-based OCXOs that are ideal for timing and synchronization in microwave applications. Mercury™ ASIC-based OCXOs combine the stability and noise performance of traditional discrete OCXOs with the advantages of lower power, significantly higher reliability and smaller size (industry's smallest OCXOs: 9×7 mm and 14×9 mm). Rakon is a key supplier to leading OEMs, ODMs and silicon vendors throughout the telecommunications and defense industries with a global R&D, manufacturing and customer service footprint.
RAKON
www.rakon.com

RoHS Compliant Voltage-Controlled Oscillator
VENDOR**VIEW**

Z-Communications Inc. announced a RoHS compliant voltage-controlled oscillator (VCO) model USSP3300-LF in the S-Band. The USSP3300-LF operates from 3050 to 3550 MHz within a tuning voltage range of 0 to 5 VDC. This VCO features phase noise of -105 dBc/Hz at 100 kHz offset while operating off a 3 VDC supply and typically drawing only 13 mA of current. The low cost USSP3300-LF provides the end user an output power of 1±3 dBm into a 50 Ω load.
Z-Communications Inc.
www.zcomm.com

ANTENNAS

MIMO Omni Antennas with Magnetic Mount Base
VENDOR**VIEW**

Southwest Antennas offers two and four input MIMO omni antennas with integrated magnetic mount base. These are ideal for vehicle mount antenna applications, especially where permanent installation is not desired or rapid deployment is needed. Both antennas are designed for S-Band communication at 2.1 to 2.5 GHz and are 45° slant polarized, and include 12 feet of integrated low-loss RF cable with Type-N(m) RF connectors (other cable length and RF connector options available upon request). Part # 1055-301 2-Input, Part # 1055-302 4-Input.
Southwest Antennas
www.southwestantennas.com

TEST EQUIPMENT

Miniature MS-Series Matrix

The new miniature MS-series matrix is an ideal switch solution for test & measurement requirements; designed and built with the Reliant Switch™ product series in mind. It is equipped with high performance Reliant Switches™ with 0.03 dB insertion loss repeatability across DC to 26.5 GHz and a minimum of 10 million life cycles for SPDT and 5 million life cycles for SP6T. The MMS-series can be used in many applications where RF switches are needed and it is not restricted to VNA's extension only but also supports extensive testing on DUT's.
Dow-Key Microwave
www.dowkey.com

NewProducts

Laser Powered E-Field Probe

The LSProbe offers a significant reduction in measurement time and effort for radiation immunity testing. Continuous streaming of 500,000 samples per second provides precise timing and characteristics of the electric field strength in reverberation chambers and multiple probes can measure synchronously. From 10 kHz to 6 GHz, the LSProbe is claimed to deliver best-in-class dynamic range (70 to 100 dB) for electric field strengths from 0.1 V/m to 10 kV/m. Extensive frequency and temperature compensation data is supplied for each probe.

LUMILOOP GmbH
www.lumiloop.de/en

WR-12 Source Frequency Extension Module

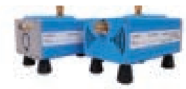

Expand your existing signal generator capabilities to conduct measurements in WR-12 (60 to 90 GHz) with OML's source module. With high output power of +10 dBm, this module provides high performance source for DUT characterization activities. It offers options such as manual (0 to 25 dB) and electronic (0 to 20 dB, 0 to 40 dB and 0 to 60 dB) adjustable attenuation.

OML Inc.
www.omlinc.com

High Performance DC to 18 GHz Modular Matrix

VENDORVIEW

System MS2010A is a high performance DC to 18 GHz coaxial blocking matrix designed for high reliability, very low MTTR, and is available in configurations from 4×4 to 10×10 in an elegant and compact 2RU unit. Enjoy the known benefits of mechanical relay elements without worry of relay-life, or hassle of maintenance. The company's new proprietary high reliability relay element coupled with its sophisticated rack-mount design gives you the performance and maintainability you demand.

Universal Switching Corp.
www.uswi.com

MATERIALS

Tape and Reel Packaging

SV Microwave now offers in-house tape and reel packaging. Now you can automate your pick to place assembly process and protect your parts from electrostatic discharge (ESD). SV's new packaging allows customers to save time and money while simultaneously protecting your parts during shipping, processing and assembly. Contact SV today for more information on this newest value added feature.

SV Microwave
www.svmicro.com

2016 IEEE International Symposium on Phased Array Systems and Technology

Revolutionary Developments in Phased Arrays

18–21 October 2016

Westin Waltham Hotel,
Greater Boston,
Massachusetts, USA
www.array2016.org

Sponsors

Platinum
Raytheon

Gold
Georgia Tech Research Institute

Silver
SRC
Lincoln Laboratory, Massachusetts Institute of Technology
MITRE

Banquet Sponsor
Rockwell Collins

Other Sponsors
Applied Radar
STR Systems & Technology Research

Technical Co–Sponsors
MTT-S
APS
AESS

Our Blog

Conference Committee

Conference Chair:
Jeffrey S. Herd, (MIT LL)

Vice Chair:
William Weedon, Applied Radar

Honorary Chair:
Eli Brookner, Raytheon (retired)

Technical Program Chair:
Alan J. Fenn, MIT LL

Technical Program Vice Chair:
Wajih Elsallal, MITRE

Special Sessions Chair:
Sean Duffy, MIT LL

Plenary Session Chairs:
David Mooradd, MIT LL
Eli Brookner, Raytheon (retired)

Tutorials Chairs:
Jonathan Williams, STR
Jonathan Doane, MIT LL

Student Program Chairs:
Bradley T. Perry, MIT LL
Justin Kasemodel, Raytheon

Secretary:
Duane J. Matthiesen, Technia

International Liaison:
Alfonso Farina, Selex (retired)

Exhibits Chair:
Dan Culkin, NGC

Publicity Chairs:
Glenn Meurer, MITRE
Don McPherson, SRC, Inc.

Social Media Chair:
Gregory Charvat, Humatics, Inc.

Publications Chairs:
Raoul Ouedraogo, MIT LL
Will Moulder, MIT LL

Poster Sessions Chairs:
Greg Arlow, Lockheed Martin
Mark McClure, STR

Local Arrangements/Finance:
Robert Alongi, IEEE Boston

Website:
Kathleen Ballos, Ballos Associates

Advisors:
Ellen Ferraro, Raytheon
Robert J. Mailloux, Arcon
Hans Steyskal, Arcon
Chris McCarroll, Raytheon

v.19

Microwave and RF Semiconductor Control Device Modeling

Robert H. Caverly

The goal of any RF/microwave design is "first pass design success." The industry has made great strides toward that goal through continuous advances in computing power and software, enabling sophisticated electromagnetic simulation and semiconductor device modeling. While power amplifiers arguably pose the greatest design challenge, requiring simulation of both linear and nonlinear domains, control circuits should not be considered easy. They are likely the second most challenging, requiring models that accurately track changes in voltage, current, power and frequency.

Robert Caverly has spent most of his career working with RF/microwave control circuits and their constituent devices and has converted his knowledge into a book treating the physical operation and modeling of PIN diodes and FETs as control components. He hopes his insight, as he writes in the preface, "will be of some aid to design engineers to help them wisely choose and adapt device and circuit parameters during design optimization for best circuit performance."

To establish a foundation, Caverly begins with basic control circuit concepts, such as quality factor, noise figure and power handling. He then outlines the common control circuits: reflective switches and attenuators, matched attenuators and phase shifters and the PIN diode and FET control elements that are the building blocks for these circuits. Beginning with the second chapter, he addresses the real world factors that designers face: parasitics, thermal behavior and nonlinearity (Chapter 2); the linear and nonlinear performance of PIN diodes (Chapters 3 and 4); the characteristics and modeling of MOSFET control devices (Chapter 5); and the characteristics and modeling of MESFET and HEMT control devices (Chapter 6). The final two chapters discuss applications using these PIN diode, MOSFET, MESFET and HEMT components. Chapter 7 focuses on T/R switches, and Chapter 8 addresses attenuators, limiters and phase shifters.

Caverly wrote "Microwave and RF Semiconductor Control Device Modeling" to be a practical reference for the design engineer — not a text book. So you won't find homework problems at the end of each chapter; however, you will find the theory is thorough, with many equations to derive the practical design techniques. The blend of theory and practice makes this another good reference to have on your bookshelf.

To order, contact:

Artech House
www.artechhouse.com
ISBN: 978-1-63081-021-4
272 pages
$189
Available in hardcover and eBook formats

Advertising Index

Advertisers in blue are enabled with the layar app

Sales Representatives

Microwave Journal
Frequency Matters.

Eastern and Central Time Zones
Chuck Boyd
Northeast Reg. Sales Mgr.
(New England, New York, Eastern Canada)
685 Canton Street
Norwood, MA 02062
Tel: (781) 619-1942
FAX: (781) 769-5037
cboyd@mwjournal.com

Michael Hallman
Eastern Reg. Sales Mgr.
(NJ, Mid-Atlantic, Southeast, Midwest, TX)
4 Valley View Court
Middletown, MD 21769
Tel: (301) 371-8830
FAX: (301) 371-8832
mhallman@mwjournal.com

Pacific and Mountain Time Zones
Brian Landy
Western Reg. Sales Mgr.
(CA, AZ, OR, WA, ID, NV, UT, NM, CO, WY, MT, ND, SD, NE & Western Canada)
144 Segre Place
Santa Cruz, CA 95060
Tel: (831) 426-4143
FAX: (831) 515-5444
blandy@mwjournal.com

International Sales
Richard Vaughan
International Sales Manager
16 Sussex Street
London SW1V 4RW, England
Tel: +44 207 596 8742
FAX: +44 207 596 8749
rvaughan@horizonhouse.co.uk

Germany, Austria, and Switzerland (German-speaking)
WMS.Werbe- und Media Service
Brigitte Beranek
Gerhart-Hauptmann-Street 33,
D-72574 Bad Urach
Germany
Tel: +49 7125 407 31 18
FAX: +49 7125 407 31 08
bberanek@horizonhouse.com

Korea
Young-Seoh Chinn
JES Media International
2nd Floor, ANA Bldg.
257-1, Myungil-Dong
Kangdong-Gu
Seoul, 134-070 Korea
Tel: +82 2 481-3411
FAX: +82 2 481-3414
yschinn@horizonhouse.com

China
Shenzhen
Michael Tsui
ACT International
Tel: 86-755-25988571
FAX: 86-10-58607751
michaelt@actintl.com.hk

Shanghai
Linda Li
ACT International
Tel: 86-21-62511200
lindal@actintl.com.hk

Beijing
Oasis Guo
ACT International
Tel: 86-13011108861
oasisg@actintl.com.hk

Hong Kong, Taiwan, Singapore
Mark Mak
ACT International
Tel: 852-28386298
markm@actintl.com.hk

Japan
Katsuhiro Ishii
Ace Media Service Inc.
12-6, 4-Chome,
Nishiiko, Adachi-Ku
Tokyo 121-0824, Japan
Tel: +81 3 5691 3335
FAX: +81 3 5691 3336
amskatsu@dream.com

Ed Kiessling Traffic Manager/Inside Sales • 685 Canton Street Norwood, MA 02062 • Tel: (781) 619-1963 FAX: (781) 769-6178 • ekiessling@mwjournal.com

FABS and LABS

The Lattice Organization - W. L. Gore & Associates

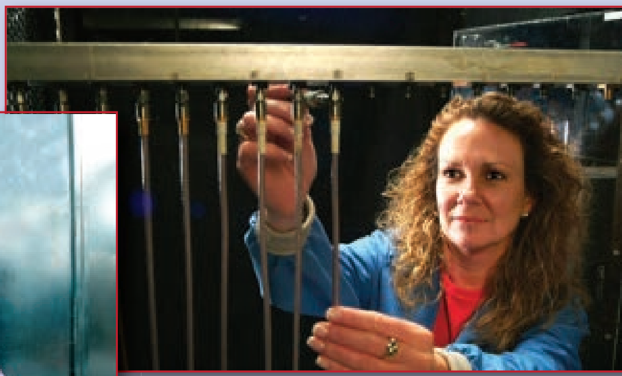

Gore's best known product is Gore-Tex fabric, but they manufacture a diverse portfolio of products that include microwave/electronic cable assemblies, filters, guitar strings, dental floss, sealants, vents and medical devices. Almost all of their products are based on polytetrafluoroethylene (PTFE), a fluoropolymer discovered by Roy Plunkett in 1938 at DuPont. Bill Gore and his wife Genevieve founded the company in 1958 in their basement, while working to develop products after licensing the material technology from DuPont.

Their first product was an insulated ribbon cable called Multi-Tet cable that won Gore a contract from the Denver Water Co. for 7.5 miles of cable in 1960, forcing them out of the basement and into their first facility in Delaware. Bob's son joined Gore in 1969 researching a process to stretch extruded PTFE. He discovered that if PTFE is heated and quickly stretched, it forms a microporous structure that they named expanded PTFE (ePTFE). Today, Gore employs more than 10,000 people at more than 50 facilities around the world with estimated sales exceeding $3 billion.

The main Gore manufacturing site for their microwave cable assemblies is in Landenburg, Pa. Most of their cable assemblies are produced using custom equipment that they design and maintain. They machine most of their own connectors and produce cables with all types of jackets. All of the microwave cable assemblies use a wrapped insulator that provides the highest performance and most reliable products. Their cables are 100 percent tested for S-parameters and test data is provided on each one. An interesting fact is that each employee must successfully manufacture their own cable assembly when they start work in order to learn how it is done.

Gore has a separate Space Flight assembly area in a cleanroom environment. Each space qualified cable goes though X-ray inspection of all solder joints to ensure high-reliability. They measure shielding effectiveness in their anechoic chamber (to 40 GHz) and have separate areas for QC and custom measurements. They can provide matched assemblies to less than pico seconds batch-to-batch, and maintain their records so that even previously sold batches can be matched.

The Gore Capabilities Center nearby fosters collaboration as the 5,000 square foot center features technology displays, multimedia presentations and hands-on activities. Gore has interactive modules that introduce guests to their capabilities in physics, chemistry, biology and electromagnetics. Guests can even stretch PTFE into ePTFE at one of the displays.

Gore has earned a position on Fortune magazine's "100 Best Companies to Work For" list since the late 90's. Their organization is completely flat with everyone carrying the title of associates and managers carrying the title of sponsors. Associates are organized into teams that typically pursue market opportunities, new product concepts, or businesses. As teams evolve, leaders frequently emerge as they gain followership. Bill Gore first presented the concept of a "lattice" organization to Gore associates in 1967 and presented what he termed "culture principles" in a paper entitled, "The Lattice Organization – A Philosophy of Enterprise." He articulated four culture principles that he called freedom, fairness, commitment and waterline.

This non-traditional organizational structure and culture has been shown to be a significant contributor to associate satisfaction and retention with one of the best retention rates in the world (full-time voluntary turnover is only about 3 percent). The Gore culture fosters exceptional, self-motivated and entrepreneurial associates who create some of the most innovative products in the industry.

www.gore.com

WERLATONE®

Mismatch Tolerant

HIGH POWER, MULTI-OCTAVE PERFORMANCE

Radial Combiners

- Multi-kW Power Levels
- Lowest Loss
- Custom Designs Available

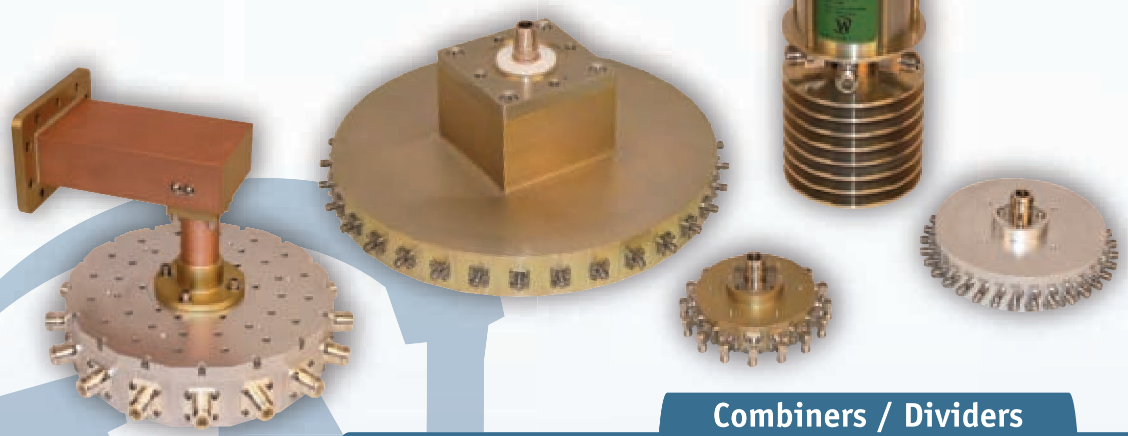

Combiners / Dividers

Model	Type	Frequency (MHz)	Power (W CW)	Insertion Loss (dB)	VSWR	Connectors (Sum Port, Inputs/Outputs)
D8182	5-Way	1175-1375	1,500	0.4	1.35:1	1 5/8" EIA, N Female
D8454	8-Way	370-450	10,000	0.25	1.30:1	3 1/8" EIA, N Female
D9710	8-Way	1000-2500	2,000	0.3	1.40:1	1 5/8" EIA, N Female
D9529	8-Way	2305-2360	1,000	0.2	1.15:1	7/16 Female, N Female
D9528	8-Way	2305-2360	2,000	0.2	1.15:1	7/8" EIA, N Female
D5320	12-Way	470-860	500	0.3	1.30:1	All N Female
D9194	16-Way	2305-2360	1,000	0.2	1.15:1	7/16 Female, SMA Female
D9527	16-Way	2305-2360	2,000	0.2	1.15:1	7/8" EIA, N Female
D9706	16-Way	2700-3500	6,000	0.35	1.35:1	Waveguie, N Female
D6857	32-Way	1200-1400	4,000	0.5	1.35:1	1 5/8" EIA, TNC Female

Werlatone®, Inc.
17 Jon Barrett Road
Patterson, NY 12563
T 845.278.2220
F 845.278.3440
www.werlatone.com

Directional Couplers

0° Combiners/Dividers

90° Hybrid Couplers

180° Hybrid Combiners

Absorptive Filters